NASA Contractor Report 3925

Unsteady Flow in a Supersonic Cascade With Two In-Passage Shocks

Willis H. Braun

CONTRACT NAS3-24100
SEPTEMBER 1985

NASA

NASA Contractor Report 3925

Unsteady Flow in a Supersonic Cascade With Two In-Passage Shocks

Willis H. Braun
Berea, Ohio

Prepared for
Lewis Research Center
under Contract NAS3-24100

National Aeronautics
and Space Administration

**Scientific and Technical
Information Branch**

1985

UNSTEADY FLOW IN A SUPERSONIC CASCADE WITH TWO IN-PASSAGE SHOCKS

Willis H. Braun

National Aeronautics and Space Administration
Lewis Research Center
Cleveland, Ohio 44135

ABSTRACT

A model for a supersonic blade row with two in-passage shock waves is developed. It accounts for three-dimensional effects in observed flows by using a hypothetical blade shape in a two-dimensional cascade. There is enough flexibility in the choice of blade shape to accommodate a desired entrance angle, exit angle, boundary-layer thickness and stage pressure ratio at a given entrance Mach number.

The model divides the mean flow into regions of uniform or one-dimensional flow in which the solutions for the superimposed unsteady flow may be found successively. The analysis makes use of previous solutions for unsteady flow in cascades and over an oscillating wedge.

Six flow conditions are chosen in the range of parameters for which the two-shock model is valid for studies of flutter in torsion and bending. It is found, in keeping with previous results from a single-shock model, that in each case there is increasing instability with decreasing frequency.

INTRODUCTION

The analysis of unsteady flows in blade rows has been facilitated by the use of models for the underlying steady flow which permit the governing differential equations to be written with constant coefficients. This has been true for both supersonic flows and mixed flows with a single shock wave (ref. 1) in which the mean flows were assumed to be uniform. A number of experimental measurements (refs. 2 to 5), using both pressure sensors and laser anemometers, has shown that multiple shock waves are a common occurrence in the tip region of the blades, especially near the operating point of the compressor. One of the frequent patterns (fig. 1) observed in the experimental studies has an oblique shock wave at the leading edge of each blade and a nearly normal shock wave at the trailing edge. It is that flow which we shall investigate for bending and torsional flutter.

We shall first introduce a model for the mean flow which incorporates the two shock waves and modifies the actual blade surfaces to account for three-dimensional flow effects. There are three mean-flow domains which are modeled as either uniform or one-dimensional flow so that the greatest use can be made of previous solutions for unsteady duct flow (ref. 1) and flow around an oscillating wedge (ref. 6). The range of validity of the model is estimated and six numerical examples are calculated covering the intervals of inlet Mach number and stage pressure ratio for which the model is valid. The stability characteristics of the examples are discussed.

Considerable use is made of the analysis previously developed in reference 1 for the flow in a blade passage with a single normal shock wave present. Some familiarity with that paper is assumed in parts of the exposition. The stability analysis of a mean-flow configuration related to those treated here and in reference 1 has recently been completed (unpublished data by E. Acton, Unsteady Flow in a Supersonic Cascade with Strong Oblique Leading Edge Shocks (1982)); it treats the case of a single strong shock wave emanating from the blade leading edge. It uses the principal elements of the blade model employed here.

A computer program, TIPS (Two In-Passage Shocks), has been written which uses the analysis described in this report to calculate the stability of a flow in a cascade. The user provides inlet flow conditions, geometric parameters and disturbance characteristics and the program yields corresponding unsteady lifts and moments. Contact COSMIC, The University of Georgia, Athens, Georgia 30602, concerning the availablity of this program. Frank Molls programmed the model and supplied the numerical calculations.

MODEL

An example of a double-shock configuration observed in an experimental rotor (ref. 5) is shown in figure 2 which exhibits static pressure contours measured at the blade tips. The dashed line beginning at the leading edge of a blade corresponds to an oblique shock wave whose angle is calculated from the pressure ratio across the contours. The position of the shock is in good agreement with the direction of the contours. A nearly normal shock wave emanates from the trailing edge of the blade. The apparent discrepancy between the angle of the oblique shock wave and the small wedge angle of blade at its leading edge is attributed in reference 5 to a radial contraction of the flow in the blade passage.

Following the course set in an earlier analysis (ref. 1) we wish to use a model of the flow in the blade passage which represents the main features of the mean flow to a good approximation and at the same time keeps the equations governing the unsteady motion as amenable to solution as possible. In figure 3 the incremental rotor annulus at the blade tips has been unrolled into a two-dimensional cascade. In it a two-dimensional contraction is imposed by the presence of a wedge at the leading edge. The wedge angle, δ , while much larger than the metal angle of the blade, correctly accounts for the shock angle, χ . Where the oblique shock intersects the lower blade, the surface of the blade is turned parallel to the flow behind the shock. Consequently the shock is not reflected, in accordance with the observed flow in figure 2.

In order to terminate the blade in a small thickness comparable to the combined thicknesses of the upper- and lower-surface boundary layers, the upper surface of the blade after its intersection with the oblique shock wave is represented by a (cubic) function $f_u(x_3)$ whose initial direction is that of the turned flow, β_3', and whose final slope corresponds to the exit angle, β_2', which is a free parameter of the blade design. Likewise, the lower surface over the same range of the coordinate x_3 is designated by the function $f_\ell(x_3)$. The shock wave terminating this region of flow is normal to the exit direction, u_2. The last segment of the lower surface along which the flow is subsonic following the second shock wave, is parallel to the exit flow direction.

The mean flow used in this model is uniform in the entrance region, the triangular region immediately behind the oblique shock wave and in the exit region behind the normal shock wave. Solutions to the unsteady equations of motion can, therefore, be obtained analytically in those regions. The flow in the channel between the curvilinear surfaces is assumed to be one-dimensional so that the unsteady motion in that region may be obtained subject to a slowly-varying flow approximation.

The unit of length in the model is the length of the blade as measured in the turned flow direction β_3'. The chord length is, then,

$$\ell_c = \frac{1}{\cos(\chi_o - \beta_3')} \geq 1$$

Other lengths are

$$s = \ell_c \cos \beta_1'/\mathrm{sol}, \quad s^+ = \ell_c \sin \beta_1'/\mathrm{sol}$$

$$s_3 = s \sin(\chi - \delta)/\sin \chi, \quad s_3^+ = \ell_c \sin \beta_3'/\mathrm{sol}$$

$$d_s = 1 - (s^+ + s \cot \chi) \cos \delta, \quad \ell_b = (1 - d_s) \tan \delta$$

(Here "sol" denotes the solidity of the blade row.)

The trailing-edge values of the boundary-layer displacements are specified in fractions δ_u and δ_ℓ of the base width, ℓ_b, of a blade with unidirectional flow after the oblique shock. The chord intersects the base at a fraction v of its width measured from the lower side.

$$v = \frac{\mathrm{sol} \sin \chi \sin\left(\chi_o - \beta_3'\right)}{\cos(\beta_1' - \chi) \sin \delta}$$

The two cubic functions defining the curved portions of the blade surface are

$$f_u(x_3) = -\ell_u \left[3\left(\frac{x_3}{d_s}\right)^2 - 2\left(\frac{x_3}{d_s}\right)^3\right] - d_s \tan(\beta_2' - \beta_3')\left[\left(\frac{x_3}{d_s}\right)^2 - \left(\frac{x_3}{d_s}\right)^3\right]$$

and

$$f_\ell(x_3) = s_3 + \ell_\ell \left[3\left(\frac{x_3}{d_s}\right)^2 - 2\left(\frac{x_3}{d_s}\right)^3\right] - d_\ell \tan(\beta_2' - \beta_3')\left[\left(\frac{x_3}{d_s}\right)^2 - \left(\frac{x_3}{d_s}\right)^3\right]$$

The cross-sectional area of the blade passage per unit blade height of the cascade is

$$A(x_3) = \sqrt{\left(1 - \frac{d_\ell}{d_s}\right)^2 x_3^2 + \left(f_\ell - f_u\right)^2}$$

In these expressions,

$$\ell_u = \ell_b(1 - v - \delta_u)$$

$$\ell_\ell = -\frac{\ell_c}{sol} \sin \beta_2' \sin(\beta_2' - \beta_3') + \ell_b \left[v + \delta_u \sin^2(\beta_2' - \beta_3') - \delta_\ell \cos^2(\beta_2' - \beta_3')\right]$$

and

$$d_\ell = d_s - s_2 \sin(\beta_2' - \beta_3')$$

A convenient but not necessary assumption in this model is that the elastic axis for torsion lies on the chord at some fraction f of its length measured from the leading edge. Then the distance d_o of the elastic axis from the origin of x_1 in the inlet direction is

$$d_o = -s^+ + f[\cos \delta + v(1 - d_s) \sin \delta \tan \delta]$$

which reduces to the value appropriate for a system of infinitesimally thin blades (ref. 1) when $\delta = 0$.

In region 2 the corresponding moment arm of the elastic axis is

$$d_{o,2} = 1 - s_2^+ - \ell_c(1 - f) \cos(\beta_2' - x_o)$$

When allowance for the trailing-edge boundary-layer thicknesses is made, the blade separation and stagger lengths are

$$s_2 = \ell_c \cos \beta_2'/sol - (\delta_u + \delta_\ell)\ell_b \cos(\beta_2' - \beta_3'),$$

$$s_2^+ = \ell_c \sin \beta_2'/sol - (\delta_u + \delta_\ell)\ell_b \sin(\beta_2' - \beta_3')$$

At any entrance Mach number M_1 and for any cascade geometry this model is valid if the static pressure ratio P_{21} across the blade row is not so low that the oblique shock fails to intersect the adjacent blade or so high that the velocity behind this shock is subsonic. Figure 4 shows the region of validity in the M_1, P_{21} plane for a cascade of solidity 1.4, stagger angle 62° and entrance-flow angle 67°.[1] To the left of the valid area is the region of low pressure ratio in which the flow through the blade passage is

---

[1]The blades are untapered at the trailing edge and take the shape indicated by the dashed lines in figure 3.

likely to be entirely supersonic. To the right is the region of high pressure ratio in which a strong oblique shock is a likely configuration.

In general, even though the blades are tapered near the trailing edge to more nearly approximate the shape of real blades, there is a finite trailing-edge thickness, corresponding to a boundary-layer displacement thickness, and a wake of finite thickness as well. It is assumed, in keeping with the boundary conditions on the infinitesimally thin wake in reference 1, that the pressure and normal component of velocity are also continuous across the wake of the present model.

ANALYSIS

The unsteady flow produced by the oscillating blade row in the supersonic region upstream of the leading shock has been treated in reference 1 for the case where there is a single normal shock at the leading edge of each blade. In the present double-shock configuration the upstream supersonic region extends an additional length $s \cot \chi$ along the upper blade surface before the oblique shock from the adjacent blade touches down. The upstream solution is the same as in reference 1 and extends without modification through this region up to the leading shock. Likewise, the unsteady solution in the subsonic flow region 2 downstream of the normal shock wave is, with slight modification, the same as the downstream subsonic solution of the single-shock analysis of reference 1. The main new features of the present model are the oblique shock and the supersonic region between this shock and the trailing normal shock.

Boundary Conditions on the Blade

With the bending motion of amplitude H_0 assumed normal to the entrance-region surface and with $x = d_0$ the projection of the elastic axis upon that surface, the amplitude of the upper surface oscillation of the zeroth blade is

$$W_1 = H_0 + A_0(x - d_0)$$

The motion of the lower surface of the same blade is

$$W_3 = H_0 \cos \delta + A_0(x_3 + 1 - d_s - f)$$

(Subscript 1 refers to the entrance flow, subscript 3 to the region behind the oblique shock. Subscript 2 is reserved for the subsonic exit region. See fig. 3.)

As indicated in reference 7, the most general blade motion is the superposition of motions with constant interblade phase angle, σ, so we need only consider motions of this type. Then in the cascade, the motion of the n^{th} blade is determined by

$$V_3\left(x_3 + ns_3^+, y_3 + n(\ell_b + s_3)\right) = e^{in\sigma} V_3(x_3, y_3) \qquad (1)$$

where V_3 can be any of the physical variables. In particular, on the lower surface of the first blade,

$$W_3 = e^{i\sigma}\left[H_0 \cos \delta + A_0(x_3 + \alpha s_3 - f)\right]$$

(We shall see later that there is an additional motion with $\alpha = \cot(x - \delta)$ associated with the perturbation of shock position. However, it does not enter into the shock relations which are the immediate concern of this discussion.)

Conditions on the Oblique Shock Wave

As discussed in reference 1, the pressure disturbances generated in the upstream supersonic region distort the oblique shock and may be transmitted by it, but not reflected, i.e., the flow region 1 is unaffected by the shock. The perturbed Rankine-Hugoniot equations have been given by Carrier (ref. 6) for an oblique shock in a disturbance-free upstream flow, and by Moore (ref. 8) when there are upstream disturbances. A particular case of the latter is given in reference 1 for the normal shock wave. It also applies to oblique shock waves when the coordinates move with the component of the mean velocity parallel to the shock. The dimensionless time derivative in the moving coordinates transforms as

$$\frac{\partial}{\partial t} \to \frac{1}{\sin \chi}\left(\frac{\partial}{\partial t} - \cos \chi \frac{\partial}{\partial y}\right) \equiv \frac{1}{\sin \chi}\frac{D_s}{Dt}$$

since time was normalized by $c/\mathscr{U}_1 \sin \chi$. With the displacement of the shock normal from its mean position denoted by $x_s(y,t)$, the pressure perturbation by p', the disturbance normal and tangent velocities by $u^{(n)}$ and $u^{(t)}$, respectively, then the shock conditions, to first order in the disturbance quantities, are

$$p_3' = \left(\frac{2M_1^2 \sin^2\chi - \mu + 1}{\mu + 1}\right) p_1' + \frac{4}{\mu + 1} \sin \chi \left[u_1^{(n)} - \frac{D_s x_s}{Dt}\right]$$

$$u_3^{(n)} - \frac{D_s x_s}{Dt} = \left[\frac{(\mu - 1)M_1^2 \sin^2\chi - 2}{(\mu + 1)M_1^2 \sin^2\chi}\right]\left[u_1^{(n)} - \frac{D_s x_s}{Dt}\right] + 2\left(\frac{\mu - 1}{\mu + 1}\right)\frac{p'}{\sin \chi}$$

$$u_3^{(t)} - u_1^{(t)} = \left[1 - \frac{\mathscr{U}_3 \sin(\chi - \delta)}{\mathscr{U}_1 \sin \chi}\right]\frac{\partial x_s}{\partial y_s} \sin \chi$$

where, as indicated previously, the subscripts 1 and 3 refer to conditions upstream and downstream of the shock. When these relations are expressed in terms of the streamwise and cross-stream velocities in the upstream and post shock flows

$$u_1 = u_1^{(n)} \sin \chi - u_1^{(t)} \cos \chi, \quad v_1 = u_1^{(t)} \sin \chi + u_1^{(n)} \cos \chi$$

$$u_3 = u_3^{(n)} \sin(\chi - \delta) - u_3^{(t)} \cos(\chi - \delta), \quad v_3 = u_3^{(t)} \sin(\chi - \delta) + u_3^{(n)} \cos(\chi - \delta)$$

they take the form

$$p_3 + I_1 \frac{\mathscr{U}_1}{\mathscr{U}_3} \frac{D_s x_s}{Dt} = \alpha_{11} p_1 + \alpha_{12} u_1 + \alpha_{13} v_1 \tag{2}$$

$$u_3 + I_2 \frac{\mathscr{U}_1}{\mathscr{U}_3} \frac{D_s x_s}{Dt} + K_2 \frac{\partial x_s}{\partial y_s} = \alpha_{21} p_1 + \alpha_{22} u_1 + \alpha_{23} v_1 \tag{3}$$

$$v_3 + I_3 \frac{\mathscr{U}_1}{\mathscr{U}_3} \frac{D_s x_s}{Dt} + K_3 \frac{\partial x_s}{\partial y_s} = \alpha_{31} p_1 + \alpha_{32} u_1 + \alpha_{33} v_1 \tag{4}$$

where we have equated tangential velocities at the shock wave to obtain $\cos(\chi - \delta)/\cos \chi = \mathscr{U}_1/\mathscr{U}_3$. The coefficients I_m, K_m, α_{pq} are the functions of the entrance Mach number and shock angle listed in appendix A. The quantities on the right side are known from the solution for the unsteady flow in the upstream supersonic region which, as we indicated, is independent of the downstream flow.

Solution in Region 3

Carrier (ref. 6) developed the solution to the small amplitude, unsteady flow behind a shock wave attached to a wedge that is oscillating about its apex as Bessel series for the unsteady potential, vorticity and shock displacement. We adapt his solution to the region behind the oblique shock by generalizing the wedge motion and replacing a portion of the potential series representing the effect of the boundary condition on the blade by a form characteristic of duct solutions as, for example, in reference 1. The potential, stream function, and shock displacement in region 3 between the zeroth blade and the first blade (figure 3) are, in our notation,

$$\Phi_3 = e^{ik_3 M_3 (x_3 + \alpha s_3)} \sum_{n=1}^{\infty} \tilde{A}_n \cosh n\theta \, J_n(k_3 r) + \Phi_b \tag{5}$$

$$\Psi_3 = e^{i\omega_3 (x_3 + \alpha s_3 M_3^2/\beta_3^2 - \alpha y_3/\beta_3^2)} \sum_{n=1}^{\infty} \tilde{C}_n J_n\left[k_3 \sqrt{\alpha^2 - \beta_3^2} \, (s_3 - y_3)\right] \tag{6}$$

$$x_s = e^{i\omega_3 \alpha M_3^2 (s_3 - y_3)/\beta_3^2} \sum_{n=0}^{\infty} \tilde{D}_n J_n \left[k_3 \sqrt{\alpha^2 - \beta_3^2}\, (s_3 - y_3) \right] \tag{7}$$

where

$$r^2 = (x_3 + \alpha s_3)^2 - \beta_3^2 (s_3 - y_3)^2$$

$$\theta = \tanh^{-1} \left[\frac{\beta_3 (s_3 - y_3)}{(x_3 + \alpha s_3)} \right]$$

The potential Φ_b is given by

$$\Phi_b = i\omega_1 \left[H_o \cos \delta + A_o (x_3 + 1 - d_s - f) \right] f_1(y_3; M_3\omega_3)$$

$$- A_o \left[\frac{\partial}{\partial \omega_3} \omega_3 f_1(y_3; M_3\omega_3) + \omega_3 f_2(y_3; M_3\omega_3) \right] \frac{\omega_1}{\omega_3}$$

in which the functions $f_1(y;\omega)$ and $f_2(y,\omega)$ are those already defined for region 1 in reference 1 and represent duct effects having contributions from all the blades. We have followed Van Dyke (ref. 9) in adding to the series for the shock displacement the term

$$\tilde{D}_o J_o \left[k_3 \sqrt{\alpha^2 - \beta_3^2}\, (s_3 - y_3) \right]$$

which describes the change in shock position due to the motion of the blade leading edge. When the blade has both a plunging motion and an oscillation around an axis not at the apex,

$$\tilde{D}_o = e^{i\sigma} \left[H_o \cos \chi - A_o \ell_c f \cos(\chi + \chi_o - \beta_1') \right] \tag{8}$$

The perturbation pressure and velocities are obtained from the velocity potential and stream function from the relations

$$p_3 = - \frac{s}{s_3} \left(\frac{\partial \Phi_3}{\partial t} + \frac{\partial \Phi_3}{\partial x_3} \right), \quad u_3 = \frac{\partial \Phi_3}{\partial x_3} + \frac{\partial \Psi_3}{\partial y_3}, \quad v_3 = \frac{\partial \Phi_3}{\partial y_3} - \frac{\partial \Psi_3}{\partial x_3} \tag{9}$$

From the first of these and the periodicity relation (1) the pressure on the blade surface behind the oblique shock wave is

$$P_3(x_3,-\ell_b) = -\frac{k_3 s}{2s_3} e^{i[k_3M_3(x_3+1-d_s)-\sigma]} \sum_{n=0}^{\infty}\left(\tilde{A}_{n+1} + \frac{2i}{M_3}\tilde{A}_n - \tilde{A}_{n-1}\right)$$

$$\times J_n\left[k_3(x_3 + 1 - d_s)\right] - \frac{\omega_1 e^{-i\sigma_s}}{s_3}\left\{\omega_3\left[H_o \cos\delta\right.\right.$$

$$\left.\left. + A_o(x_3 + 1 - d_s + s_3^+ - f)\right] + iA_o\right\} f_1(s_3;M_3\omega_3)$$

$$- \frac{i\omega_1 A_o s}{s_3} e^{-i\sigma}\left\{\omega_3 f_2(s_3;M_3\omega_3) - \frac{M_3\omega_3 s_3}{\sin(M_3\omega_3 S_3)} f_1(0;M_3\omega_3)\right\}$$

$$d_s - 1 < x_3 < \beta_3 s_3 - s_3^+$$

The coefficients $\tilde{A}_n$, $\tilde{C}_n$, $\tilde{D}_n$ remaining unspecified in the solutions (5), (6), (7) must be determined from the shock conditions (2), (3), (4) in a manner to be described below.

For convenience in the later computation of the lift and moment on the blade we record here the contributions to those quantities obtained from the foregoing expression for the pressure.

The lift developed on the blade surface from the leading edge to $x_3 = -s_3^+$ is

$$L_{33} \equiv \int_{d_s-1}^{-s_3^+} P_3(x_3,-\ell_b)dx_3$$

$$= -\frac{k_3 s}{2s_3} e^{-i\sigma} \sum_{n=0}^{\infty}\left(\tilde{A}_{n+1} + \frac{2i}{M_3}\tilde{A}_n - \tilde{A}_{n-1}\right)\hat{A}_n$$

$$- \alpha s\omega_1\left[\omega_3\left(\hat{H}_3 + \frac{\alpha s_3}{2} A_o\right) f_1(s_3;M_3\omega_3) + iA_o\hat{\hat{H}}_3(s_3)\right] e^{-i\sigma}$$

where

$$\hat{\Delta}_n \equiv \int_0^{\alpha s_3} e^{iM_3k_3\eta} J_n(k_3\eta)d\eta = \frac{i^{n+1}}{M_3k_3} \sum_{\ell=0}^{\infty} \frac{\gamma(2\ell + n + 1, -iM_3k_3\alpha s)}{(2M_3)^{2\ell+n}\, \ell!(n + \ell)!}$$

$$\hat{H}_3 \equiv H_o \cos\delta + A_o(s_3^+ - f)$$

and

$$\hat{\hat{H}}_3(s_3) \equiv f_2(s_3; M_3\omega_3, s_3^+)\omega_3 + f_1(s_3; M_3\omega_3) - \frac{M_3\omega_3 s_3}{\sin(M_3\omega_3 s_3)} f_1(0; M_3\omega_3)$$

The evaluation of $\hat{\Delta}_n$ is made by expanding the Bessel function in its power series at $\eta = 0$ and integrating to obtain a sum of incomplete gamma functions $\gamma(2\ell + n + 1, -iM_3k_3\alpha s_3)$.

Likewise, the moment contributed by this blade surface, measured about the leading edge, is

$$M_{33} \equiv \int_{d_s-1}^{-s_3^+} (x_3 - d_s + 1)P_3(x_3, -\ell_b)dx_3$$

$$= -\frac{k_3 s}{2s_3} e^{-i\sigma} \sum_{n=0}^{\infty} \left(\tilde{A}_{n+1} + \frac{2i}{M_3}\tilde{A}_n - \tilde{A}_{n-1}\right)\hat{\hat{\Delta}}_n$$

$$- \frac{\omega_1\alpha^2 s s_3 e^{-i\sigma}}{2} \left[\left(\hat{H}_3 + A_o \frac{2}{3}\alpha s_3\right)\omega_3 f_1(s_3; M_3\omega_3) + iA_o\hat{\hat{H}}_3(s_3)\right]$$

where

$$\hat{\hat{\Delta}}_n \equiv \int_0^{\alpha s_3} \eta e^{iM_3k_3\eta} J_n(k_3\eta)d\eta = \frac{-i^n}{(M_3k_3)^2} \sum_{\ell=0}^{\infty} \frac{\gamma(2\ell + n + 2, -iM_3k_3\alpha s_3)}{(2M_3)^{2\ell+n}\ell!(n + \ell)!}$$

Upstream Shock Quantities

The unsteady pressures and velocities ahead of the shock wave can be obtained from reference 1 as

$$p_1 e^{i\omega t} = \sum_{n=0}^{\infty} \left[e^{i(M_1 k_1 - \lambda_n)x} R_n^+ + e^{i(M_1 k_1 + \lambda_n)x} R_n^- \right] \cos\left(\frac{n\pi y}{s}\right)$$

$$- \omega_1^2 \left[H_0 + A_0(x - d_0) \right] f_1(y; M_1\omega_1)$$

$$- iA_0 \left[\frac{\partial}{\partial \omega_1} \omega_1^2 f_1(y; M_1\omega_1) + \omega_1^2 f_2(y; M_1\omega_1) \right]$$

$$u_1 e^{i\omega t} = \sum_{n=0}^{\infty} \left[e^{i(M_1 k_1 - \lambda_n)x} Q_n^+ + e^{i(M_1 k_1 + \lambda_n)x} Q_n^- \right] \cos\left(\frac{n\pi y}{s}\right) + iA_0\omega_1 f_1(y; M_1\omega_1)$$

$$v_1 = \frac{1}{i\omega_1} \frac{\partial}{\partial y} \left[p_1(x,y) + u_1(x,y) \right]$$

In order to bring these quantities into a form appropriate for the shock conditions we write them in terms of the argument $\xi = k_3 \sqrt{\alpha^2 - \beta_2^3}\ (s_3 - y_3)$ of Carrier's solution and transform them to Bessel series.

On the shock locus

$$x = (s - y)\cot \chi$$

$$y = \frac{s y_3}{s_3}$$

an argument of the functions f_1 and f_2 of Φ_b becomes

$$\pm M_1\omega_1(y - s) = q_1^{\pm} k_3 \sqrt{\alpha^2 - \beta_3^2}\ (s_3 - y_3) + \alpha k_3 M_3 (s_3 - y_3)$$

where

$$q_1^{\pm} = - \frac{\pm \frac{M_1\omega_1}{k_3} \sin\chi + M_3 \cos(\chi - \delta)}{\sqrt{1 - M_3^2 \sin^2(\chi - \delta)}}$$

If the generating function for the Bessel functions, and its parametric derivative,

$$e^{-iM\eta} = J_0(\eta) + \sum_{\nu=1}^{\infty} |t^{\nu} + (-t)^{-\nu}| J_{\nu}(\eta),\ t = -i(M + \beta),\ \beta = \sqrt{M^2 - 1}$$

$$i\eta e^{+iM\eta} = \frac{1}{\beta} \sum_{\nu=1}^{\infty} \nu \left[\bar{t}^{\nu} - (-\bar{t})^{-\nu} \right] J_{\nu}(\eta),\ \bar{t} = i(M + \beta)$$

are introduced, it follows that

$$e^{\pm iM_1\omega_1(y-s)} = e^{i\alpha k_3 M_3(s_3-y_3)}\left\{J_0(\xi) + \sum_{m=1}^{\infty}\left[(t_{\pm})^m + (-t_{\pm})^{-m}\right]J_m(\xi)\right\}$$

with

$$t_{\pm} = \left(q_1 \pm \sqrt{q_1^2 - 1}\right)$$

and that

$$ik_3 \frac{\sqrt{1 - M_3^2 \sin^2(\chi - \delta)}}{\cos \chi} x e^{\pm iM_1\omega_1(y-s)}$$

$$= \frac{1}{\sqrt{q_{\pm}^2 - 1}} e^{i\alpha k_3 M_3(s_3-y_3)} \sum_{m=1}^{\infty} m\left[t_{\pm}^m - (-t_{\pm})^{-m}\right] J_m(\xi)$$

Consequently, the functions f_1, f_2, appearing in Φ_b, can be transformed to Bessel series by using the identities

$$\cos M_1\omega_1(y - s) = e^{i\alpha k_3 M_3(s_3-y_3)} \sum_{m=0}^{\infty} (1)\Theta_m^+ J_m(\xi)$$

$$\sin M_1\omega_1(y - s) = e^{i\alpha k_3 M_3(s_3-y_3)} \frac{1}{i} \sum_{m=0}^{\infty} (1)\Theta_m^- J_m(\xi)$$

$$\cos M_1\omega_1 y = e^{i\alpha k_3 M_3(s_3-y_3)} \sum_{m=0}^{\infty} (1)\tilde{\Theta}_m^+ J_m(\xi)$$

$$\sin M_1\omega_1 y = -ie^{i\alpha k_3 M_3(s_3-y_3)} \sum_{m=0}^{\infty} (1)\tilde{\Theta}_m^- J_m(\xi)$$

$$x \cos M_1\omega_1(y - s) = e^{i\alpha k_3 M_3(s_3-y_3)} \sum_{m=1}^{\infty} (1)\Psi_m^+ J_m(\xi)$$

$$x \sin M_1\omega_1(y - s) = -ie^{i\alpha k_3 M_3(s_3-y_3)} \sum_{m=1}^{\infty} {}^{(1)}\Psi_m^- J_m(\xi)$$

$$x \cos M_1\omega_1 y = e^{i\alpha k_3 M_3(s_3-y_3)} \sum_{m=1}^{\infty} {}^{(1)}\tilde{\Psi}_m^+ J_m(\xi)$$

$$x \sin M_1\omega_1 y = -ie^{i\alpha k_3 M_3(s_3-y_3)} \sum_{m=1}^{\infty} {}^{(1)}\tilde{\Psi}_m^- J_m(\xi)$$

The quantities ${}^{(1)}\Theta_m^{\pm}$, ${}^{(1)}\tilde{\Theta}_m^{\pm}$, ${}^{(1)}\Psi_m^{\pm}$, ${}^{(1)}\tilde{\Psi}_m^{\pm}$ are defined in appendix B.[2]

The Fourier cosine series appearing in each of p_1, u_1, and v_1 is transformed by again introducing coordinates of region 3 to obtain

$$\left[M_1k_1 \mp \lambda_n^{(1)}\right]x - \frac{n\pi y}{s} = r_n^{\pm}\xi + \alpha k_3 M_3(s_3 - y_3)$$

Then, for example, in the pressure the Fourier series becomes

$$\sum_{n=0}^{\infty}\left\{e^{i\left[M_1k_1-\lambda_n^{(1)}\right]x}R_n^+ + e^{i\left[M_1k_1+\lambda_n^{(1)}\right]x}R_n^-\right\}\cos\left(\frac{n\pi y}{s}\right)$$

$$= \frac{1}{2}e^{i\alpha k_3 M_3(s_3-y_3)}\sum_{m=0}^{\infty}(-1)^m\left[R_m^+\left(e^{ir_m^+\xi} + e^{ir_{-m}^+\xi}\right) + R_m^-\left(e^{ir_m^-\xi} + e^{ir_{-m}^-\xi}\right)\right]$$

$$r_n^{\pm} = \frac{M_1k_1\cos\chi - M_3k_3\cos(\chi - \delta) - \left(\frac{n\pi}{s} \pm \lambda_n\cot\chi\right)\sin\chi}{k_3\sqrt{1 - M_3^2\sin^2(\chi - \delta)}}$$

We approximate the summation in this last form by a least-squares fit to a polynomial of order 50, say,

---

[2]The functions f_1, f_2 and expressions involving them are also listed in appendix B.

$$\sum_{m=0}^{50} \mathscr{A}_m^{(1)} \left(\frac{\xi}{2}\right)^m$$

The polynomial is, in turn, converted to a Bessel series by using Gegenbauer's expansion (ref. 10)

$$\left(\frac{1}{2}\, z\right)^{\mu} = \sum_{n=0}^{\infty} \frac{(\mu + 2n)\Gamma(\mu + n)}{n!}\, J_{\mu+2n}(z)$$

with the result for the Fourier series in the pressure p,

$$\sum_{m=0}^{\infty} \left[e^{i(M_1 k_1 - \lambda_n)x} R_n^+ + e^{i(M_1 k_1 + \lambda_n)x} R_n^- \right] \cos\left(\frac{n\pi y}{s}\right)$$

$$\equiv e^{i\alpha k_3 M_3 (s_3 - y_3)} \sum_{n=0}^{\infty} J_n(\xi) \sum_{m=0}^{[n/2]} \mathscr{A}_{n-2m}^{(1)} \frac{n\Gamma(n - m)}{m!}$$

The alternate expression for the upstream pressure for application in the shock relations is, then,

$$p_1 e^{i\omega t} = e^{i\omega_3 \alpha M_3^2 (s_3 - y_3)/\beta_3^2} \sum_{n=0}^{\infty} J_n(\xi) \left\{ \sum_{m=0}^{[n/2]} \mathscr{A}_{n-2m}^{(1)} \frac{n\Gamma(n - m)}{m!} \right.$$

$$- \left[\frac{\omega_1 (H_0 - A_0 d_0)}{M_1 \sin(M_1 \omega_1 s)} + iA_0 \frac{\partial}{\partial \omega_1} \left(\frac{\omega_1^2}{M_1 \omega_1 \sin(M_1 \omega_1 s)} \right) \right] \left[e^{i\sigma}\, {}^{(1)}\tilde{\Theta}_n^+ - {}^{(1)}\Theta_n^+ \right]$$

$$- \frac{A_0 \omega_1}{M_1 \sin(M_1 \omega_1 s)} \left[e^{i\sigma}\, {}^{(1)}\tilde{\Psi}_n^+ - {}^{(1)}\Psi_n^+ + M_1 \tan \chi \left[e^{i\sigma}\, {}^{(1)}\tilde{\Psi}_n^- - {}^{(1)}\Psi_n^- \right] \right.$$

$$\left. \left. - e^{i\sigma} \left[s^+\, {}^{(1)}\tilde{\Theta}_n^+ + M_1 s\, {}^{(1)}\tilde{\Theta}_n^- \right] \right] \right\}$$

$$\equiv e^{i\alpha k_3 M_3 (s_3 - y_3)} \sum_{n=0}^{\infty} J_n(\xi)\, {}^{(1)}\mathscr{R}_n^{(1)} \tag{10}$$

and similarly for the velocity fluctuations

$$u_1 e^{i\omega t} = e^{i\omega_3 \alpha M_3^2 (s_3 - y_3)/\beta_3^2} \sum_{n=0}^{\infty} J_n(\xi) \left[\sum_{m=0}^{[n/2]} \mathscr{A}_{n-2m}^{(2)} \frac{n\Gamma(n-m)}{m!} + iA_o \frac{e^{i\sigma\, (1)\tilde{\Theta}_n^+} - {}^{(1)}\Theta_n^+}{M_1 \sin(M_1 \omega_1 s)} \right]$$

$$\equiv e^{i\alpha k_3 M_3 (s_3 - y_3)} \sum_{n=0}^{\infty} J_n(\xi)\ {}^{(1)}\mathscr{R}_n^{(2)} \tag{11}$$

$$v_1 e^{i\omega t} = e^{i\omega_3 \alpha M_3^2 (s_3 - y_e)/\beta_3^2} \sum_{n=0}^{\infty} J_n(\xi) \left(\sum_{m=0}^{[n/2]} \mathscr{A}_{n-2m}^{(3)} \frac{n\Gamma(n-m)}{m!} \right.$$

$$- \left\{ \frac{\omega_1 (H_o - A_o d_o)}{\sin(M_1 \omega_1 s)} + iA_o \frac{\partial}{\partial \omega_1} \left[\frac{\omega_1}{\sin(M_1 \omega_1 s)} \right] \right\} \left[e^{i\sigma\, (1)\tilde{\Theta}_n^-} - {}^{(1)}\Theta_n^- \right]$$

$$+ \frac{A_o \omega_1}{\sin(M_1 \omega_1 s)} \left\{ - M_1 \tan x \left[e^{i\sigma\, (1)\tilde{\Psi}_n^+} - {}^{(1)}\Psi_n^+ \right] - \left[e^{i\sigma\, (1)\tilde{\Psi}_n^-} - {}^{(1)}\Psi_n^- \right] \right.$$

$$\left. \left. + e^{i\sigma} \left[s^+\, {}^{(1)}\tilde{\Theta}_n^- + sM_1\, {}^{(1)}\tilde{\Theta}_n^+ \right] \right\} \right)$$

$$\equiv e^{i\alpha k_3 M_3 (s_3 - y_3)} \sum_{n=0}^{\infty} J_n(\xi)\ {}^{(1)}\mathscr{R}_n^{(3)} \tag{12}$$

Recursion Relations

To illustrate the method of preparing the downstream quantities for substitution into the shock relations (2), (3), (4) we compute the pressure along the oblique shock wave in its proper form.

From equations (5) and (9)

$$p_3 = \frac{s}{s_3}\left(i\omega_3 - \frac{\partial}{\partial x_3}\right)e^{ik_3M_3(x_3+\alpha s_3)}\sum_{n=1}^{\infty}\tilde{A}_n \cosh n\theta\, J_n(k_3r) + \frac{s}{s_3}\left(i\omega_3 - \frac{\partial}{\partial x_3}\right)\Phi_b$$

By employing the relations

$$\frac{\partial r}{\partial x_3} = \cosh\theta, \qquad \frac{\partial \theta}{\partial x_3} = -\frac{\sinh\theta}{r}$$

$$J_{p-1}(x) + J_{p+1}(x) = \frac{2p}{x}J_p(x)$$

and the derivative of the Bessel function we obtain for the derivative in the first term of p_3,

$$\frac{\partial}{\partial x_3}e^{ik_3M_3(x_3+\alpha s_3)}\sum_{n=1}^{\infty}\tilde{A}_n \cosh n\theta\, J_n(k_3r) = e^{ik_3M_3(x_3+\alpha s_3)}$$

$$\times\left[iM_3k_3\sum_{n=1}^{\infty}\tilde{A}_n \cosh n\theta\, J_n(k_3r) + \frac{k_3}{2}\sum_{n=1}^{\infty}\tilde{A}_n\, J_{n-1}(k_3r)\cosh(n-1)\theta\right.$$

$$\left. - \frac{k_3}{2}\sum_{n=1}^{\infty}\tilde{A}_n\, J_{n+1}(k_3r)\cosh(n+1)\theta\right]$$

Introducing a new summation index $N = n - 1$ in the second term in the brace, $N = n + 1$ in the third term, and adding the time-derivative term yields

$$\left(i\omega_3 - \frac{\partial}{\partial x_3}\right)e^{ik_3M_3(x_3+\alpha s_3)}\sum_{n=1}^{\infty}\tilde{A}_n \cosh n\theta\, J_n(k_3r) = \frac{k_3}{2}e^{ik_3M_3(x_3+\alpha s_3)}$$

$$\times\sum_{n=0}^{\infty}\cosh n\theta\, J_n(k_3r)\left[\tilde{A}_{n-1}(1-\delta_{n0})(1-\delta_{n1}) - \frac{2i}{M_3}\tilde{A}_n(1-\delta_{n0}) - \tilde{A}_{n+1}\right]$$

For the term involving Φ_b we again use the generating function of the Bessel functions to obtain

$$e^{\pm iM_3\omega_3(y_3-s_3)} \equiv e^{i\alpha k_3 M_3(s_3-y_3)} e^{iq_3^{\pm}\xi}$$

$$= e^{i\alpha k_3 M_3(s_3-y_3)}\left\{J_0(\xi) + \sum_{m=1}^{\infty}\left[(\tilde{t}^{\pm})^m + (-\tilde{t}^{\pm})^{-m}\right]J_m(\xi)\right\}$$

and, on the shock wave,

$$\frac{ik_3\sqrt{1 - M_3^2\sin^2(\chi - \delta)}}{\cos(\chi - \delta)}(x_3 + \alpha s_3)e^{\pm iM_3\omega_3(y_3-s_3)}$$

$$\equiv i\xi e^{iq_3^{\pm}\xi} e^{i\alpha k_3 M_3(s_3-y_3)} = \frac{e^{i\alpha k_3 M_3(s_3-y_3)}}{\sqrt{(q_3^{\pm})^2 - 1}}\sum_{n=1}^{\infty} n\left[t^n - (-t)^{-n}\right]J_n(\xi)$$

$$t = i\left[q_3^{\pm} + \sqrt{(q_3^{\pm})^2 - 1}\right]$$

From these expressions all of the functions of x_3 and y_3 in the potential Φ_b may be represented as expansions in Bessel functions in the same way as the corresponding quantities in the upstream region. After considerable manipulation one can write

$$\frac{s}{s_3}\left(i\omega_3 - \frac{\partial}{\partial x_3}\right)\Phi_b = \frac{s}{s_3} e^{i\alpha M_3 k_3(s_3-y_3)}\sum_{n=1}^{\infty} {}^{(3)}\mathscr{R}_n^{(1)} J_n(\xi)$$

with ${}^{(3)}\mathscr{R}_n^{(1)}$ defined as in appendix C. Thus, on the oblique shock where

$$x_3 + \alpha s_3 = \alpha(s_3 - y_3),$$

$$e^{i\omega_1 t} p_3 = \frac{s}{s_3} e^{ik_3 M_3\alpha(s_3-y_3)}\sum_{n=0}^{\infty} J_n(\xi)\left\{\frac{k_3}{2}\cosh n\theta\left[\tilde{A}_{n-1}(1 - \delta_{n1})(1 - \delta_{n0})\right.\right.$$

$$\left.\left. - \frac{2i}{M_3}\tilde{A}_n(1 - \delta_{n0}) - \tilde{A}_{n+1}\right] + {}^{(3)}\mathscr{R}_n^{(1)}\right\}$$

Likewise, the unsteady velocities and shock displacement are given by

$$e^{i\omega_1 t} u_3 = \frac{k_3}{2} e^{i\alpha M_3 k_3 (s_3 - y_3)} \sum_{n=0}^{\infty} J_n(\xi) \left\{ 2iM_3 \tilde{A}_n \cosh n\theta_0 \right.$$

$$\left. - \sqrt{\alpha^2 - \beta_3^2} \left(\tilde{C}_{n+1} - \tilde{C}_{n-1} \right) - \frac{2i\alpha}{M_3} \tilde{C}_n + \left(\tilde{A}_{n+1} - \tilde{A}_{n-1} \right) \cosh n\theta_0 + {}^{(3)}\mathscr{R}_n^{(2)} \right\}$$

$$e^{i\omega_1 t} v_3 = - \frac{k_3 \beta_3}{2} e^{i\alpha M_3 k_3 (s_3 - y_3)} \sum_{n=0}^{\infty} J_n(\xi) \left\{ 2i \frac{\beta_3}{M_3} \tilde{C}_n \right.$$

$$\left. + \left(\tilde{A}_{n+1} + \tilde{A}_{n-1} \right) \sinh n\theta_0 + {}^{(3)}\mathscr{R}_n^{(3)} \right\}$$

$$e^{i\omega_1 t} \frac{Dx_s}{Dt} = \frac{\mathscr{U}_3}{\mathscr{U}_1} \frac{k_3}{2} e^{ik_3 M_3 \alpha (s_3 - y_3)} \sum_{n=0}^{\infty} J_n(\xi) \left\{ \frac{2i}{M_3} \left[1 - M_3^2 \sin^2(\chi - \delta) \right] \tilde{D}_n \right.$$

$$\left. + \cos(\chi - \delta) \sqrt{1 - M_3^2 \sin^2(\chi - \delta)} \left(\tilde{D}_{n+1} - \tilde{D}_{n-1} \right) \right\}$$

We can now substitute the expressions for p_1, u_1, p_3, u_3, v_3 into the shock relations (2), (3), (4), multiply the first equation by $2s_3M_3/sk_3$, the other two by $2/k_3$, and by equating coefficients of the Bessel functions of like order obtain the following recursion relations for the $\tilde{A}_n$, $\tilde{C}_n$, and $\tilde{D}_n$:

$$\mathscr{M}_{ij} C_j^{(n+1)} + \mathscr{N}_{ij} C_j^{(n)} + \mathscr{L}_{ij} C_j^{(n-1)} = \mathscr{R}_i^{(n)} \tag{13}$$

where

$$C_j^{(n+1)} = \begin{pmatrix} \tilde{A}_{n+1} \\ \tilde{C}_{n+1} \\ \tilde{D}_{n+1} \end{pmatrix}, \qquad C_j^{(n)} = \begin{pmatrix} \tilde{A}_n \\ \tilde{C}_n \\ \tilde{D}_n \end{pmatrix},$$

$$C_j^{(n-1)} = \begin{pmatrix} \tilde{A}_{n-1} \\ \tilde{C}_{n-1} \\ (1 + \delta_{n1}) \tilde{D}_{n-1} \end{pmatrix}, \qquad \mathscr{R}_i^{(n)} = \begin{pmatrix} \frac{2s_3 M_3}{sk_3} R_n^{(1)} \\ \frac{2}{k_3} R_n^{(2)} \\ \frac{2}{k_3} R_n^{(3)} \end{pmatrix}$$

The matrices $\mathcal{M}_{ij}$, $\mathcal{N}_{ij}$, $\mathcal{L}_{ij}$ and the vector $\mathcal{R}_n^{(1)}$ are defined in appendix C. The recursion system is entered at $n = 0$ with

$$\tilde{A}_{-1} = \tilde{C}_{-1} = \tilde{D}_{-1} = 0 = \tilde{A}_0 = \tilde{C}_0$$

and with $\tilde{D}_0$ given by equation (8).

Channel Region

The wedge-flow solution is valid up to the point where the shock wave intersects the adjacent blade. At the intersection the flow is at the angle β_3' (see fig. 3). We construct a perpendicular to the blade at this point (in the y_3-direction) and designate the region downstream of it up to the normal shock wave as the "channel region". The passage diverges slowly from its initial width $S(x_3) = s_3$ to its final value $S(x_3) = s_2$. Provided $dS(x_3)/dx_3 \ll 1$, it is appropriate to represent the mean flow as one-dimensional, i.e., $\mathcal{U}_3 = \mathcal{U}_3(x_3)$. For the unsteady flow also to be slowly varying it is necessary that the wavelength of the disturbance $\lambda \sim S(x_3)$.

The slowly varying approximation for the unsteady flow is a straight channel solution modified to account for the slowly varying channel width. The potential and stream function respectively, are

$$\Phi_3 = \sum_{n=0}^{\infty} \left[T_n^+ e^{i\int_0^{x_3} (M_3 k_3 - \lambda_n^{(3)}) dx_3} + T_n^- e^{i\int_0^{x_3} (M_3 k_3 + \lambda_n^{(3)}) dx_3} \right] \cos\left(\frac{n\pi y_3}{S}\right) + \Phi_b + \Phi_s \tag{14}$$

$$\Psi_3 = \sum_{n=1}^{\infty} B_n^{(3)} \sin\left(\frac{n\pi y_3}{S}\right) e^{i\int_0^{x_3} \omega_3 \, dx_3} \tag{15}$$

where the parameters M_3, $\omega_3 = \omega c/\mathcal{U}_3$, $k_3 \equiv \omega_3 M_3/\beta_3^2$, and

$\lambda_n^{(3)} \equiv \sqrt{k_3^2 + (n\pi/\beta_3 S)^2}$ vary slowly with x_3.

The additional potential Φ_s, appearing in equation (14), arises from the motion of the upper blade surface in following the disturbance of the oblique shock wave. In figure 5 the dashed line represents the displaced position of the model wall due to a displacement $x_s(0)$ of the oblique shock wave from its mean position. The displacement of the wall in region 3 normal to itself is

$$W_s = \frac{x_s(0)\ \sin\delta}{\sin\chi}$$

where from equation (7),

$$x_s(0) = e^{i\alpha k_3(0)M_3(0)s_3}\ \hat{D} \tag{16}$$

$$\hat{D} = \sum_{n=0}^{\infty} \tilde{D}_n J_n\left(k_3\sqrt{\alpha^2 - \beta_3^2}\ s_3\right)$$

The upwash condition on the blade,

$$V_s = -\ i\omega_1 W_s$$

is satisfied, along with the convective wave equation governing the flow (eq. (2.2), ref. 1) by

$$\Phi_s = -\ i\omega_1 W_s\ \frac{\cos[M_3(0)\omega_3(0)(s_3 - y_3)]}{\omega_3(0)M_3(0)\ \sin[M_3(0)\omega_3(0)s_3]}$$

In order to find the expansion constants $T_n^{\pm}$, $B_n^{(3)}$ in equations (14), (15) we match the latter quantities to the wedge solution (5), (6) at $x_3 = 0$. To expedite this we can, without affecting p_3, u_3, v_3, replace Φ_3 and Ψ_3 in the wedge region by

$$\tilde{\Phi}_3 \equiv e^{ik_3M_3(x_3+\alpha s_3)} \sum_{n=1}^{\infty} \tilde{A}_n \cosh n\theta\ J_n(k_3 r) + \Phi_b$$

$$- \frac{\cosh\omega_3(s_3 - y_3)}{i\ \sinh\omega_3 s_3}\ e^{i\omega_3(x_3+\alpha s_3 M_3^2/\beta_3^2)}\hat{C}$$

$$\tilde{\Psi}_3 = e^{i\omega_3(x_3+\alpha s_3M_3^2/\beta_3^2-\alpha y_3/\beta_3^2)} \sum_{n=1}^{\infty} \tilde{C}_n\ J_n\left[k_3\sqrt{\alpha^2 - \beta_3^2}\ (s_3 - y_3)\right]$$

$$- \frac{\sinh\omega_3(s_3 - y_3)}{\sinh\omega_3 s_3}\ e^{i\omega_3(x_3+\alpha s_3M_3^2/\beta_3^2)}\hat{C}$$

The vorticity, $\tilde{\Psi}^3$, contributes no normal velocity at the blade surface, a characteristic shared by equation (15).

In order to match pressures at $x_3 = 0$, it is necessary to match both Φ_3 and $\partial\Phi/\partial x_3$. Equating Φ_3 and $\tilde{\Phi}_3$ at $x_3 = 0$, multiplying by $\sin m\pi y_3/s_3$, integrating and employing orthogonality properties of the trigonometric functions yields

$$T_m^+ + T_m^- = \frac{2}{s_3(1 + \delta_{mo})} (I_{11} - I_{12} - I_{13}) \tag{17}$$

where

$$I_{11} = e^{ik_3M_3\alpha s_3} \sum_{n=1}^{\infty} \tilde{A}_n \left[\int_0^{s_3} \cosh n\theta \, J_n(k_3 r) \cos\left(\frac{m\pi y_3}{s_3}\right) dy_3 \right]_{x_3=0} \equiv e^{ik_3M_3\alpha s_3} \Delta_{n,m}$$

$$I_{12} \equiv \frac{e^{ik_3M_3\alpha s_3} \hat{C}}{i \sin \omega_3 s_3} \int_0^{s_3} \cosh \omega_3(s_3 - y_3) \cos\left(\frac{m\pi y_3}{s_3}\right) dy_3 = \frac{-i\omega_3 e^{ik_3M_3 s_3 \alpha} \hat{C}}{\omega_3^2 + (m\pi/s_3)^2}$$

$$I_{13} \equiv \int_0^{s_3} \Phi_s(y_3) \cos\left(\frac{m\pi y_3}{s_3}\right) dy_3 = \frac{-i\omega_1 W_s}{(M_3\omega_3)^2 - (m\omega/s_3)^2}$$

The integral $\Delta_{n,m}$ appearing in I_{11} is evaluated in appendix D.

Similarly, matching $\partial\Phi/\partial x_3$ and $\partial\tilde{\Phi}/\partial x_3$ yields

$$T_m^+(M_3k_3 - \lambda_m) + T_m^-(M_3k_3 + \lambda_m) = \frac{2}{is_3(1 + \delta_{mo})} (I_{21} - I_{22}) \tag{18}$$

where

$$I_{21} \equiv e^{i\alpha k_3M_3s_3} \sum_{n=1}^{\infty} \tilde{A}_n \int_0^{s_3} \left[ik_3M_3 \cosh n\theta \, J_n(k_3r) \right.$$

$$\left. + n \frac{\partial\theta}{\partial x_3} \sinh n\theta \, J_n(k_3r) + k_3 \frac{\partial r}{\partial x_3} \cosh n\theta \, J_n'(k_3r) \right]_{x_3=0} \cos\left(\frac{m\pi y_3}{s_3}\right) dy_3$$

and

$$I_{22} = i\omega_3 I_{12}$$

To evaluate I_{21} we use

$$\frac{\partial\theta}{\partial x_3} = -\frac{\sinh\theta}{r}, \quad J_n = \frac{1}{2}\left(J_{n-1} + J_{n+1}\right)$$

in the second term of the integrand, and

$$\frac{\partial r}{\partial x_3} = \cosh\theta,\ J_n' = \frac{1}{2}\left(J_{n-1} - J_{n+1}\right)$$

in the third term, and

$$\cos\frac{m\pi(s_3 - y_3)}{s_3} = (-1)^m \cos\left(\frac{m\pi y_3}{s_3}\right)$$

to obtain

$$I_{21} = \sum_{n=1}^{\infty} \tilde{A}_n \int_0^{s_3} \Big[2iM_3 \cosh n\theta\, J_n + \cosh(n-1)\theta J_{n-1} - \cosh(n+1)\theta J_{n+1}\Big]_{x_3=0} \cos\frac{m\pi(s_3-y_3)}{s_3}\, dy_3$$

Introducing a new summation index $N_1 = n - 1$ in the second term of the integrand and $N_2 = n + 1$ in the third term leads to

$$I_{21} = e^{ik_3M_3s_3\alpha}\ \frac{k_3}{2}\sum_{n=1}^{\infty}\left(2iM_3\tilde{A}_n + \tilde{A}_{n+1} - \tilde{A}_{n-1}\Delta_{n,m}\right)$$

When equations (16) and (17) are combined one finds

$$T_n^{\pm} = \frac{e^{iM_3(0)k_3(0)s_3\alpha}}{s_3(1+\delta_{n,0})}\sum_{m=0}^{\infty}\left[A_m \pm \frac{ik_3(0)}{2\lambda_n^{(3)}(0)}(A_{m+1} - A_{m-1})\right]\Delta_{m,n}$$

$$+ i\left(1 \pm \frac{k_3(0)}{M_3(0)\lambda_n^{(3)}(0)}\right)\frac{\omega_3(0)\hat{C}}{\omega_3^2(0) + (n\pi/s_3)^2}$$

$$- i\left(1 \pm \frac{M_3(0)k_3(0)}{\lambda_n^{(3)}(0)}\right)\frac{\omega_1 \sin\delta}{(n\pi/s_3)^2 - M_3^2(0)\omega_3^2(0)}\quad\frac{\hat{D}}{\sin x}$$

Equating vorticities Ψ_3 and $\tilde{\Psi}_3$ at $x_3 = 0$, multiplying by $\sin m\pi y_3/s_3 \equiv (-1)^{m+1} \sin(s_3 - y_3)m\pi/s_3$ and integrating across the channel yields

$$B_n^{(3)} \frac{s_3}{2} = (-1)^{m+1} e^{i\omega_3 \alpha s_3} \sum_{n=1}^{\infty} \tilde{C}_m \int_0^{s_3} e^{i\omega_3 \alpha y/\beta_3^2} J_n\left(k_3 \sqrt{\alpha^2 - \beta_3^2}\, y\right)$$

$$\times \sin\left(\frac{m\pi y}{s_3}\right) dy - \frac{e^{i\alpha k_3 M_3 s_3} \hat{C}}{\sinh \omega_3 s_3} (-1)^{m+1} \int_0^{s_3} \sinh \omega_3 y \sin\left(\frac{m\pi y}{s_3}\right) dy$$

$$\equiv e^{i\omega_3 \alpha s_3} \sum_{n=1}^{\infty} \tilde{C}_n \Delta_{n,m}^{(0)} - \frac{e^{i\alpha k_3 M_3 s_3}\, m\pi/s_3}{\omega_3^2 + (m\pi/s_3^2)} \hat{C}$$

or

$$B_n^{(3)} = \frac{2}{s_3}\left[e^{i\omega_3(0)\alpha s_3} \sum_{m=1}^{\infty} C_m \Delta_{m,n}^{(0)} - \frac{(n\pi/s_3)\hat{C}}{\omega_3^2(0) + (n\pi/s_3)^2} e^{iM_3(0)k_3(0)s_3\alpha}\right]$$

The integral

$$\Delta_{m,n}^{(0)} \equiv (-1)^{m+1} \int_0^{s_3} e^{i\omega_3 \alpha y/\beta_3^2} J_m\left(k_3 \sqrt{\alpha^2 - \beta_3^2}\, y\right) \sin\left(\frac{n\pi y}{s_3}\right) dy$$

is evaluated in appendix D.

The pressure obtained from the potential Φ_3 of equation (14) is, on the upper surface of the blade,

$$P(x_3,0+) = \frac{s}{s_3}\left(\sum_{n=0}^{\infty}\left\{{}^{(3)}R_n^{+}\, e^{i\int_0^{x_3}\left[M_3(x_3)k_3(x_3)-\lambda_n^{(3)}(x_3)\right]d\hat{x}_3}\right.\right.$$

$$\left. + {}^{(3)}R_n^{-}\, e^{i\int_0^{\hat{x}_3}\left[M_3(x_3)k_3(x_3)+\lambda_n^{(3)}(x_3)\right]d\hat{x}_3}\right\}$$

$$- \omega_3\omega_1\left[H_o\cos\delta + A_o(x_3 - s_3^{+} + f)\right]f_1(0;M_3\omega_3)$$

$$\left. - iA_o\left[\frac{\partial}{\partial\omega_3}\,\omega_3^2 f_1(0;M_3\omega_3) + \omega_3^2 f_2(0;M_3\omega_3,s_3^{+})\right]\frac{\omega_1}{\omega_3}\right)$$

$$+ \frac{\omega_1 sW_s}{M_3\omega_3\tan(M_3\omega_3 s_3)}$$

where

$$\hat{x}_3 \equiv x_3 - d_s$$

$${}^{(3)}R_n^{\pm} \equiv -ie^{i\int_0^{d_s}\left[M_3(x_3)k_3(x_3)\mp\lambda_n^{(3)}(x_3)\right]dx_3}\left[\frac{k_3(x_3)}{M_3(x_3)} \mp \lambda_n^{(3)}(x_3)\right]T_n^{\pm}$$

On the lower surface

$$P(x_3,0-) = e^{-i\sigma \frac{s}{s_3}}\left(\sum_{n=0}^{\infty}(-1)^n\left\{{}^{(3)}R_n^+ \, e^{i\int_0^{\hat{\hat{x}}_3}\left[M_3(x_3)k_3(x_3)-\lambda_n^{(3)}(x_3)\right]d\hat{\hat{x}}_3}\right.\right.$$

$$\left. + {}^{(3)}R_n^- \, e^{i\int_0^{\hat{\hat{x}}_3}\left[M_3(x_3)k_3(x_3)+\lambda_n^{(3)}(x_3)\right]d\hat{\hat{x}}_3}\right\}$$

$$- \omega_3\omega_1\left[H_0 \cos\delta + A_0(x_3 + f)\right] f_1(A(x_3);M_3\omega_3)$$

$$\left. - iA_0 \frac{\omega_1}{\omega_3}\left[\frac{\partial}{\partial\omega_3}\omega_3^2 f_1(A(x_3);M_3\omega_3) + \omega_3^2 f_2(A(x_3);M_3\omega_3)\right]\right)$$

$$+ \frac{e^{-i\sigma_{\omega_1} sW_s}}{M_3\omega_3 \sin(M_3\omega_3 s_3)}$$

with $\hat{\hat{x}}_3 = x_3 - d_s + s_3^+$. In calculating the lifts from these pressures we must allow for the difference in the slope of the curved blade surface in region 3 and the slope of the blade surface in region 1. On the upper surface the contribution to the lift is

$$L_{31} \equiv \int_0^{d_s} P_3(x_3,0+) \cos(\delta - \alpha_u)dx_3$$

$$\cos(\delta - \alpha_u) = \frac{\cos\delta + f_u'(x_3)\sin\delta}{\sqrt{1 + [f_u'(x_3)]^2}}$$

Defining the moment with respect to the trailing edge, we have

$$M_{31} = \int_0^{d_s} \frac{(x_3 - d_s)P_3(x_3,0+)dx_3}{\sqrt{1 + [f_u'(x_3)]^2}}$$

On the lower surface of the blade we also allow for the altered length of the channel (d_ℓ versus d_s) and obtain for the lift

$$L_{32} \equiv \int_{-s_3^+}^{d_s - s_3^+} P_3(x_3, 0-) \left\{ \frac{\cos\delta + f_p'(x_3)\sin\delta}{\sqrt{1 + [f_\ell'(x_3)]^2}} \right\} \frac{d_\ell}{d_s}\, dx_3$$

The corresponding moment about the end of the channel is

$$M_{32} = \int_{-s_3^+}^{-s_3^+ + d_s} \frac{x_3 P(x_3, 0-)\left(\frac{d_\ell}{d_s}\right)^2 dx_3}{\sqrt{1 + [f_\ell'(x_3)]^2}} + (s_3^+ - d_3) \int_{-s_3^+}^{s_3^+ + d_s} \frac{P_3(x_3, 0-)dx_3}{\sqrt{1 + [f_\ell'(x_3)]^2}} \left(\frac{d_\ell}{d_s}\right)$$

Region 2

The solution for the unsteady flow in the subsonic region that follows the normal shock wave proceeds as in reference 1 after allowing for the downstream displacement of the shock to the trailing edge of the blade and including the effects of upstream vorticity. The downstream pressure is still given by equations (G1) and (G2) of reference 1, but now the coefficients $B_n^{(2)}$ of a downstream propagating wave are determined by the equation

$$-\frac{2}{s_2}\frac{F_n}{1 + \delta_{n,o}} = B_n^{(2)} e^{i\eta^+(1 - s_2^+ - \varepsilon_o)} a_n^+ + a_n^- e^{-i\bar{\eta}_n \varepsilon_o} \sum_{m=0}^{\infty} B_m^{(2)} K_{mn}$$

rather than by equation (3.33) of reference 1. The small quantity ε_o represents the length of a nominal channel between the shock position and the end of the blade. The quantities $a_n^{\pm}$, K_{mn} remain as defined in reference 1, and F_n is defined in appendix E.

The pressure on the blade surface in region 2 is given by equations (G1) and (G2) of reference 1. The lift and moment derived from them are included in appendix E.

Shock Lifts and Moments

The unsteady displacements of the two shock waves where they impinge upon the blade surfaces contribute to the unsteady lifts and moments by shifting the boundary between adjacent regions of the flow and thereby altering the domain of influence of the mean pressures, as discussed in reference 1. The oblique shock, for example, forms the boundary between regions 1 and 3 on the top of the blade. From figure 5 it can be seen that $x_s(0)/\sin\chi$ is the penetration of region 1 into region 3, for which $(p_1^{(0)} - p_3^{(0)})x_s(0)/\sin\chi$ is a correction to the downward pressure force normal to the surface in region 1. Since the dimensionless pressure difference is

$$\left(\frac{p_3^{(0)} - p_1^{(0)}}{\rho_1 \mathscr{U}_1^2}\right) = \sin^2\chi \left[1 - \frac{\tan(\chi - \delta)}{\tan \chi}\right]$$

it follows from equation (18) that the lift due to the oblique shock is

$$\mathscr{L}_s^{(1)} = \frac{\sin \delta \, \hat{D}s}{\sin \chi \, \alpha s_3} e^{i\alpha M_3(0) k_3(0) s_3}$$

The corresponding moment is

$$\mathscr{M}_s^{(1)} = (s \cot \chi - d_0)\mathscr{L}_s^{(1)}$$

where d_0 is the value of x at which the elastic axis projects upon the surface in region 1.

The expression for the lift due to the normal shock is similar to that given in reference 1 with modifications required for the downstream displacement of the shock and its impingement on the lower surface rather than the upper:

$$\mathscr{L}_s^{(2)} = \frac{-i}{2k_3(d_s)M_3(d_s)} \left[\frac{2M_3^2(d_s) - \mu + 1}{\mu + 1} P_3(d_s - s_3^+, 0) + \frac{4}{\mu + 1} U_3(d_s - s_3^+, 0) \frac{s}{s_2} - P_2(1 - 2s_2^+, 0)\right]$$

The moment is

$$\mathscr{M}_s^{(2)} = \left[\ell_c(1 - f) \cos(\beta_2' - \chi_0) - s_2^+\right]\mathscr{L}_s^{(1)}$$

RESULTS AND DISCUSSION

A set of six blades which are examples of the two-shock model is shown in figure 6. For all blades the solidity is 1.4, the stagger angle is 62° and the entrance angle is 67°. The exit angle is 65° except in the first case for which it is 63°. The initial choices of entrance Mach number, M_1, and pressure ratios, P_{21}, were made to provide a distribution of flow conditions over the shaded region of figure 4. Since figure 4 was constructed for the simplest geometry having straight surfaces and a boat-tail trailing edge (dashed lines in fig. 6) it is necessary to recompute the pressure ratio after the choice of boundary-layer thickness and exit angle to account for the isentropic expansion of the gas in the channel and the strengthened normal shock wave. The expansion and the enhanced normal shock strength tend to counteract each other; thus the actual pressure ratios stay within 15 percent of the initial estimate and are sometimes much closer.

Each blade has been given a trailing-edge thickness to represent the displacement effect of surface boundary layers. The displacement thickness on the upper surface is denoted by $\delta_u \ell_b$ and the displacement thickness on the lower surface by $\delta_\ell \ell_b$. The values for δ_u and δ_ℓ were chosen to yield a combined thickness of about 10 percent of ℓ_b. In one case $\delta_u = \delta_\ell$ and in two cases $\delta_\ell = 0$. In the remaining three blades δ_ℓ is actually negative, thereby reducing blade thickness, but simultaneously increasing the effective stagger angle. This suggests that in some applications it may be desirable to begin the model design with an initially undervalued stagger angle and to use negative boundary-layer thickness and the exit angle to bring it up to the desired value.

Some representative pressure distributions on the blade surfaces are shown in figures 7 to 12, for blades pitching about their centers (f = 0.5). The pressures for four interblade phase angles are given in each case. On the upper surface, the pressures in the entrance region exhibit the same characteristics that occur in the normal-shock configuration of reference 1, namely, that they are relatively uniform and low in magnitude over the full length of the surface $-s^+ < \chi < s \cot \chi$ except, perhaps, for phase angles of $\pi/2$ or π, or at high frequency. The pressures on the additional surface $0 < \chi < s \cot \chi$ now included in the entrance region have no unusual characteristics. In the second supersonic region behind the oblique shock wave, however, the pressures are sharply peaked, a characteristics observed previously (ref. 1) in the subsonic region behind a normal shock wave, and now seen to be feature of the unsteady flow behind a weak shock as well. These peaks appear to be even more predominant at low frequencies than at high.

On the lower surface, as well, the unsteady pressure behind the oblique shock wave has generally several times the magnitude of the pressure in the entrance region, although it is likely to be more uniform in spatial distribution except at the high frequency. At the point on the blade surface where the curved surface of the channel begins, the pressures are usually strongly affected. There is often a sharp reversal in the magnitude of the pressure which then falls to a lower magnitude at the end of the channel, just preceding the normal shock wave.

When the disturbances are transmitted through the second, normal, shock wave there is once again apt to be an amplification of their strength, especially when the blades are out of phase ($\sigma = \pi/2$) or of opposing phase ($\sigma = \pi$). When the blades are moving in phase ($\sigma = 0$) the pressure amplitude in the subsonic region is likely to be low. In general, however, the effect of successive shock waves appears to compound, thus raising the disturbance magnitude to a high level.

The dimensionless lifts and moments in regions 2 and 3 have been derived or recorded in the Analysis section. The lift and moment in region 1 can be obtained from the pressures given in equations (D1) and (D2) of reference 1. They are defined and recorded here in appendix F. The separate lift forces when added vectorially and referred to the normal of the entrance-region surface yield for the total lift

$$L = (L_{33} + L_{32} - L_{32}) \cos \delta + L_{21} \cos(\beta_1' - \beta_2') - L_{11} + L_s^{(1)} + L_s^{(2)} \cos(\beta_1' - B_2')$$

Likewise, after each moment M_{ij} has been translated to a corresponding moment $\bar{M}_{ij}$ referred to the elastic axis, the complete moment is given by

$$M = \bar{M}_{33} + \bar{M}_{32} + \bar{M}_{21} - \bar{M}_{11} - \bar{M}_{31} + M_s^{(1)} + M_2^{(2)}$$

The total complex moment M is plotted for each of the blade models at three reduced frequencies, ω_1, in figures 13 to 18. When $\mathcal{I}m\, M$ in these figures is negative, the blade is receiving energy from the flow and flutter is the result. The interblade phase angle σ is the parameter along the curves. Black dots denote an interval of $\pi/8$ in σ.

In all cases the figures indicate that there is instability in torsion at the moderate and low frequencies but in only one case at the high frequency. The exception is blade 4 which has the largest thickness ratio of all the blades. This progression to greater instability as the frequency is decreased was also the characteristic of the cascade with one normal shock wave in reference 1. The instability is more apparent in the double shock case with flow at the intermediate frequency being decisively unstable. The increased complication of the flow in the double-shock model is reflected in the more complicated stability figure than for the single-shock flow. The number of loops and crossings has increased and the moment wanders more erratically in the complex plane.

The complex lifts are displayed in figures 19 to 24. A negative $\mathcal{I}m\, L$ means that the blade is receiving energy from the flow and there is instability in bending. Qualitatively, the trend towards instability in bending at lower frequencies is the same as in torsion. Blade 4 is seen to be the most stable of the six examples, and, again, the figures display considerably more structure than in the single-shock model.

CONCLUDING REMARKS

The model for a supersonic blade row with shock waves which has been presented here has extended the operating range of turbomachinery for which stability calculations can be made. Based on the single geometry explored here, the model is appropriate at $M_1 \geq 1.3$ at the lowest applicable stage pressure ratio and, for any pressure ratio, at higher entrance Mach numbers than the single shock model. The calculations for specific cases show that in this operating region the presence of shock waves has a strong influence on the unsteady flow and that the tendency for instability at low frequencies observed in the single-shock model of reference 1 persists in the two-shock model. Thickness ratio appears to have significant influence on stability of the flow at high frequencies.

APPENDIX A - COEFFICIENTS OF SHOCK CONDITIONS

$$I_1 = \frac{4 \sin \chi \cos \chi}{(\mu + 1) \cos(\chi - \delta)} \qquad I_2 = - \alpha_0 \tan(\chi - \delta) \cos \chi$$

$$I_3 = - \alpha_0 \cos \chi \qquad \alpha_0 = \frac{2(M_1^2 \sin^2 \chi + 1)}{(\mu + 1) M_1^2 \sin^2 \chi}$$

$$K_2 = \sin \chi \cos(\chi - \delta) \left[1 - \frac{\tan(\chi - \delta)}{\tan \chi}\right]$$

$$K_3 = - \sin \chi \sin(\chi - \delta) \left[1 - \frac{\tan(\chi - \delta)}{\tan \chi}\right]$$

$$\alpha_{11} = \frac{2M_1^2 \sin^2 \chi - \mu + 1}{\mu + 1} \qquad \alpha_{12} = \frac{4 \sin^2 \chi}{\mu + 1} \qquad \alpha_{13} = \frac{4 \sin \chi \cos \chi}{\mu + 1}$$

$$\alpha_{22} = - \alpha_0 \sin \chi \sin(\chi - \delta) + \cos \delta$$

$$\alpha_{23} = - \alpha_0 \cos \chi \sin(\chi - \delta) - \sin \delta$$

$$\alpha_{32} = - \alpha_0 \sin \chi \cos(\chi - \delta) + \sin \delta$$

$$\alpha_{33} = - \alpha_0 \cos \chi \cos(\chi - \delta) + \cos \delta$$

APPENDIX B - FUNCTIONS IN THE UPSTREAM SHOCK QUANTITIES

$$q^{\pm} = -\frac{\pm \frac{M_1\omega_1}{k_3} \sin\omega + M_3 \cos(\chi - \delta)}{\sqrt{1 - M_3^2 \sin^2(\omega - \delta)}}, \qquad t_{\pm} = q \pm \sqrt{q^2 - 1}$$

$$(1)\theta_m^{\pm} = \frac{i^m}{2}\left\{t_-^m(q_+) + t_+^m(q_+) \pm \left[t_-^m(q_-) + t_+^m(q_-)\right]\right\} \frac{1}{1 + \delta_{mo}}$$

$$(1)\tilde{\theta}^{\pm} = \frac{i^m}{2(1 + \delta_{mo})}\left\{e^{iM_1\omega_1 s}\left[t_-^m(q_+) + t_+^m(q_+)\right] \pm e^{-iM_1\omega_1 s}\left[t_-^m(q_-) + t_+^m(q_-)\right]\right\}$$

$$(1)\Psi_m^{\pm} = \frac{\cos\chi\, m i^{m-1}}{2k_3\sqrt{1 - M_3^2 \sin^2(\chi - \delta)}}\left[\frac{t_-^m(q_+) - t_+^m(q_+)}{\sqrt{q_+^2 - 1}} \pm \frac{t_-^m(q_-) - t_+^m(q_-)}{\sqrt{q_-^2 - 1}}\right]$$

$$(1)\tilde{\Psi}_m^{\pm} = \frac{\cos\chi\, m i^{m-1}}{2k_3\sqrt{1 - M_3^2 \sin^2(\omega - \delta)}}\left\{e^{iM_1\omega_1 s}\left[\frac{t_-^m(q_+) - t_+^m(q_+)}{\sqrt{q_+^2 - 1}}\right] \pm e^{-iM_1\omega_1 s}\left[\frac{t_-^m(q_-) - t_+^m(q_-)}{\sqrt{q_-^2 - 1}}\right]\right\}$$

$$f_1(y;M_1\omega_1) = e^{i\alpha k_3 M_3(s_3 - y_3)}\sum_{m=0}^{\infty}\frac{e^{i\sigma\,(1)\tilde{\theta}_m^{+}} - \theta_m^{(1)}}{\omega_1 M_1 \sin(M_1\omega_1 s)} J_m(\xi)$$

$$xf_1(y;M_1\omega_1) = e^{i\alpha k_3 M_3(s_3 - y_3)}\sum_{m=1}^{\infty}\frac{e^{i\sigma\,(1)\tilde{\Psi}_m^{+}} - (1)\Psi_m^{+}}{\omega_1 M_1 \sin(M_1\omega_1 s)} J_m(\xi)$$

$$f_1'(y;M_1\omega_1) = -e^{i\alpha k_3 M_3(s_3-y_3)} \sum_{m=0}^{\infty} \frac{e^{i\sigma\ (1)\tilde{\Theta}_m^-} + {}^{(1)}\Theta_m^-}{i\ \sin(M_1\omega_1 s)}\ J_m(\xi)$$

$$f_2(y;M_1\omega_1) = e^{i\alpha k_3 M_3(s_3-y_3)} \sum_{m=0}^{\infty} \frac{is^+ e^{i\sigma\ (1)\tilde{\Theta}_m^+}}{M_1\omega_1\ \sin(M_1\omega_1 s)}\ J_m(\xi)$$

$$f_2'(y;M_1\omega_1) = -e^{i\alpha k_3 M_3(s_3-y_3)} \sum_{m=0}^{\infty} \frac{s^+ e^{i\sigma\ (1)\tilde{\Theta}_m}}{\sin(M_1\omega_1 s)}\ J_m(\xi)$$

$$xf_1'(y;M_1\omega_1) = -e^{i\alpha k_3 M_3(s_3-y_3)} \sum_{m=0}^{\infty} \frac{e^{i\sigma\ (1)\tilde{\Psi}_m^-} - {}^{(1)}\Psi_m^-}{i\ \sin(M\omega_1 s_1)}\ J_m(\xi)$$

$$\frac{\partial}{\partial\omega_1}\left[\omega_1^2 f_1(y;M_1\omega_1) + \omega_1^2 f_2(y;M_1\omega_1)\right]$$

$$= e^{i\alpha k_3 M_3(s_3-y_3)} \sum_{m=0}^{\infty} \left\{ \left(e^{i\sigma\ (1)\tilde{\Theta}_m^-} - {}^{(1)}\Theta_m^+ \right) \frac{\partial}{\partial\omega_1} \left[\frac{\omega_1^2}{M_1\omega_1\ \sin(M_1\omega_1 s)} \right] \right.$$

$$+ \frac{\omega_1\ \tan x}{i\ \sin(M_1\omega_1 s)} \left[e^{i\sigma\ (1)\tilde{\Psi}_m^-} - {}^{(1)}\Psi_m^- \right]$$

$$\left. + \frac{e^{i\sigma}\left[i\omega_1 s^+\ {}^{(1)}\tilde{\Theta}_m^+ - \omega_1 M_1 s\ {}^{(1)}\tilde{\Theta}_m^- \right]}{M_1\ \sin(M_1\omega_1 s)} \right\} J_m(\xi)$$

$$\xi \equiv k_3\sqrt{\alpha^2 - \beta_3^2}\ \ (s_3 - y_3)$$

APPENDIX C - MATRICES OF THE RECURSION RELATIONS

$$\Lambda_1 = \frac{4 \cos\chi \tan(\chi - \delta)}{\mu + 1} \qquad \Lambda_2 = \frac{2\,(M_1^2 \sin^2\chi + 1)\cos\chi}{(\mu + 1)\tilde{n}_3 M_1^2 \sin^2\chi} \qquad \alpha = \cot(\chi - \delta)$$

$$\Lambda_3 = \frac{2(M_1^2 \sin^2\chi - 1)}{(\mu + 1)M_1^2 \sin\chi} \qquad \tilde{n}_3 = M_3 \cos(\chi - \delta) \qquad \tilde{m}_3 = M_3 \sin(\chi - \delta)$$

$$\mathscr{M} = \begin{pmatrix} -M_3 \cosh n\theta_o & 0 & \tilde{n}_3 \sqrt{1 - \tilde{m}_3^2}\,\Lambda_1 \\ \cosh n\theta_o & -\sqrt{\alpha^2 - \beta_3^2} & -\tilde{n}_3 \sqrt{1 - \tilde{m}_3^2}\,(\tilde{m}_3\Lambda_2 + \Lambda_3)/M_3 \\ -\beta_3 \sinh n\theta_o & 0 & -\sqrt{1 - \tilde{m}_3^2}\,(\tilde{n}_3^2\Lambda_2 - \tilde{m}_3\Lambda_3)/M_3 \end{pmatrix}$$

$$\mathscr{N} = \begin{pmatrix} -2i \cosh n\theta_o & 0 & 2i(1 - \tilde{m}_3^2)\Lambda_1 \\ 2iM_3 \cosh n\theta_o & -2i\alpha/M_3 & -2i\left[(1 - \tilde{m}_3^2)\tilde{m}_3\Lambda_2 + \tilde{n}_3\Lambda_3\right]/M_3 \\ 0 & -2i\beta_3^2/M_3 & -2i\tilde{n}_3\left[(1 - \tilde{m}_3^2)\Lambda_2 - \tilde{m}_3\Lambda_3\right] \end{pmatrix}$$

$$\mathscr{L} = \begin{pmatrix} -M_3 \cosh n\theta_o & 0 & -\tilde{n}_3 \sqrt{1 - \tilde{m}_3^2}\,\Lambda_1 \\ -\cosh n\theta_o & -\sqrt{\alpha^2 - \beta_3^2} & \tilde{n}_3 \sqrt{1 - \tilde{m}_3^2}\,(\tilde{m}_3\Lambda_2 + \Lambda_3) \\ -\beta_3 \sinh n\theta_o & 0 & \sqrt{1 - \tilde{m}_3^2}\,(\tilde{n}_3^2\Lambda_2 - \tilde{m}_3\Lambda_3) \end{pmatrix}$$

$$R_n^{(i)} = \sum_{J=1}^{3} \alpha_{ij}\, {}^{(1)}\mathscr{R}_n^{(j)} - {}^{(3)}\mathscr{R}_n^{(i)} \qquad i = 1, 2, 3$$

$${}^{(\ell)}\mathscr{R}_n^{(1)} = \left\{ {}^{(\ell)}\mathscr{L}_n^{(1)} - g_\ell\, {}^{(\ell)}\hat{\tilde{\Theta}}_n^{\pm}/M_\ell - \frac{A_o\omega_1}{M_\ell \sin(M_\ell\omega_\ell s_\ell)} \left[\left(\hat{\Psi}_n^{+} + M_\ell \tan\chi_\ell\, {}^{(\ell)}\hat{\Psi}_n \right) - e^{i\sigma} \left(s_\ell^{+}\, {}^{(\ell)}\tilde{\Theta}_n^{+} + M_\ell s_\ell\, {}^{(\ell)}\tilde{\Theta}_n^{-} \right) \right] \right\} \frac{\sin\chi}{\sin\chi_\ell}$$

$$ {}^{(\ell)}\mathscr{R}_n^{(2)} = {}^{(\ell)}\mathscr{L}_n^{(2)} + \frac{iA_0\omega_1 \, {}^{(\ell)}\tilde{\Theta}_n^{+}}{M_\ell\omega_\ell \sin(M_\ell\omega_\ell s_\ell)} $$

$$ {}^{(\ell)}\mathscr{R}_n^{(3)} = {}^{(\ell)}\mathscr{L}_n^{(3)} - g_\ell \, {}^{(\ell)}\hat{\Theta}_n - \frac{A_0\omega_1}{\sin(M_\ell\omega_\ell s_\ell)} \left[M_\ell \tan \chi_\ell \, {}^{(\ell)}\hat{\Psi}_n^{+} + {}^{(\ell)}\hat{\Psi}_n^{-} - e^{i\sigma} \left(s_\ell^{+} \, {}^{(\ell)}\tilde{\Theta}_n^{-} + s_\ell M_\ell \, {}^{(\ell)}\tilde{\Theta}_n^{+} \right) \right] $$

$$ {}^{(3)}\mathscr{L}_n^{(j)} \equiv 0 $$

$$ g_\ell = \frac{\omega_1}{\omega_\ell \sin(M_\ell\omega_\ell s_\ell)} \left[\omega_\ell \hat{H}_\ell + iA_0 \left(1 - \frac{M_\ell\omega_\ell s_\ell}{\sin(M_\ell\omega_\ell s_\ell)} \right) \right] $$

$$ \hat{H}_\ell = (H_0 - A_0 d_0) \cos(x - x_\ell) - A_0 s \sin(x - x_\ell) $$

$$ {}^{(\ell)}\Psi_n^{\pm} = \frac{i^{n-1} n \cos \chi_\ell}{\sqrt{2k_3 \; 1 - \tilde{m}_3^2}} \left\{ \left[e^{i(M_\ell\omega_\ell s_\ell + \sigma)} - 1 \right] \left[\frac{t_-^n(q_\ell^+) - t_+^n(q_\ell^+)}{\sqrt{(q_\ell^+)^2 - 1}} \right] \pm \left[e^{i(\sigma - M_\ell\omega_\ell s_\ell)} - 1 \right] \left[\frac{t_-^n(q_\ell^-) - t_+^n(q_\ell^-)}{\sqrt{(q_\ell^-)^2 - 1}} \right] \right\} $$

$$ {}^{(\ell)}\hat{\Theta}_n^{\pm} = \frac{i^n}{2(1 + \delta_{no})} \left\{ \left[e^{i(\sigma + M_\ell\omega_\ell s_\ell)} - 1 \right] \left[t_-^n(q_\ell^+) + t_+^n(q_\ell^+) \right] \pm \left[e^{i(\sigma - M_\ell\omega_\ell s_\ell)} - 1 \right] \left[t_-^n(q_\ell^-) + t_+^n(q_\ell^-) \right] \right\} $$

$$ {}^{(1)}\mathscr{S}_n^{(j)} = \begin{cases} \sum_{m=0}^{[n/2]} {}^{'}\mathscr{A}_{n-2m}^{(j)} \left[\frac{n(n - m - 1)!}{m!} \right], & n \neq 0 \\ {}^{'}\mathscr{A}_0^{(j)}, & n \neq 0 \end{cases} $$

$$q_{\ell}^{\pm} = -\left[M_3 \cos(\chi - \delta) \pm \frac{M_{\ell}\omega_{\ell}}{k_3} \sin \chi_{\ell}\right] \Big/ \sqrt{1 - M_3^2 \sin^2(\chi - \delta)}$$

$$\chi_1 = \chi, \qquad \chi_3 = \chi - \delta$$

$$\ell = 1, 3$$

APPENDIX D - INTEGRALS ARISING IN THE MATCHING PROCESS

In the integration across the blade passage at $x_3 = 0$ there arise integrals of the type

$$\Delta^{\pm}_{m,n} \equiv (-1)^n \int_0^{s_3} J_m(k_3(0)r_o)\, e^{\pm m\theta_o} \cos\left(\frac{n\pi y}{s_3}\right) dy$$

where

$$y = s_3 - y_3,\quad r_o^2 = (\alpha s_3)^2 - (\beta_3(0)y)^2,\quad \theta_o = \frac{1}{2}\ln\left[\frac{\alpha s_3 + \beta_3(0)y}{\alpha s_3 - \beta_3(0)y}\right]$$

Letting

$$\eta \equiv \frac{y}{s_3} = 1 - \frac{y_3}{s_3},\quad b \equiv \alpha k_3(0)s_3,\quad P = \beta_3(0)k_3(0)s_3$$

puts these integrals in the form

$$\frac{\Delta^{\pm}_{m,n}}{s_3} = (-1)^n \int_0^1 J_m\left(\sqrt{b^2 - p^2\eta^2}\right)\left(\frac{b^2 + p^2\eta^2}{b^2 - p^2\eta^2}\right)^{m/2} \cos n\pi\eta\, d\eta$$

In succession one expands the Bessel function in its power series, translates to a new coordinate $\bar{\eta} = \eta \pm \lambda$ and converts factors $(\bar{\eta} \mp 2\lambda)^k$ to their binomial expansion ($\lambda \equiv b/p$). Then one has integrals of a standard type

$$\int_{\pm\lambda}^{1\pm\lambda} \bar{\eta}^{m+\ell} e^{in\pi\bar{\eta}}\, d\bar{\eta}$$

It follows that

$$\Delta^{\pm}_{mn} = \frac{\pm 1}{n\pi} \sum_{k=0}^{\infty} \frac{(b/2)^{2k+m}}{(m+k)!} \sum_{j=0}^{k} \frac{(-2)^j (m + 2k - j)!}{(k-j)!\, j!}$$

$$\times \sum_{r=0}^{\left[k + \frac{(m-j-1)}{2}\right]} \frac{(-1)^r\left[(1 \pm \mu)^{m+2k-j-2r-1} - (-1)^n\right]}{(m + 2k - j - 2r - 1)!}\left(\frac{\mu}{n\pi}\right)^{2r+1}, \qquad \mu \equiv \frac{1}{\lambda}$$

The end quantity desired is

$$\frac{\Delta_{m,n}}{s_3} \equiv \frac{(\Delta^{+}_{m,n} + \Delta^{-}_{m,n})}{2s_3} = \sum_{k=0}^{\infty} \frac{(b/2)^{2k+m}}{(m+k)!} \sum_{j=0}^{k} \frac{(-2)^j}{(k-j)!\, j!}\, \tilde{\Gamma}_{m+2k-j}$$

$$\tilde{\Gamma}_{m+2k-j} \equiv \sum_{r=0}^{\left[\frac{m+2k-j-1}{2}\right]} \frac{(-1)^r (m+2k-j)!\, (\mu/n\pi)^{2r+1}}{(m+2k-j-2r-1)!}$$

$$\times \left[(1+\mu)^{m+2k-j-2r-1} - (1-\mu)^{m+2k-j-2r-1} \right]$$

To put $\Delta_{m,n}$ in a form convenient for calculations we first introduce a new summation index $\ell = k - j$ and sum over all nonnegative values of both ℓ and j. In the ℓ,j matrix we construct a final index $k = 2\ell + j$ which sums over all nonnegative values with $0 \le \ell \le [k/2]$. Then

$$\Delta_{m,n} = \frac{s_3}{2n\pi} \sum_{j=0}^{\infty} \left[\Gamma^{(n)}_{m+j}(\mu) + \Gamma^{(n)}_{m+j}(-\mu) \right] \Lambda^{(m)}_{j}(b)$$

$$\Gamma^{(n)}_{k}(\mu) = \sum_{r=0}^{\left[\frac{k-1}{2}\right]} \frac{k!\, (-1)^r}{(k-2r-1)!} \left(\frac{\mu}{n\pi}\right)^{2r+1} (1+\mu)^{k-2r-1}$$

$$\Lambda^{(m)}_{j}(b) = \sum_{k=0}^{[j/2]} \frac{(b/2)^{m+2j-2k}\; 2^{j-2k}}{(m+j-k)!\, k!\, (j-2k)!}$$

For the case $n = 0$,

$$\frac{\Gamma_k(\pm\mu, n\pi)}{n\pi} = \frac{(1 \pm \mu)^{k+1}}{\pm \mu(k+1)}$$

Another quantity arising from the integration across the blade passage is

$$\Delta_{m,n}^{(0)} = -(-1)^n \int_0^{s_3} e^{i\omega_3(0)\alpha y/\beta_3^2(0)} J_m\left[k_3(0)\sqrt{\alpha^2 - \beta_3^2(0)}\, y\right] \sin\left(\frac{n\pi y}{s_3}\right) dy$$

$$= \frac{-s_3(-1)^n i^m}{2} \sum_{k=0}^{\infty} \frac{1}{k!\,(k+m)!} \left(\frac{\rho}{2}\right)^{2k+m}$$

$$\times \left[\frac{\gamma\left(2k+m+1, \frac{a+n\pi}{i}\right)}{(a+n\pi)^{2k+m+1}} - \frac{\gamma\left(2k+m+1, \frac{a-n\pi}{i}\right)}{(a-n\pi)^{2k+m+1}}\right]$$

$$a = \frac{\alpha k_3(0) s_3}{M_3(0)}, \qquad \rho = k_3(0) s_3 \sqrt{\alpha^2 - \beta_3^2(0)},$$

$$\beta_3^2 = M_3^2 - 1, \qquad \alpha = \cot(\chi - \delta)$$

γ is the incomplete gamma function.

APPENDIX E - EFFECTS OF UPSTREAM VORTICITY AND CHANGED SHOCK LOCATION ON SOLUTION IN SUBSONIC REGION

Equation (3.33) of reference 1 must be modified to account for the presence of vorticity upstream of the normal shock wave and for the altered position of the shock wave.

If vorticity ψ_1 is present, it affects the derivation of the shock condition (A2) (or (2.18)) as given in appendix A of reference 1. The expressions for v_1 and $\partial\phi_1/\partial t$ must be augmented to read

$$v_1 = \frac{\partial\phi_1}{\partial y} - \frac{\partial\psi_1}{\partial x}, \qquad \frac{\partial\phi_1}{\partial t} = -p'_1 - u_1 + \frac{\partial\psi_1}{\partial y}$$

corresponding to the expressions in region 2,

$$v_2 = \frac{\partial\phi_2}{\partial y} - \frac{\partial\psi_2}{\partial x}, \quad \frac{\partial\phi_2}{\partial t} = -\left(\frac{\mathscr{U}_2}{\mathscr{U}_1}\right)\left(p'_2 + u_2 - \frac{\partial\psi_2}{\partial y}\right)$$

From these one can form $\partial(v_2 - v_1)/\partial t$, employ $D_\psi/Dt = 0$ on both sides of the shock wave, and set the expression equal to the time derivative of equation (A1c) to obtain.

$$\frac{\partial}{\partial y}\left[\frac{\mathscr{U}_2}{\mathscr{U}_1}\left(p'_2 + u_2 - \frac{\partial x_s}{\partial t}\right) + p'_1 + u_1 - \frac{\partial x_s}{\partial t}\right] = \frac{\mathscr{U}_2}{\mathscr{U}_1}\left(\frac{\partial^2\psi_2}{\partial y^2} - \frac{\mathscr{U}_1^2}{\mathscr{U}_2^2}\frac{\partial^2\psi_2}{\partial t^2}\right) - \left(\frac{\partial^2\psi_1}{\partial y^2} + \frac{\partial^2\psi_1}{\partial t^2}\right)$$

When (A1a) and (A1b) are introduced, the augmented version of equation (A2) is found:

$$\frac{\partial}{\partial y}\left[p'_2 - \left(M_1^2 + \frac{\mu - 1}{\mu + 1}\beta_1^2\right)p'_1\right] = -(\mu + 1)\left(\frac{M_1 M_2}{\beta_1\beta_2}\right)^2\left(\frac{\partial^2\psi_2}{\partial y^2} + \frac{\mathscr{U}_1^2}{\mathscr{U}_2^2}\frac{\partial^2\psi_2}{\partial t^2}\right)$$

$$+ (\mu + 1)\frac{M_1^4}{\beta_1^4}\left(\frac{\partial^2\psi_1}{\partial y^2} + \frac{\partial^2\psi_1}{\partial t^2}\right) \qquad \text{(E1)}$$

When the time differentiations are carried out and the time factor is cancelled, we have an equation corresponding to equation (2.18) of reference 1,

$$\frac{\partial}{\partial y}\left[P_2 - \left(M_1^2 + \frac{\mu - 1}{\mu + 1}\beta_1^2\right)P_1\right]$$

$$= (\mu + 1)\left(\frac{M_1 M_2}{\beta_1\beta_2}\right)^2\left(\frac{\partial^2\Psi_2}{\partial y^2} - \omega_2^2\Psi_2\right) + (\mu + 1)\left(\frac{M_1}{\beta_1}\right)^4\left(\frac{\partial^2\Psi_1}{\partial y^2} - \omega_1^2\Psi_1\right) \qquad \text{(E2)}$$

Again in the companion shock relations (eq. (2.17) of ref. 1) we allow for the occurrence of upstream vorticity and write

$$\frac{\partial \Phi_2}{\partial x} + \frac{\partial \Psi_2}{\partial y} = - \frac{M_1^2 + 1}{2M_1^2} P_2 + \frac{\partial \Phi_1}{\partial x} + \frac{\partial \Psi_1}{\partial y} + \frac{1}{2} \left[M_1^2 + 1 - \frac{\beta_1^4}{M_1^2} \left(\frac{\mu - 1}{\mu + 1} \right) P_1 \right] \quad \text{(E3)}$$

If Ψ_2 is eliminated between (E2) and (E3) by differentiating (E2) with respect to y and obtaining the first and third y derivatives of Ψ_2 from (E3), the extra term in Ψ_1 in the combined equation is

$$- (\mu + 1) \frac{M_1^2}{\beta_1^2} \left[\left(\frac{M_2^2}{\beta_2^2} - \frac{M_1^2}{\beta_1^2} \right) \frac{\partial^3 \Psi_1}{\partial y^3} - \left(\omega_2^2 \frac{M_2^2}{\beta_2^2} - \frac{M_1^2}{\beta_1^2} \omega_1^2 \right) \frac{\partial \Psi_1}{\partial y} \right]$$

Using the definition

$$k_1 = \frac{\omega_1 M_1}{\beta_1^2}$$

and the relations

$$\omega_2 = \omega_1 \frac{\mathscr{U}_1}{\mathscr{U}_2}$$

$$\frac{\mathscr{U}_1}{\mathscr{U}_2} = \frac{(\mu + 1) M_1^2}{\left[(\mu + 1) M_1^2 - 2\beta_1^2 \right]} \equiv \left(\frac{\beta_2 M_1}{\beta_1 M_2} \right)^2$$

we find the vorticity term to be

$$-(\mu + 1) \left(\frac{M_1 \beta_2}{\beta_1} \right)^2 \left(\frac{M_2^2}{\beta_2^2} - \frac{M_1^2}{\beta_1^2} \right) \left[\frac{1}{\beta_2^2} \frac{\partial^3 \Psi_1}{\partial y^3} + \left(\frac{\beta_1 k_1}{M_2} \right)^2 \frac{\partial \Psi_1}{\partial y} \right]$$

In reference 1 the region before the normal shock wave was region 1; here it is region 3, and we substitute for Ψ_1 the expression in equation (15) for Ψ_3, evaluated at $x_3 = d_s$:

$$\Psi_3(d_s, y_3) = \sum_{n=1}^{\infty} B_n^{(3)} \sin \frac{n\pi y_3}{s_2} e^{i \int_0^{d_s} \omega_3 dx_3}$$

Substituting $M_3(d_s)$ for M_1 everywhere in the shock condition and introducing the shock position $x = 1 - s_2^+ - \epsilon_0$ into the expressions for the potentials where they appear in the shock relation, we find the condition on the coefficients $B_n^{(2)}$ of the duct waves in the subsonic region,

$$-\frac{2}{s_2}\frac{F_n}{1+\delta_{no}} = B_n^{(2)} e^{i\eta^+(1-s_2^+-\varepsilon_o)} a_n^+ + a_n^- e^{-i\eta_n^-\varepsilon_o} \sum_{m=0}^{\infty} B_m^{(2)} K_{mn} \qquad \text{(E4)}$$

$$a_n^{\pm} \equiv \left[\lambda_n^{(2)}\right]^2 \pm 2M_2 k_2 \lambda_n^{(2)} + \left(\frac{k_2}{M_3}\right)^2$$

The inhomogeneous term F_n has the additional term

$$n\pi(1+\delta_{no})B_n^{(3)} e^{i\int_0^{d_s}\omega_3 dx_3}\left[\frac{M_2^2}{\beta_2^2} - \frac{M_3^2(d_s)}{\beta_3^2(d_s)}\right]\left[-\left(\frac{n\pi}{\beta_2 s_2}\right)^2 + \left(\frac{k_3(d_s)\beta_3(d_s)}{M_2}\right)^2\right]$$

Equation (E4) replaces equation (3.33) of reference 1. In it ε_o is the length of a nominal duct ahead of the trailing edge in which the flow is subsonic. In the calculations made for this report ε_o has been set to 0.01.

$$F_n = \frac{(1+\delta_{no})s_2}{2} a_n^- H_n e^{-i\eta_n^-\varepsilon_o} - \frac{(2M_2^2-\beta_2^2)}{\beta_2^4}\left(\frac{n^2\pi^2}{s_2^2} + M_2^2\omega_2^2 r_2\right)\omega_1 e_n^{(2)}$$

$$-\left[\frac{2M_3^2(d_s)M_2^2 - \beta_3^2(d_s)}{\beta_2^4}\right]\left(\frac{n^2\pi^2}{s_2^2} + M_2^2\omega_2^2 r_1\right)$$

$$\times\left\{\frac{(1+\delta_{no})s_2}{2}\left[{}^{(3)}R_n^+ + {}^{(3)}R_n^-\right] - \omega_1 e_n^{(3)}\right\}$$

$$-\frac{2M_2^2}{\beta_2^4}\left(\frac{n^2\pi^2}{s_2^2} + \omega_2^2\right)\left\{\frac{(1+\delta_{no})s_2}{2}\left[{}^{(3)}Q_n^+ + {}^{(3)}Q_n^-\right] - \omega_1 iA_o\left[c_n^{(2)} - c_n^{(3)}\right]\right\}$$

$$-n\pi(1+\delta_{no})\, e^{i\int_0^{d_s}\omega_3 dx_3} B_n^{(3)}\left[\frac{M_2^2}{\beta_2^2} - \frac{M_3^2(d_s)}{\beta_3^2(d_s)}\right]\left\{\left(\frac{n\pi}{S_2\beta_2}\right)^2 + \left[\frac{k_3(d_s)\beta_3(d_s)}{M_2}\right]^2\right\}$$

$$r_1 = \frac{M_3^2(d_s) + 1 - \left[\beta_3^4(d_s)/M_3^2(d_s)\right](\mu-1)/(\mu+1)}{2M_3^2(d_s)M_2^2 - \beta_3^2(d_s)}$$

$$r_2 = \frac{M_3^2(d_s) + 1}{2\,M_3^2(d_s)M_2^2 - M_3^2(d_s)\beta_2^2}$$

$$e_n^{(j)} = iA_o \frac{2(n^2\pi^2/s_2^2)c_n^{(j)} - i\omega_j s_2 + e^{i(\sigma+n\pi)}}{n^2\pi^2/s_2^2 - M_j^2\omega_j^2} + \omega_j \hat{H}_o c_n^{(j)}$$

$$c_n^{(j)} = \frac{1 - e^{i(\sigma+n\pi)}}{n^2\pi^2/s_2^2 - M_j^2\omega_j^2}, \qquad \hat{H}_o = H_o \cos\delta + A_o(1 - f)$$

$$e_n^{(3)} = e_n^{(3)} + \omega_3(0)\left[\frac{\sin\delta}{\sin\chi}\ \hat{D}e^{i\alpha k_3(0)M_3(0)s}\right] \Bigg/ \left[n^2\pi^2/s^2 - M_3^2(0)\omega_3^2(0)\right]$$

$$(3)R_n^{\pm} = e^{i\int_0^{d_s}\left[M_3k_3 \mp \lambda_n^{(3)}\right]dx_3}\,(-i)\left[\frac{k_3(d_s)}{M_3(d_s)} \mp \lambda_n^{(3)}(d_s)\right]T_n^{\pm}$$

$$(3)Q_n^{\pm} = ie^{i\int_0^{d_s}\left[M_3k_3 \mp \lambda_n^{(3)}dx_3\right]}\left[M_3(d_s)k_3(d_s) \mp \lambda_n^{(3)}\right]T_n^{\pm}$$

$$L_{21} \equiv \int_{1-2s_2^+}^{1-s_2^+} P_2\,dx, \qquad M_{21} \equiv \int_{1-2s_2^+}^{1-s_2^+} xP_2\,dx$$

$$L_{21} = \frac{s}{s_2}\sum_{n=0}^{\infty}\Bigg\{\frac{1 - e^{-i\eta_n^- s_2^+}\ \sum_{m=0}^{\infty} B_m^{(2)} K_m}{\left[e^{i(\sigma-\eta_n^- s_2^+ + n\pi)} - 1\right] i\eta_n^-}$$

$$+ B_n^{(2)}\ \left[\frac{e^{i\eta_n^+(1-s_2^+)}\left(1 - e^{-i\eta_n^+ s_2^+}\right)}{i\eta_n^+\left[e^{-i(\eta_n^+ s_2^+ - \sigma + n\pi)} - 1\right]} + \frac{e^{i(\eta_n^+ - \sigma - n\pi)} - e^{i\eta_n^+(1-s_2^+)}}{2e^{i\sigma}}\right.$$

$$\left.\times \sum_{m=-\infty}^{\infty} K_m(\lambda_n)\ \frac{\left[1 - e^{-i(\alpha_m^- + M_2 k_2)s_2^+}\right]}{i(\alpha\bar{m} + M_2 k_2)}\right]\Bigg\} + e^{-i\sigma}\sum_{m=0}^{\infty} K_m^+(M_2 k_2)$$

$$\times \frac{\left[1 - e^{-i(\alpha_m^- + M_2 k_2)s_2^+}\right]}{i(\alpha_m^- + M_2 k_2)}\ \left[D_+^{(2)} + \frac{i\omega_1 A_o}{\alpha_m^- + M_2 k_2}\right]$$

$$+ \sum_{n=0}^{\infty} \frac{H_n\left(1 - e^{-i\eta_n^- s_2^+}\right)}{i\eta_n^-\left[e^{i(\sigma-\eta_n^- s_2^+ + n\pi)} - 1\right]} - \omega_1 s_2^+\Bigg\{\left[\tilde{H}_o + A_o\left(1 - \frac{3}{2}\, s_2^+\right)\right]$$

$$\times \frac{\cot(M_2\omega_2 s_2)}{M_2} + iA_o\left[\frac{\cot(M_2\omega_2 s_2)}{M_2\omega_2} - \frac{s_2}{\sin^2(M_2\omega_2 s_2)}\right]\Bigg\}$$

$$\tilde{H}_o = H_o \cos(\beta_1' - \beta_2') - A_o d_{o,2}$$

$$M_{21} = \frac{s}{s_2}\left\{\sum_{n=0}^{\infty}\left\{\frac{\sum_{m=0}^{\infty} B_m^{(2)} K_m e^{i\bar{\eta}_n(1-s_2^+)}}{\left[e^{i(\sigma-\eta_n^- s_2^+ + n\pi)} - 1\right] i\eta_n^-}\left[(1 - s_2^+ + i/\eta_n^-)\left(1 - e^{-i\eta_n^+ s_2^+}\right)\right.\right.\right.$$

$$\left. + s_2^+ e^{-i\eta_n^+ s_2^+}\right] + B_n^{(2)}\left[\frac{e^{-i\eta_n^+(1-s_2^+)}}{(\eta_n^+)^2}\left[\left[i\eta_n^+(1 - s_2^+) - 1\right]\left(1 - e^{-i\eta_n^+ s_2^+}\right)\right.\right.$$

$$\left.\left. + i\eta_n^+ s_2^+ e^{-i\eta_n^+ s_2^+}\right] + \frac{e^{i(\eta_n^+ - \sigma - n\pi)} - e^{i\eta_n^+(1-s_2^+)}}{2e^{i\sigma}}\sum_{m=-\infty}^{\infty} K_m(\lambda_n)\right.$$

$$\left.\times \frac{\left[i(\alpha_m^- + M_2k_2)s_2^+\right] + \left[1 + i(\alpha_m^- + M_2k_2)(1 - s_2^+)\right]\left[e^{-i(\alpha_m^- + M_2k_2)s_2^+} - 1\right]}{(\alpha_m^- + M_2k_2)^2}\right]\right\}$$

$$+ e^{-i\sigma}\sum_{m=0}^{\infty} K_m^+(M_2k_2)\left\{\frac{\left[1 + i(\alpha_m^- + M_2k_2)(1 - s_2^+)\right]\left[e^{-i(\alpha_m^- + M_2k_2)s_2^+} - 1\right]}{(\alpha_m^- + M_2k_2)^2}\right.$$

$$\left. + \frac{is_2^+}{(\alpha_m^- + M_2k_2)}\right\}\left(D_+^{(2)} + \frac{i\omega_1 A_o}{\alpha_m^- + M_2k_2}\right)$$

$$+ \sum_{n=0}^{\infty}\frac{H_n\left\{\left[1 - i\eta_n^-(1 - s_2^+)\right]\left(1 - e^{-i\eta_n^- s_2^+}\right) - i\eta_n^- s_2^+ e^{-i\eta_n^- s_2^+}\right\}}{\left[e^{i(\sigma-\eta_n^- s_2^+ + n\pi)} - 1\right](\eta_n^-)^2}$$

$$- \omega_1\frac{\cot\left(M_2\omega_2 S_2\right)}{M_2\omega_2}\left\{\left(2iA_o + \omega_2\tilde{H}_o\right)s_2^+(1 - \tfrac{3}{2}s_2^+) + A_o\omega_2 s_2^+\left[1 - 3s_2^+ + \tfrac{1}{3}(s_2^+)^2\right]\right\}$$

$$\left. - i\omega_1 A_o\omega_2\frac{\partial}{\partial\omega_2}\left[\frac{\cot M_2\omega_2 s_2}{M_2\omega_2}\right]s_2^+\left(1 - \tfrac{3}{2}s_2^+\right)\right\}$$

There is a factor s/s_2 appearing in L_{21} and M_{21} which arises from the normalization of the pressure in region 2 and which merits explanation. Because time, velocities and pressure are nondimensionalized with respect to the chord, the density ρ, and velocity $\mathcal{U}_1$, whereas the material derivative in region 2 introduces the velocity $\mathcal{U}_2$, the ratio of mass fluxes $\rho_2\mathcal{U}_2/\rho_1\mathcal{U}_2$ appears in the nondimensionalization of the momentum equation. Where the blade passage is of constant width, as is the case in reference 1, the ratio is unity; but when the blade passage varies in width, as it does here, the ratio is just the reciprocal of the channel widths, s/s_2. This explains the appearance of the latter ratio in the lift and moment as well as the appearance of s/s_3 in equation (9).

APPENDIX F - LIFT AND MOMENT IN REGION 1

$$L_{11} \equiv \int_{-s^+}^{s \cot \chi} P_1 dx$$

$$= - s(\beta_1 + \cot \chi) \left\{ \omega_1^2 f_1(0;M_1\omega_1) \left[\tilde{H}_0 + A_0 \frac{s(\cot \chi - \beta_1)}{2} \right] + i\omega_1 f_3(0;M_1\omega_1) A_0 \right\}$$

$$+ \frac{1}{i} \sum_{m=0}^{\infty} \left[U_n^+ \left(e^{-i(\lambda_n - M_1 k_1)s \cot \chi} - e^{-i(M_1 k_1 - \lambda_n)s\beta_1} \right) \right.$$

$$\left. + U_n^- \left(e^{i(\lambda_n + M_1 k_1)s \cot \chi} - e^{-i(\lambda_n + M_1 k_1)s\beta_1} \right) \right]$$

$$+ s \sum_{n=-\infty}^{\infty} \frac{v_n^+ - k_1/M_1}{(v_n^+ - M_1 k_1)^2} \frac{K_1^-(M_1 k_1)}{K_-'(v_n^+)} \left(D_- + \frac{i\omega_1 A_0}{v_n^+ - M_1 k_1} \right) \frac{e^{i(v_n^+ - M_1^+ k_1)(s\beta_1 - s^+)} - 1}{d_1^+ \Gamma_n^{(1)} - v_n^+ s^+}$$

$$\tilde{H}_0 = H_0 - A_0 d_0$$

$$f_3(0;M_1\omega_1) = f_1(0;M_1\omega_1)[1 - M_1\omega_1 s \cot(M_1\omega_1 s)] + \omega_1 f_2(0;M_1\omega_1) + s$$

$$M_{11} \equiv \int_{-s^+}^{s \cot \chi} x P_1 \, dx$$

$$= \omega_1 s(\beta_1 + \cot \chi) \left\{ \left[\omega_1 \tilde{H}_0 f_1(0;M_1\omega_1) + i f_3(0;M_1\omega_1) A_0 \right] \frac{s(\beta_1 - \cot \chi)}{2} \right.$$

$$\left. - \frac{\omega_1^2 s^2}{3} A_0 f_1(0;M_1\omega_1) \left(\beta_1^2 - \beta_1 \cot \chi + \cot^2 \chi \right) \right\}$$

$$+ \sum_{n=0}^{\infty} \left(-U_n^+ \left\{ is \left[\beta_1 e^{i(\lambda_n - M_1 k_1)s\beta_1} + \cot \chi \, e^{-i(\lambda_n - M_1 k_1)s \cot \chi} \right] \right. \right.$$

$$\left. - \frac{e^{-i(\lambda_n - M_1 k_1)s\beta_1} - e^{-i(\lambda_n - M_1 k_1)s \cot \chi}}{\lambda_n - M_1 k_1} \right]$$

$$+ U_n^- \left[-is \left[\beta_1 e^{-i(\lambda_n + M_1 k_1)s\beta_1} + \cot \chi \, e^{i(\lambda_n + M_1 k_1)s \cot \chi} \right] \right.$$

$$\left. \left. - \frac{e^{-i(\lambda_n + M_1 k_1)s\beta_1} - e^{i(\lambda_n + M_1 k_1)s \cot \chi}}{\lambda_n + M_1 k_1} \right] \right\}$$

$$+ s \sum_{n=-\infty}^{\infty} \frac{v_n^+ - k_1/M_1}{(v_n^+ - M_1 k_1)^2} \frac{K_1^-(M_1 k_1)}{K_-'(v_n^+)} \left(D_- + \frac{i\omega_1 A_0}{v_n^+ - M_1 k_1} \right) \frac{1}{\Gamma_n^{(1)} d_1^+ - v_n^+ s^+}$$

$$\times \left\{ s^+ + \frac{1}{v_n^+ - M_1 k_1} - e^{i(v_n^+ - M_1 k_1)(s\beta_1 - s^+)} \left(s\beta_1 + \frac{1}{v_n^+ - M_1 k_1} \right) \right\}$$

$$U_n^{\pm} \equiv - \frac{(k_1/M_1 \mp \lambda_n) Q_n^{\pm}}{M_1 k_1 \mp \lambda_n}$$

REFERENCES

1. Goldstein, M. E.; Braun, W.; and Adamczyk, J. J.: Unsteady Flow in a Supersonic Cascade with Strong In-Passage Shocks. J. Fluid Mech., vol. 83, pt. 3, Dec. 5, 1977, pp. 569-604.

2. McDonald, P. W.; et al: A Comparison Between Measured and Computed Flow Fields in a Transonic Compressor Rotor. J. Eng. Power, vol. 102, no. 4, Oct. 1980, pp. 883-891.

3. Strazisar, A. J.; and Chima, R. V.: Comparison Between Optical Measurements and a Numerical Solution of the Flow Field Within a Transonic Axial-Flow Compressor Rotor. AIAA Paper 80-1078, 1980.

4. Chima, R. V.; and Strazisar, A. J.: Comparison of Two and Three-Dimensional Flow Computations with Laser Anemometer Measurements in a Transonic Compressor Rotor. NASA TM-82777, 1982.

5. Bilwakesh, K. R.; Koch, C. C.; and Prince, D. C.: Evaluation of Range and Distortion Tolerance for High Mach Number Transonic Fan Stages. (R71AEG195, General Electric Co.; NASA Contract NAS3-11157) NASA CR-72880, 1972.

6. Carrier, G. F.: On the Stability of the Supersonic Flows Past a Wedge. Q. Appl. Math., vol. 6, no. 4, Jan. 1949, pp. 367-378.

7. Lane, F.: System Mode Shapes in the Flutter of Compressor Blade Rows. J. Aeronaut. Sci., vol. 23, Jan. 1956, pp. 54-66.

8. Moore, F. K.: Unsteady Oblique Interaction of a Shock Wave With a Plane Disturbance. NACA TR-1165, 1954.

9. Van Dyke, M. D.: On Supersonic Flow Past an Oscillating Wedge. Q Appl. Math., vol. 11, no. 3, Oct. 1953, pp. 360-363.

10. Watson, G. N.: A Treatise on the Theory of Bessel Functions. Second ed., Cambridge University Press, 1944.

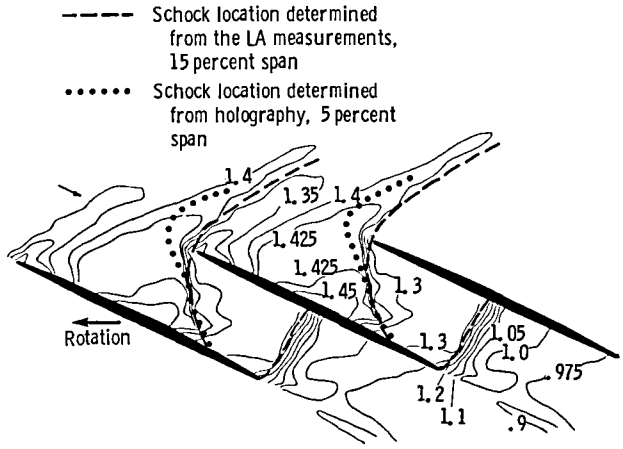

Figure 1. - Relative Mach number contours measured with the LA at 15 percent span from the tip (ref. 3).

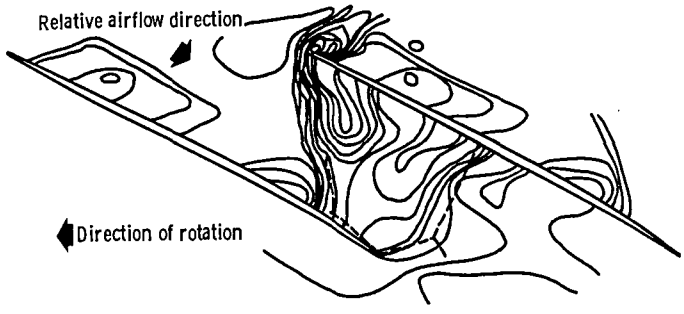

100% Speed (Near design)

Figure 2. - Rotor blade tip static pressure contours. Inlet Mach number, 1.493 (ref. 5).

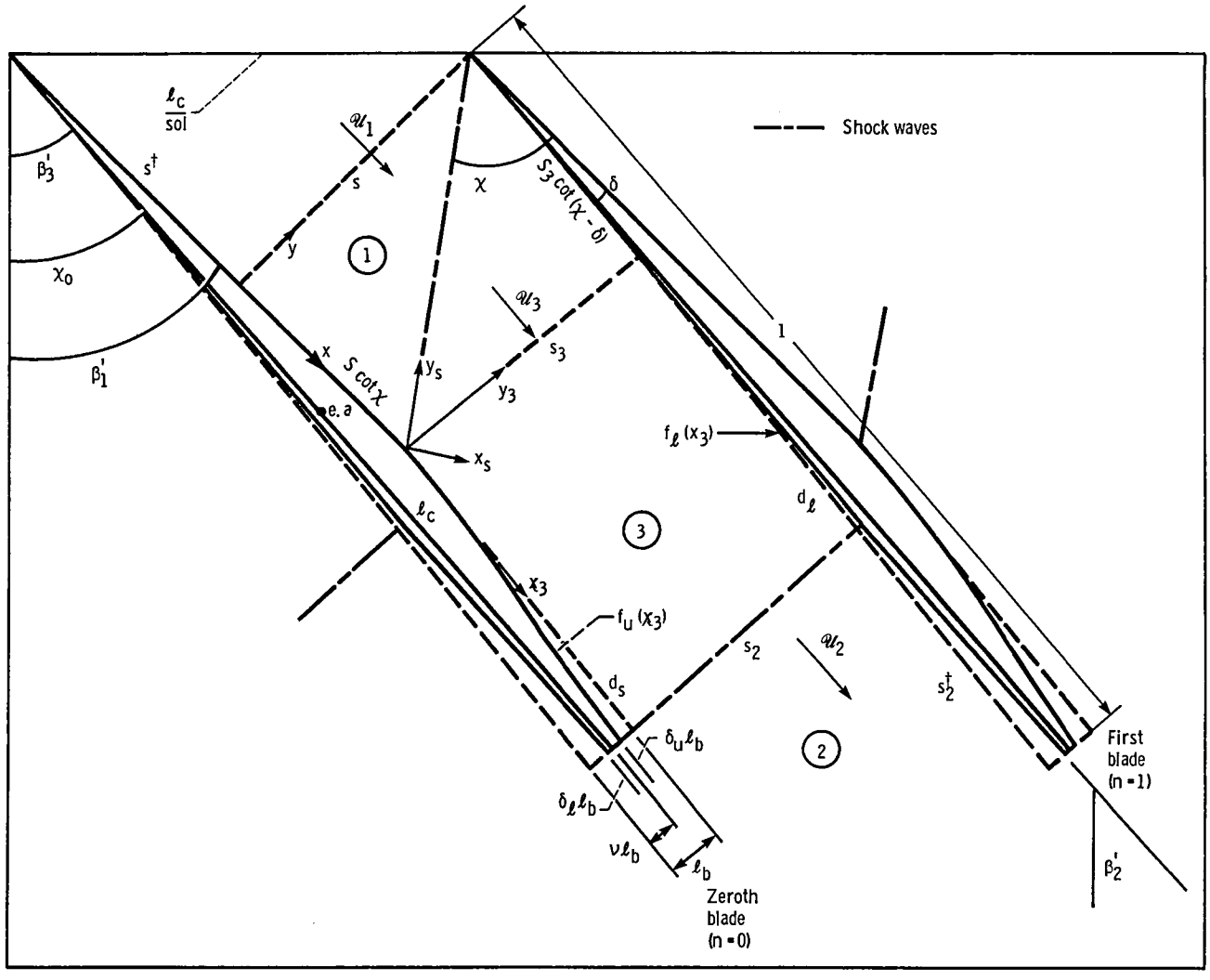

Figure 3. - Blade-passage regions and notation.

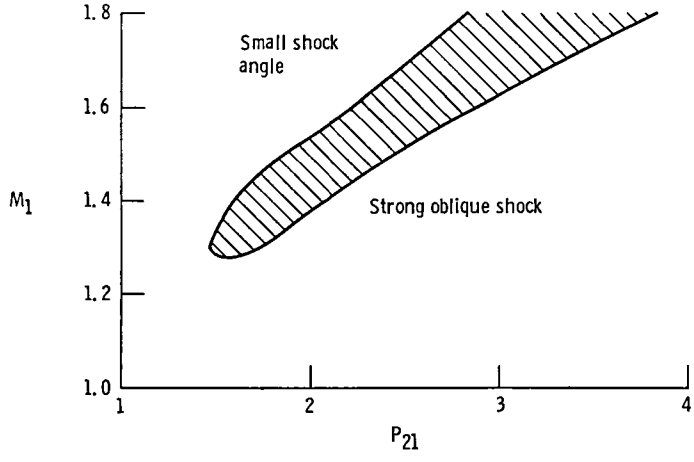

Figure 4. - Domain of validity of flow model. Solidity = 1.4; stagger angle = 62^o; entrance-flow angle = 67^o.

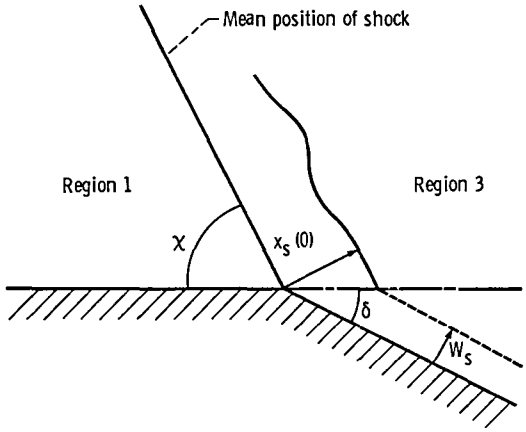

Figure 5. - Displacement of blade wall due to incremental change in oblique shock position.

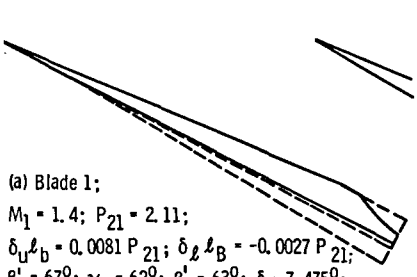

(a) Blade 1;
$M_1 = 1.4$; $P_{21} = 2.11$;
$\delta_u \ell_b = 0.0081\, P_{21}$; $\delta_\ell \ell_B = -0.0027\, P_{21}$;
$\beta_1' = 67^0$; $\chi_0 = 62^0$; $\beta_2' = 63^0$; $\delta = 7.475^0$;
estimated $P_{21} = 1.85$.

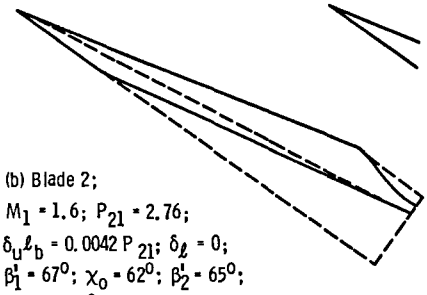

(b) Blade 2;
$M_1 = 1.6$; $P_{21} = 2.76$;
$\delta_u \ell_b = 0.0042\, P_{21}$; $\delta_\ell = 0$;
$\beta_1' = 67^0$; $\chi_0 = 62^0$; $\beta_2' = 65^0$;
$\delta = 12.947^0$; estimated $P_{21} = 2.4$.

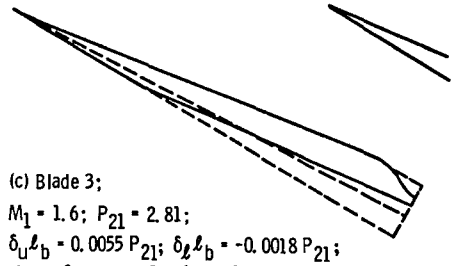

(c) Blade 3;
$M_1 = 1.6$; $P_{21} = 2.81$;
$\delta_u \ell_b = 0.0055\, P_{21}$; $\delta_\ell \ell_b = -0.0018\, P_{21}$;
$\beta_1' = 67^0$; $\chi_0 = 62^0$; $\beta_2' = 65^0$; $\delta = 8.461^0$;
estimated $P_{21} = 2.75$.

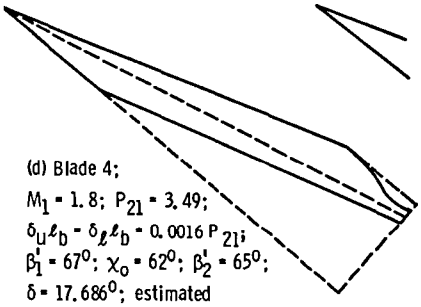

(d) Blade 4;
$M_1 = 1.8$; $P_{21} = 3.49$;
$\delta_u \ell_b = \delta_\ell \ell_b = 0.0016\, P_{21}$;
$\beta_1' = 67^0$; $\chi_0 = 62^0$; $\beta_2' = 65^0$;
$\delta = 17.686^0$; estimated
$P_{21} = 3.10$.

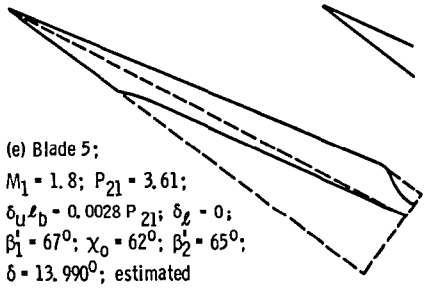

(e) Blade 5;
$M_1 = 1.8$; $P_{21} = 3.61$;
$\delta_u \ell_b = 0.0028\, P_{21}$; $\delta_\ell = 0$;
$\beta_1' = 67^0$; $\chi_0 = 62^0$; $\beta_2' = 65^0$;
$\delta = 13.990^0$; estimated
$P_{21} = 3.60$.

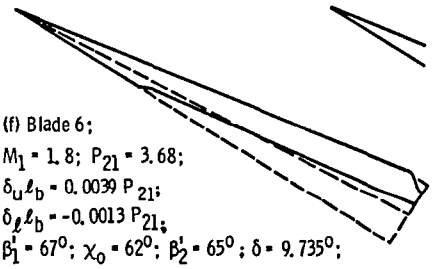

(f) Blade 6;
$M_1 = 1.8$; $P_{21} = 3.68$;
$\delta_u \ell_b = 0.0039\, P_{21}$;
$\delta_\ell \ell_b = -0.0013\, P_{21}$;
$\beta_1' = 67^0$; $\chi_0 = 62^0$; $\beta_2' = 65^0$; $\delta = 9.735^0$;
estimated $P_{21} = 3.8$.

Figure 6. - Blade models for six flow conditions. Entrance angle, 67^0; stagger angle, 62^0; solidity, 1.4.

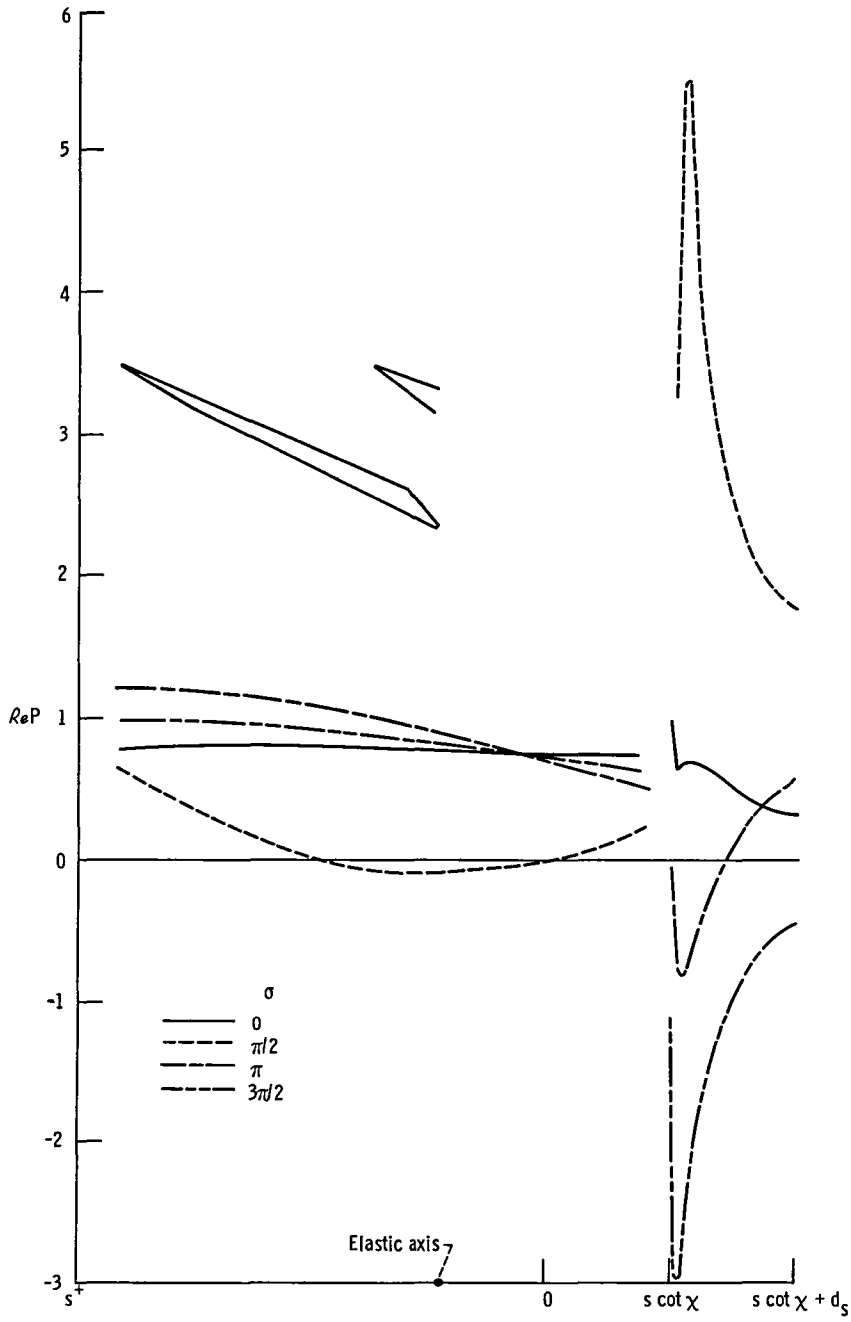

(a) In-phase component (real part) of pressure acting on upper surface.

Figure 7. - Nondimensionalized surface-pressure amplitudes on blade 1 undergoing pure pitching about its center; reduced frequency $(1/2)\omega_1 = 0.25$.

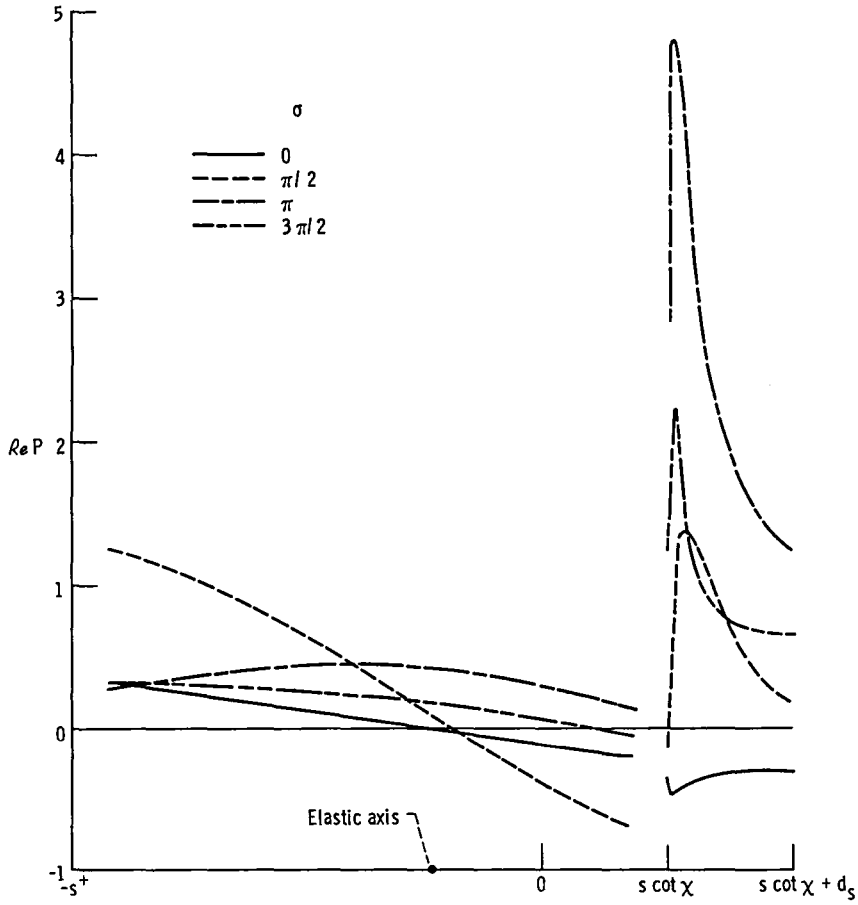

(b) Out-of-phase component (imaginary part) of pressure acting on upper surface.

Figure 7. - Continued.

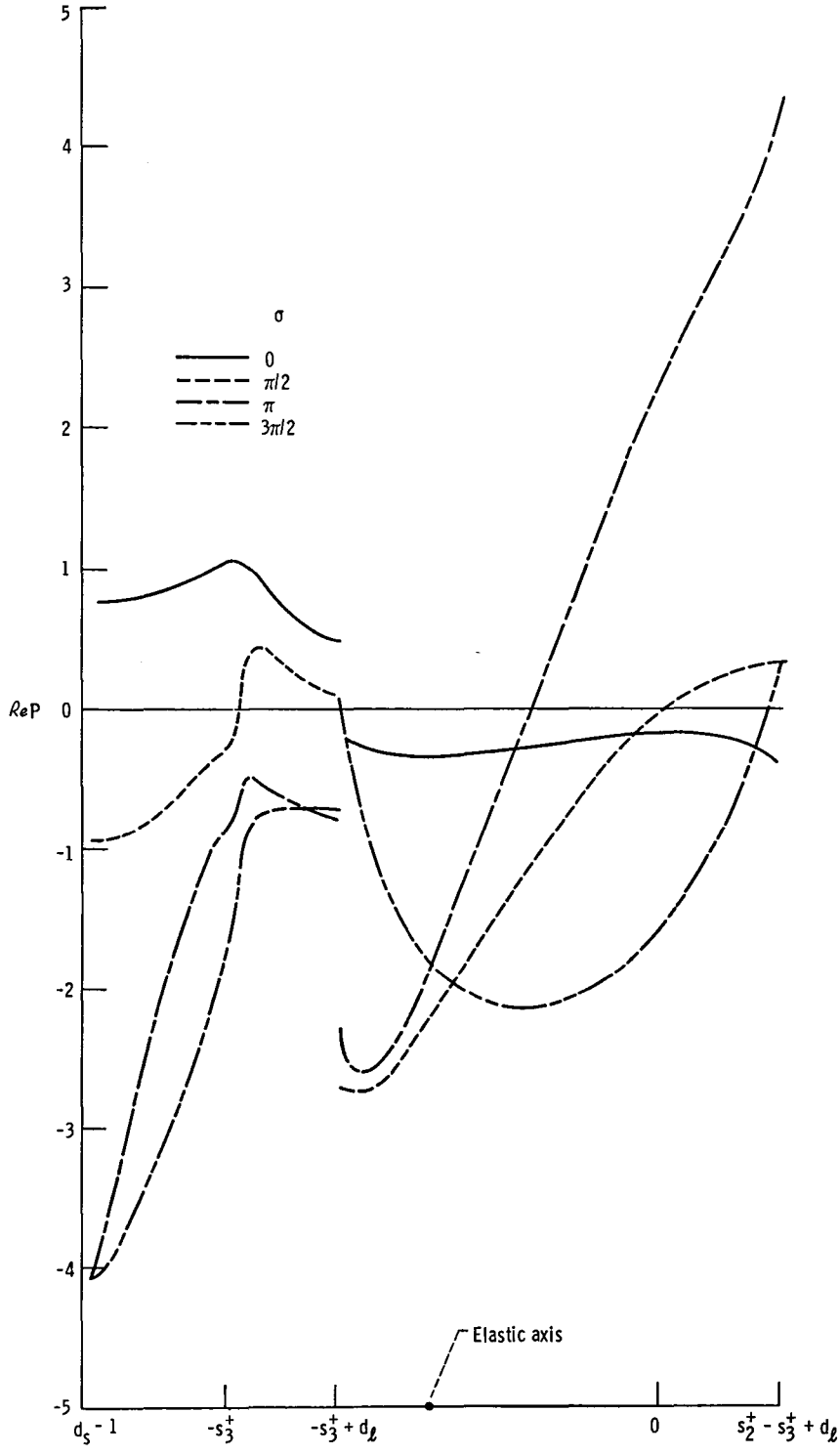

(c) In-phase component (real part) of pressure acting on lower surface.

Figure 7. - Continued.

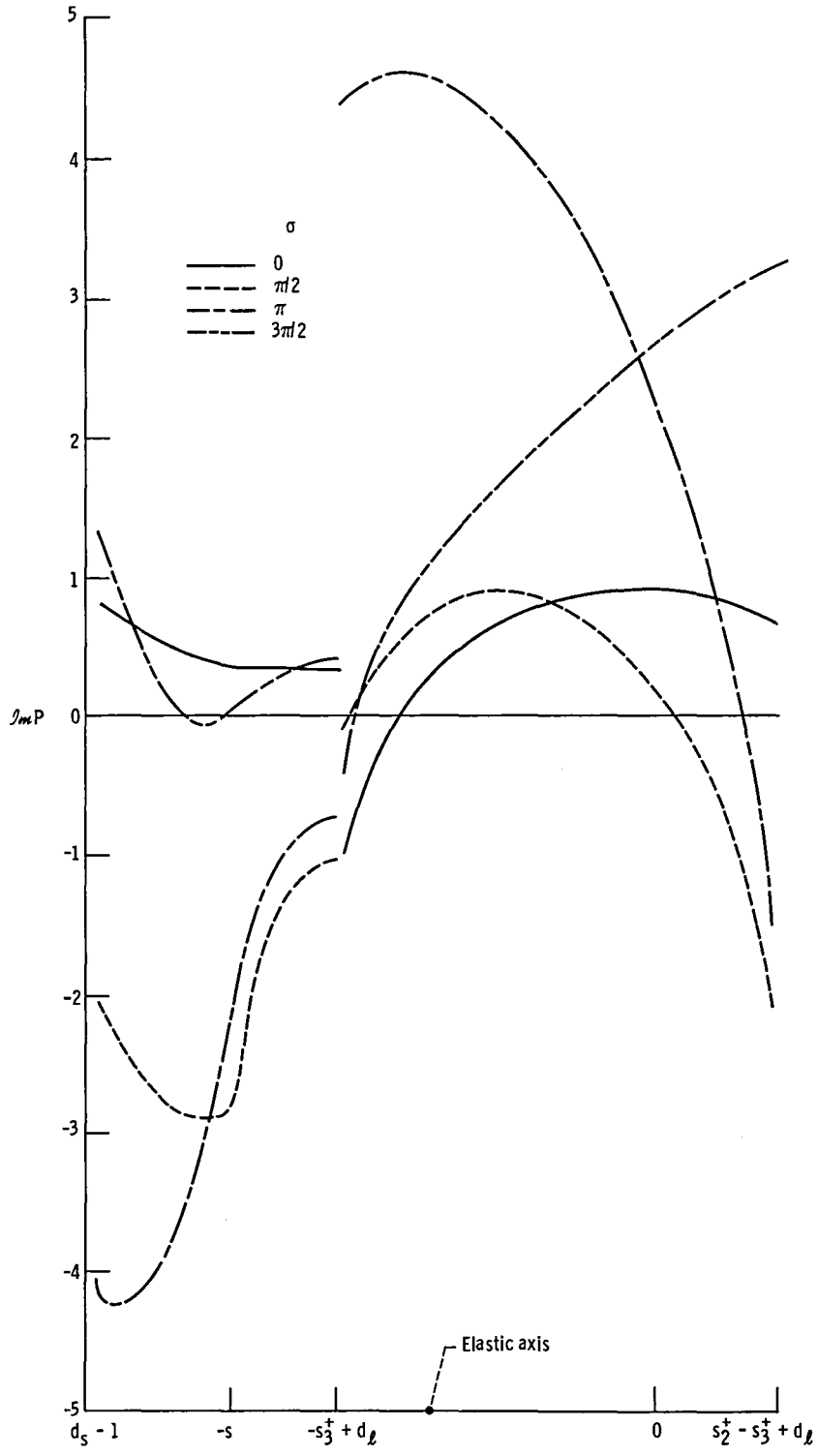

(d) Out-of-phase component (imaginary part) of pressure acting on lower surface.

Figure 7. - Concluded.

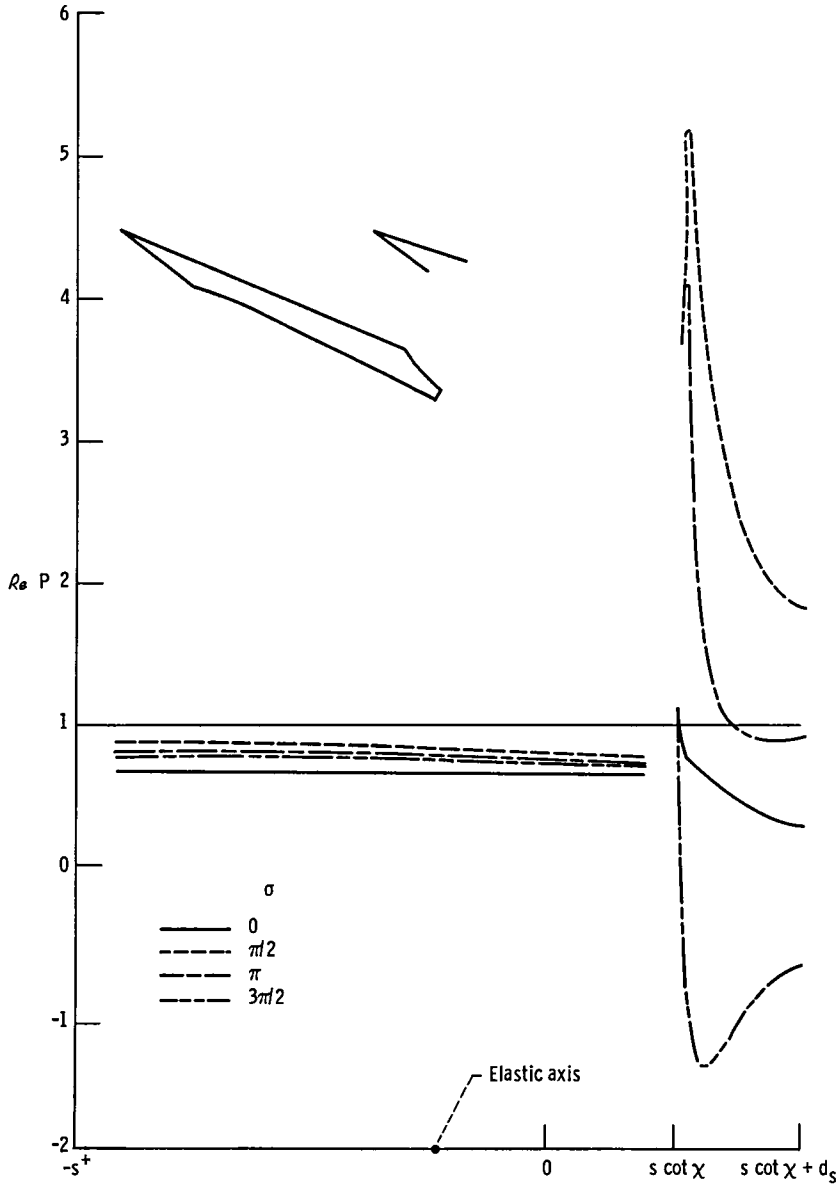

(a) In-phase component (real part) of pressure acting on upper surface.

Figure 8. - Nondimensional surface-pressure amplitudes on blade 2 undergoing pure pitching about its center; reduced frequency $(1/2)\omega_1 = 0.5$.

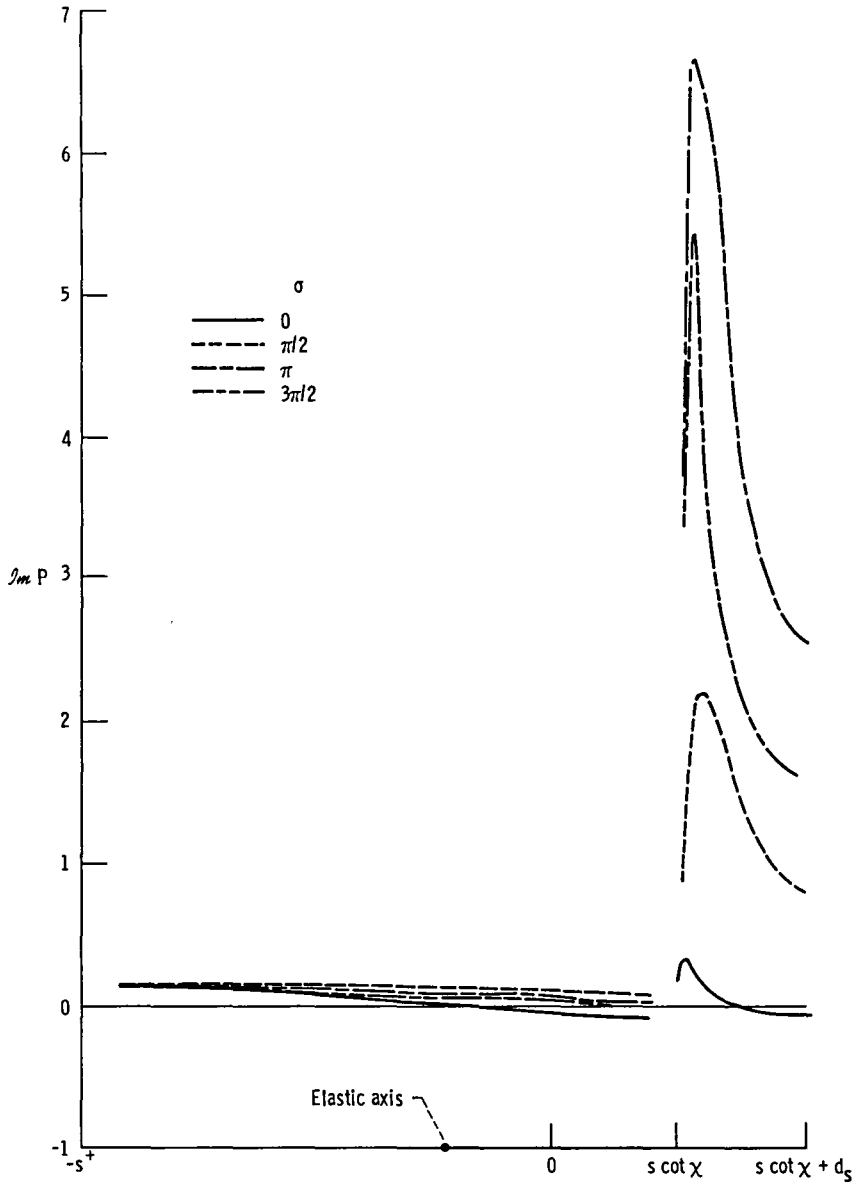

(b) Out-of-phase component (imaginary part) of pressure acting on upper surface.

Figure 8. - Continued.

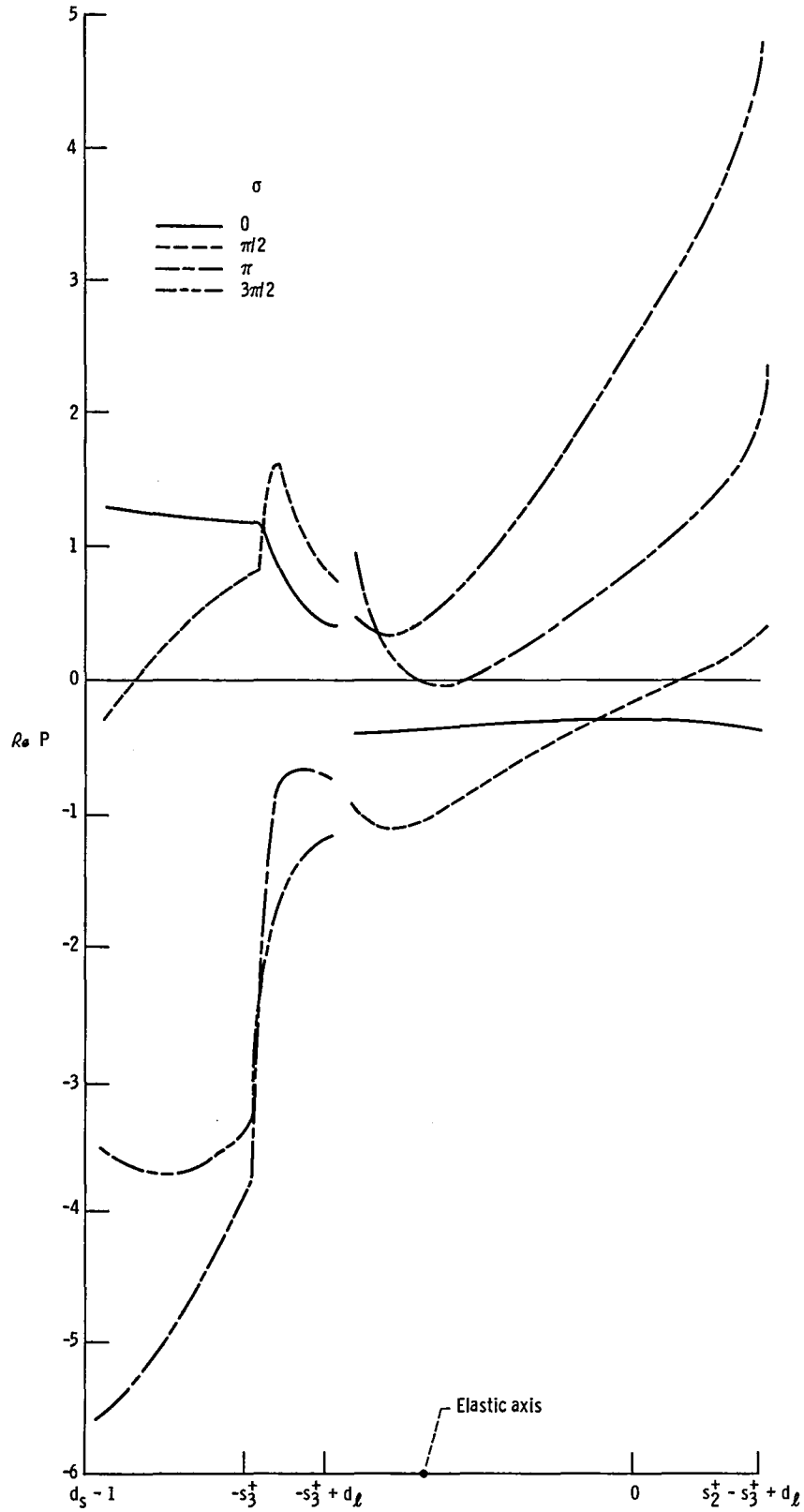

(c) In-phase component (real part) of pressure acting on lower surface.

Figure 8. - Continued.

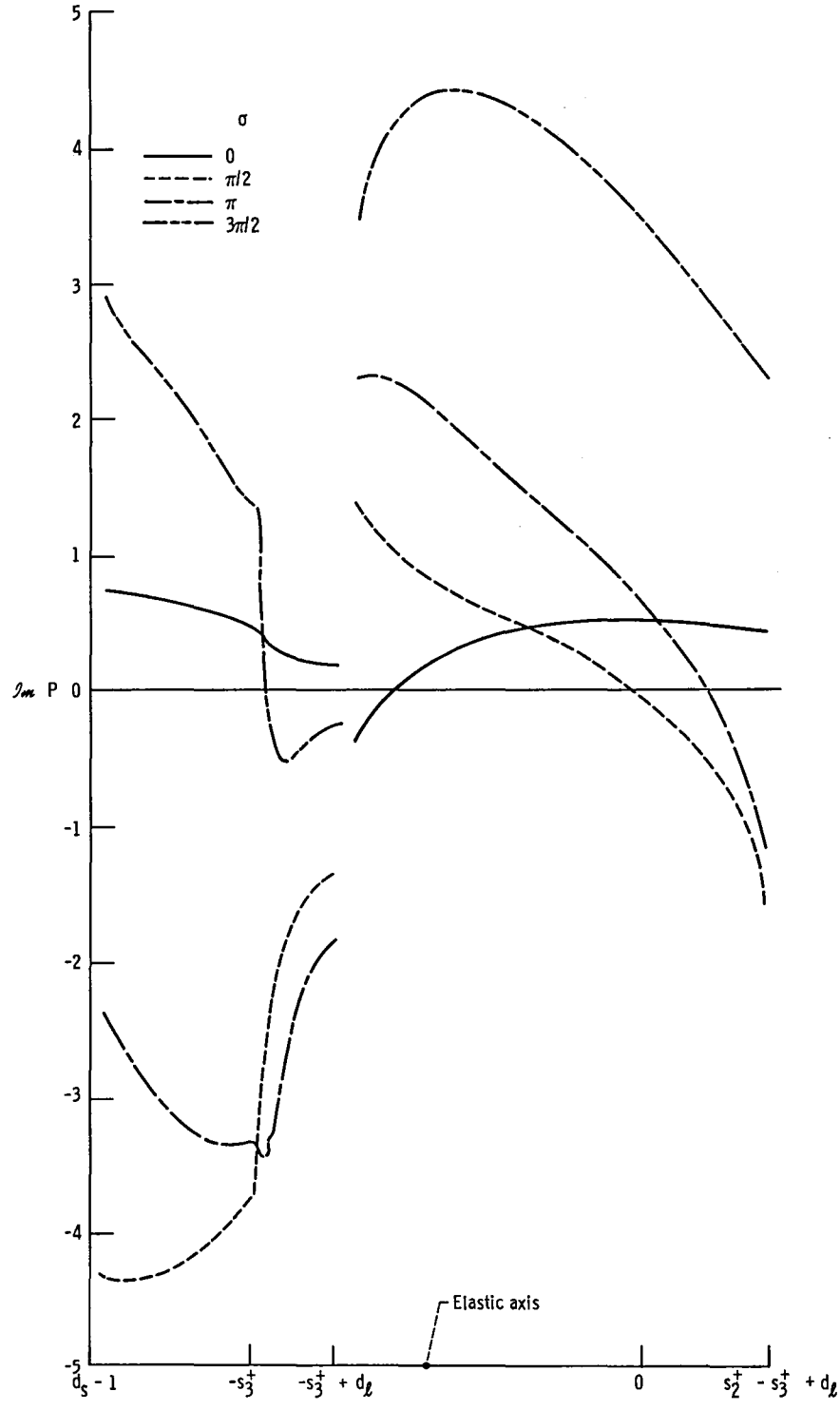

(d) Out-of-phase component (imaginary part) of pressure acting on lower surface.

Figure 8. - Concluded.

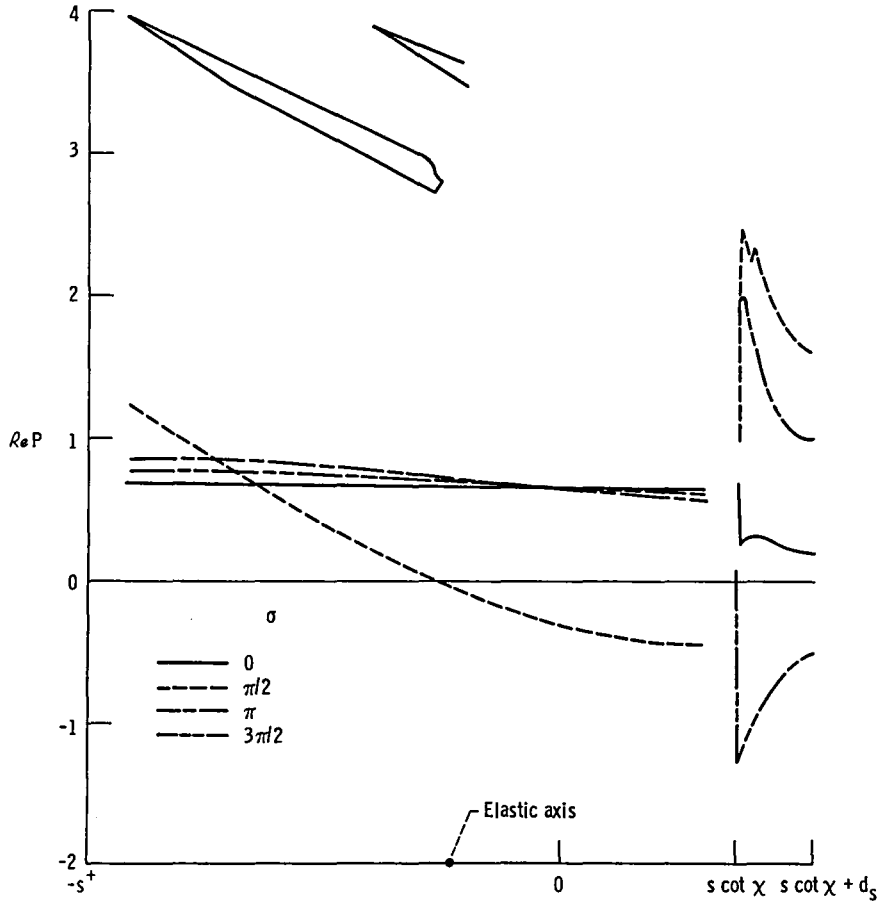

(a) In-phase component (real part) of pressure acting on upper surface.

Figure 9. - Nondimensional surface-pressure amplitudes on blade 3 undergoing pure pitching about its center; reduced frequency $(1/2)\omega_1 = 0.5$.

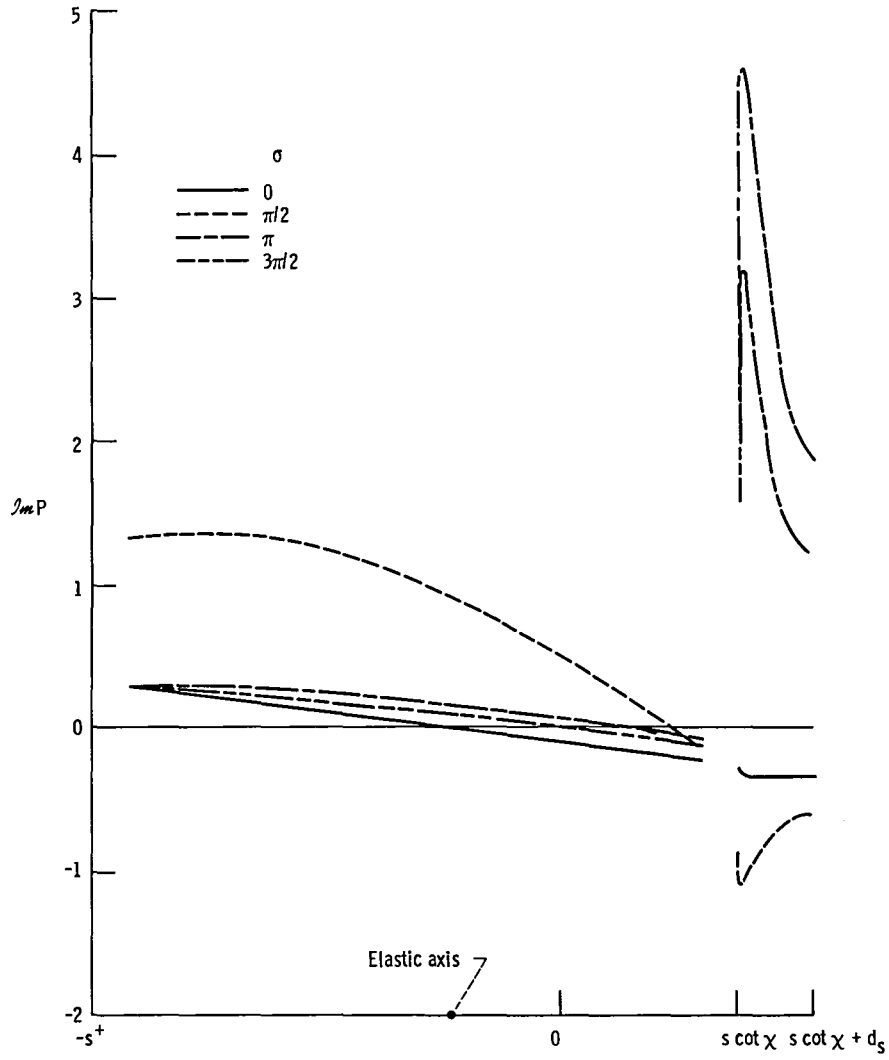

(b) Out-of-phase component (imaginary part) of pressure acting on upper surface.

Figure 9. - Continued.

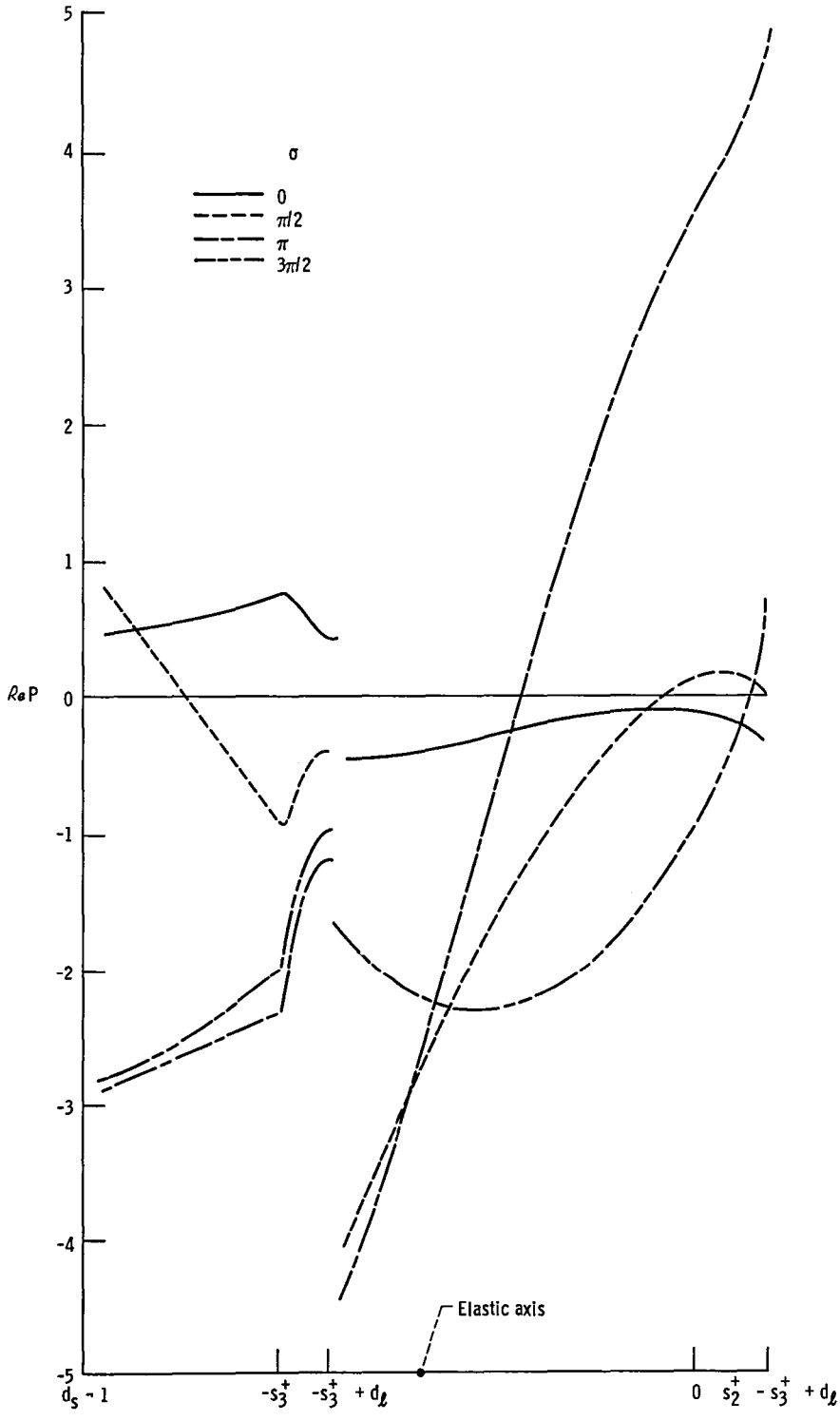

(c) In-phase component (real part) of pressure acting on lower surface.

Figure 9. - Continued.

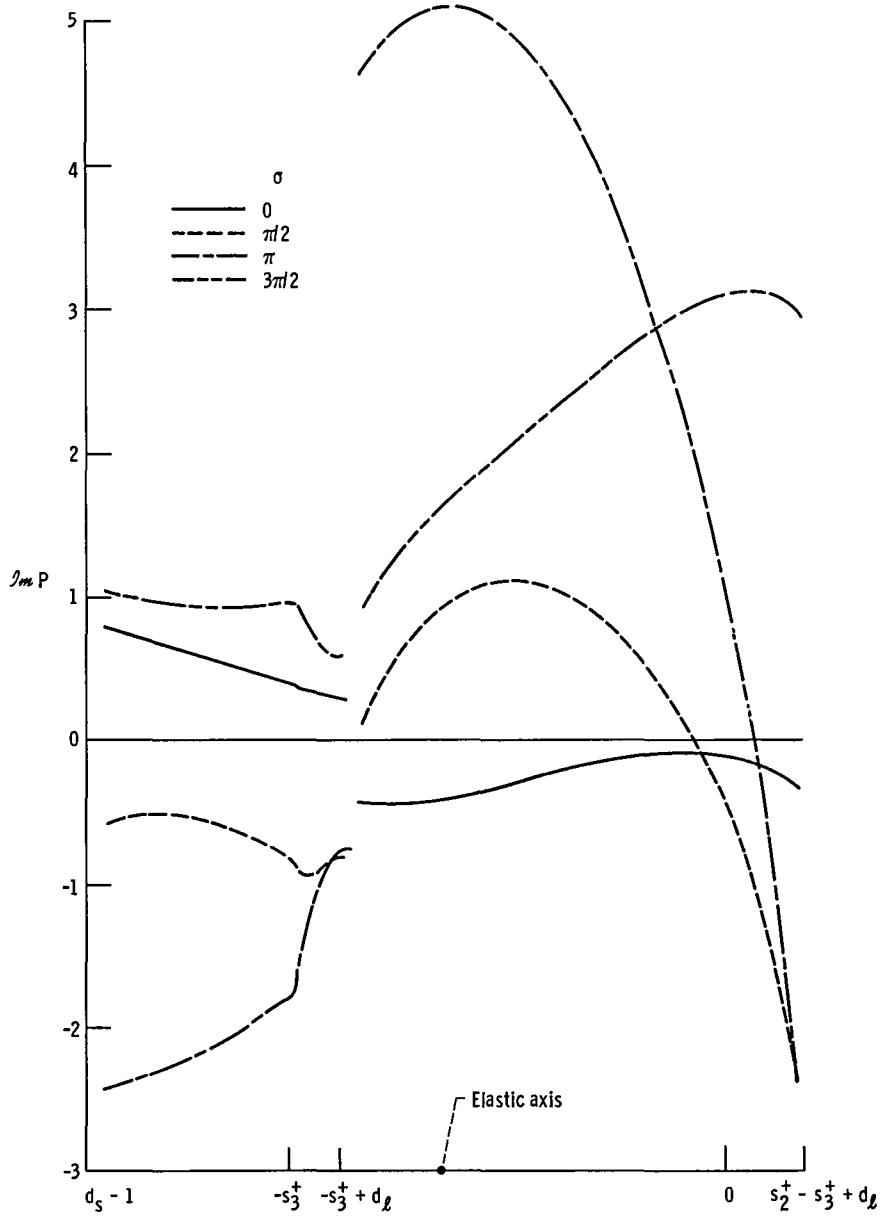

(d) Out-of-phase component (imaginary part) of pressure acting on lower surface.

Figure 9. - Concluded.

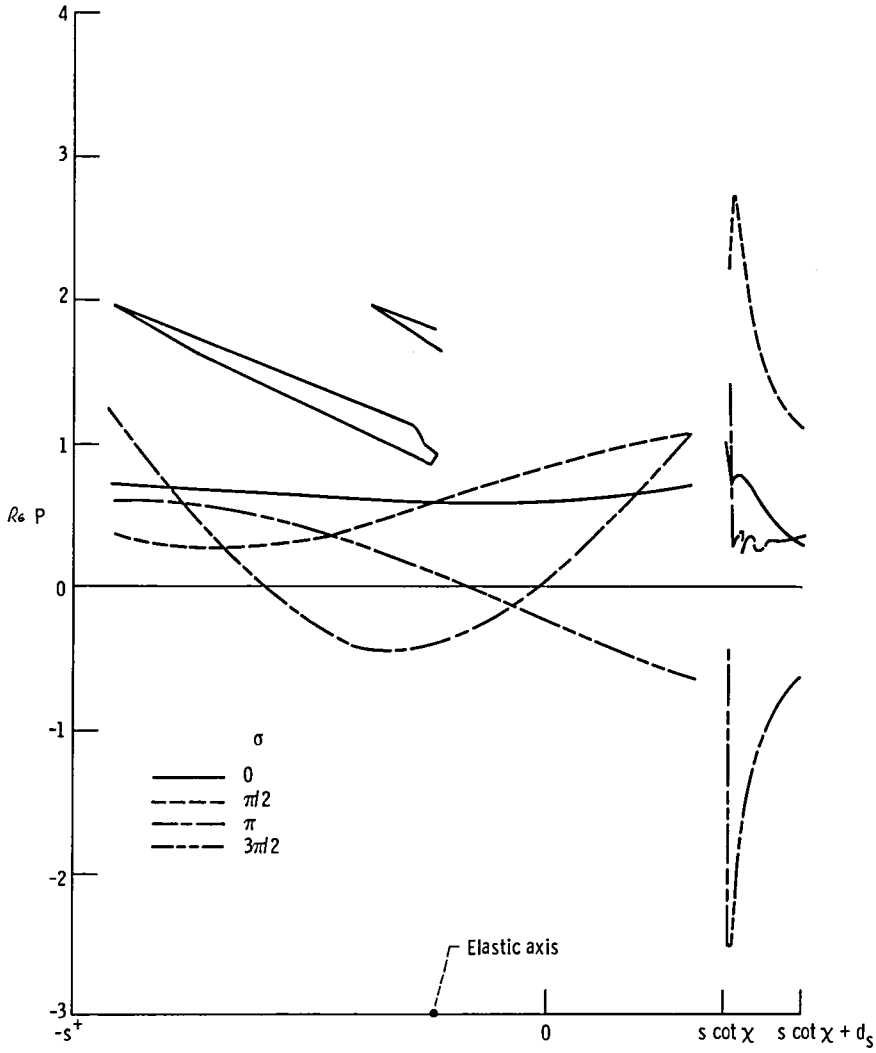

(a) In-phase component (real part) of pressure acting on upper surface.

Figure 10. - Nondimensional surface-pressure amplitudes on blade 3 undergoing pure pitching about its center; reduced frequency $(1/2)\omega_1 = 1.0$.

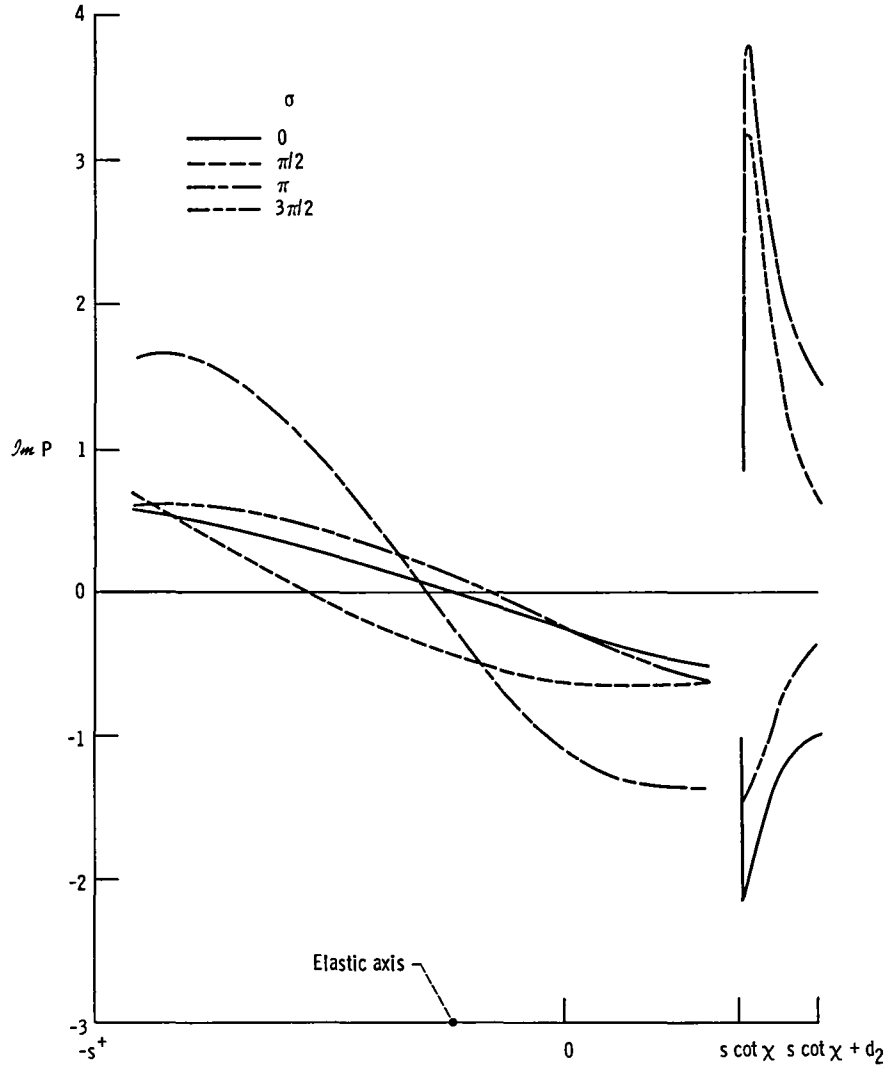

(b) Out-of-phase component (imaginary part) of pressure acting on lower surface.

Figure 10. - Continued.

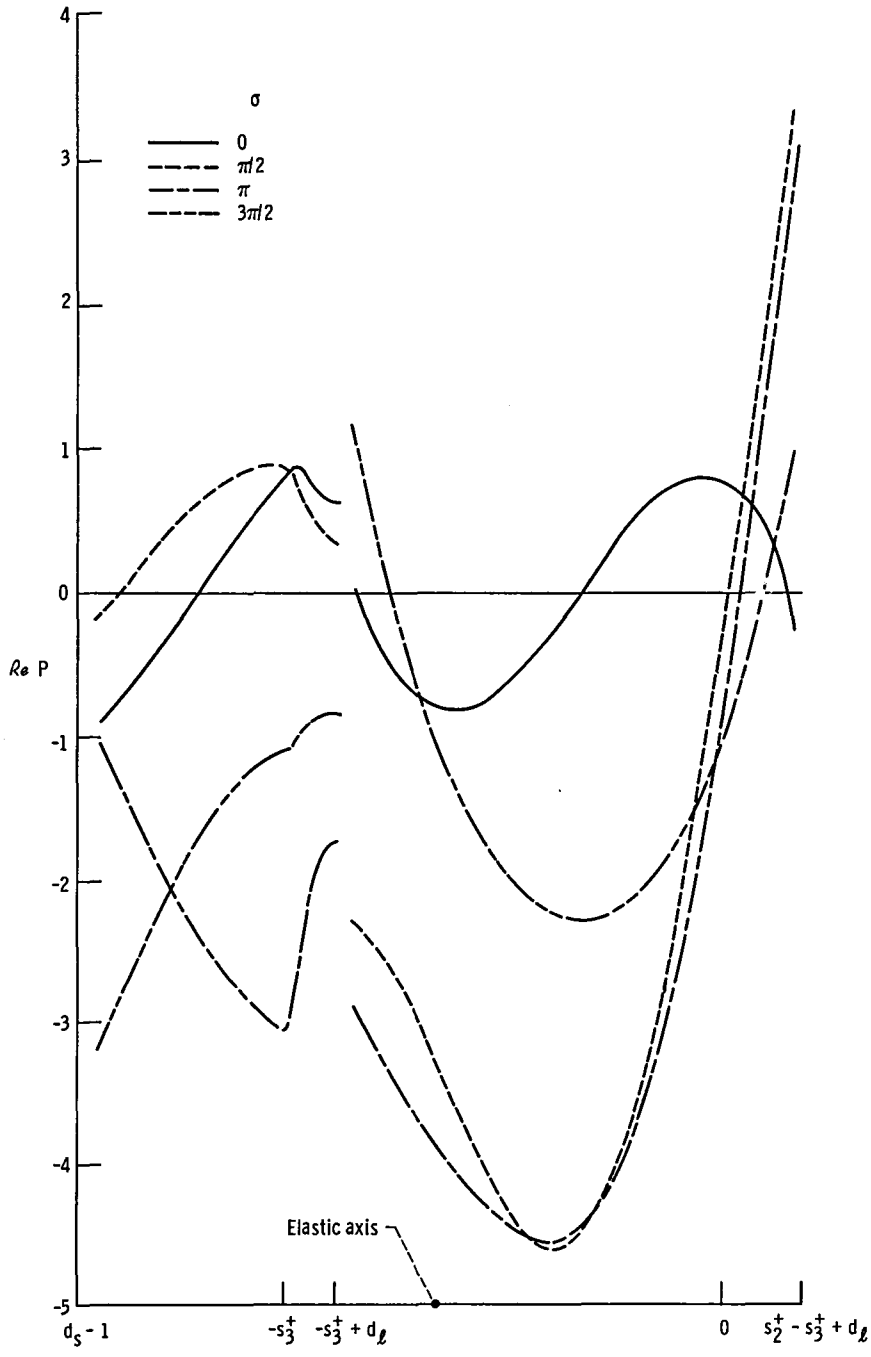

(c) In-phase component (real part) of pressure acting on lower surface.

Figure 10. - Continued.

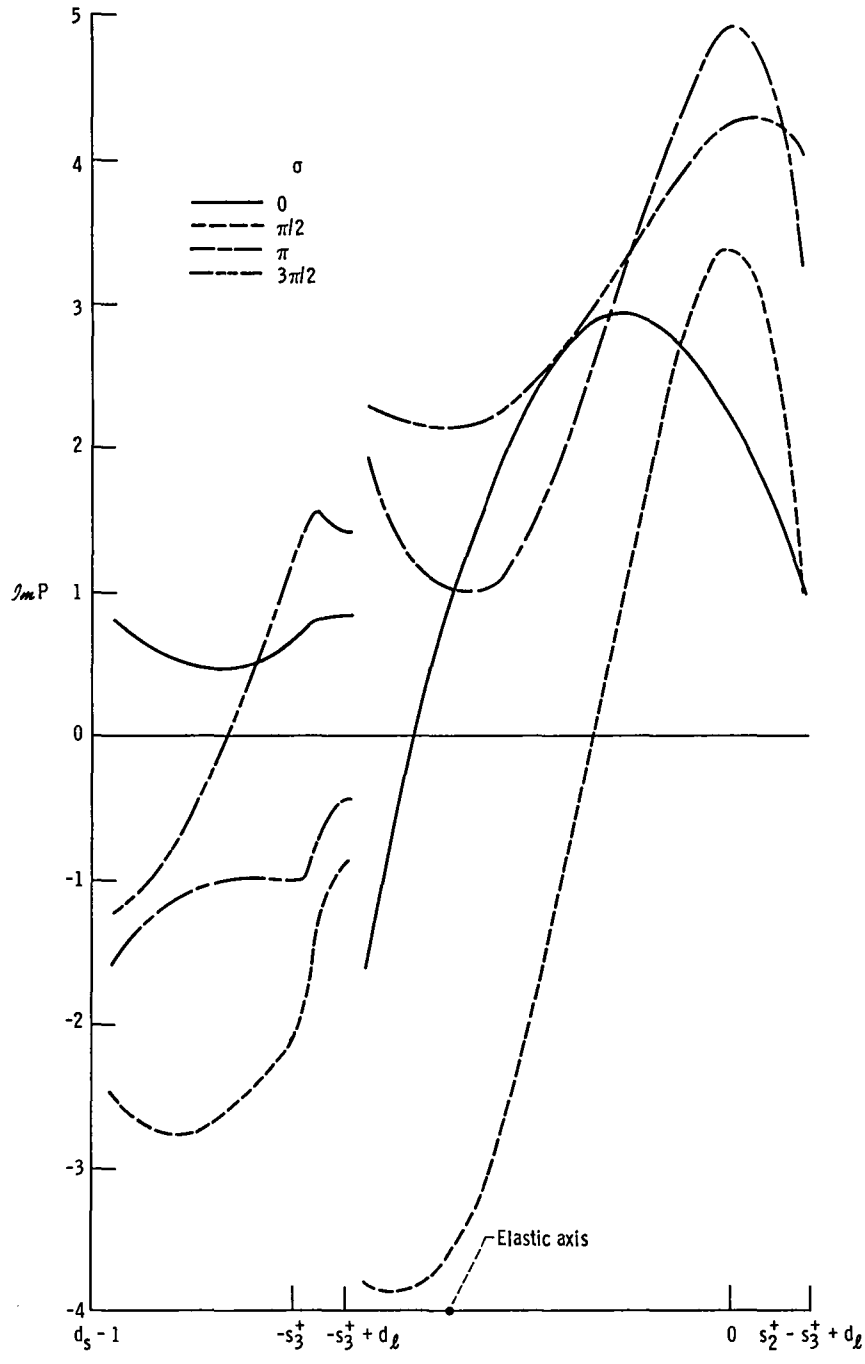

(d) Out-of-phase component (imaginary part) of pressure acting on lower surface.

Figure 10. - Concluded.

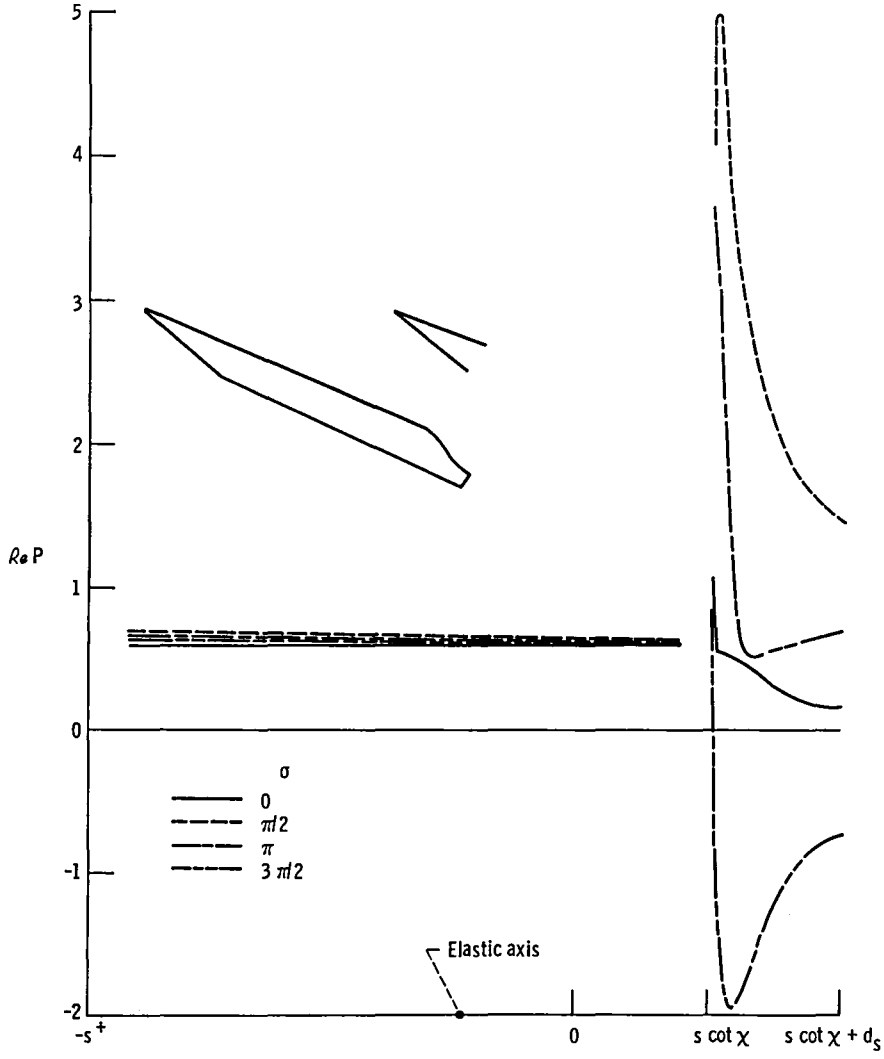

(a) In-phase component (real part) of pressure acting on upper surface.

Figure 11. - Nondimensional surface-pressure amplitudes on blade 4 undergoing pure pitching about its center; reduced frequency $(1/2)\omega_1 = 0.25$.

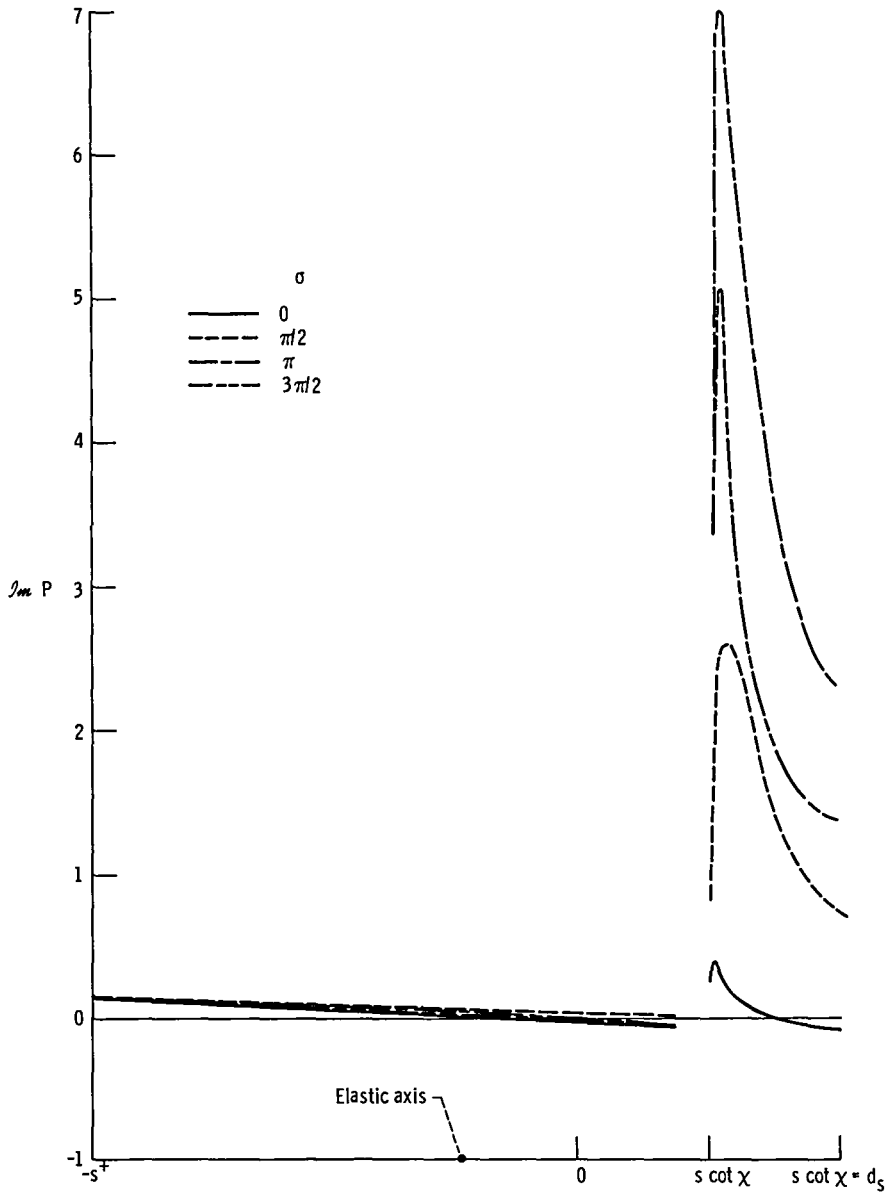

(b) Out-of-phase component (imaginary part) of pressure acting on upper surface.

Figure 11. - Continued.

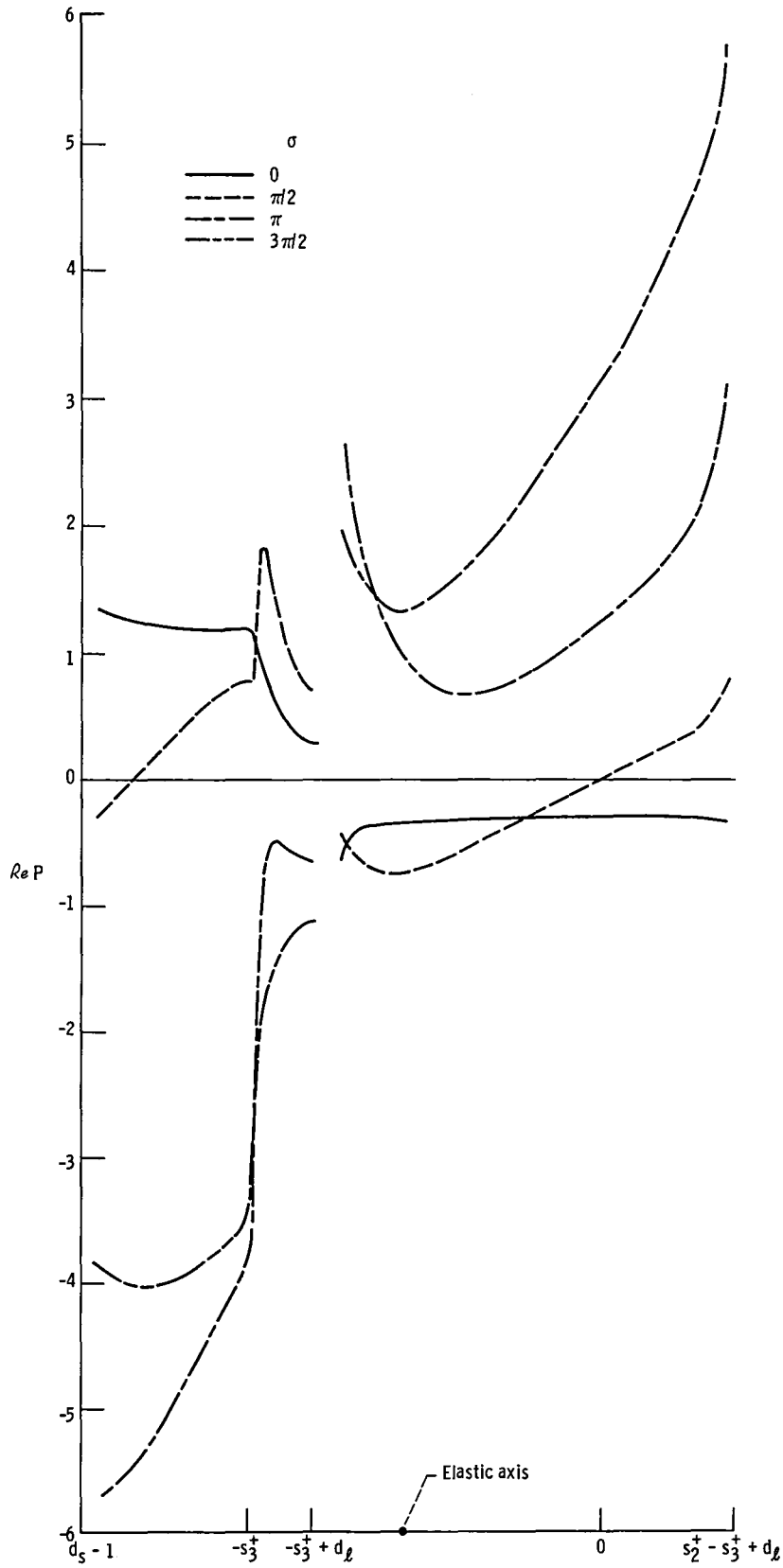

(c) In-phase component (real part) of pressure acting on lower surface.

Figure 11. - Continued.

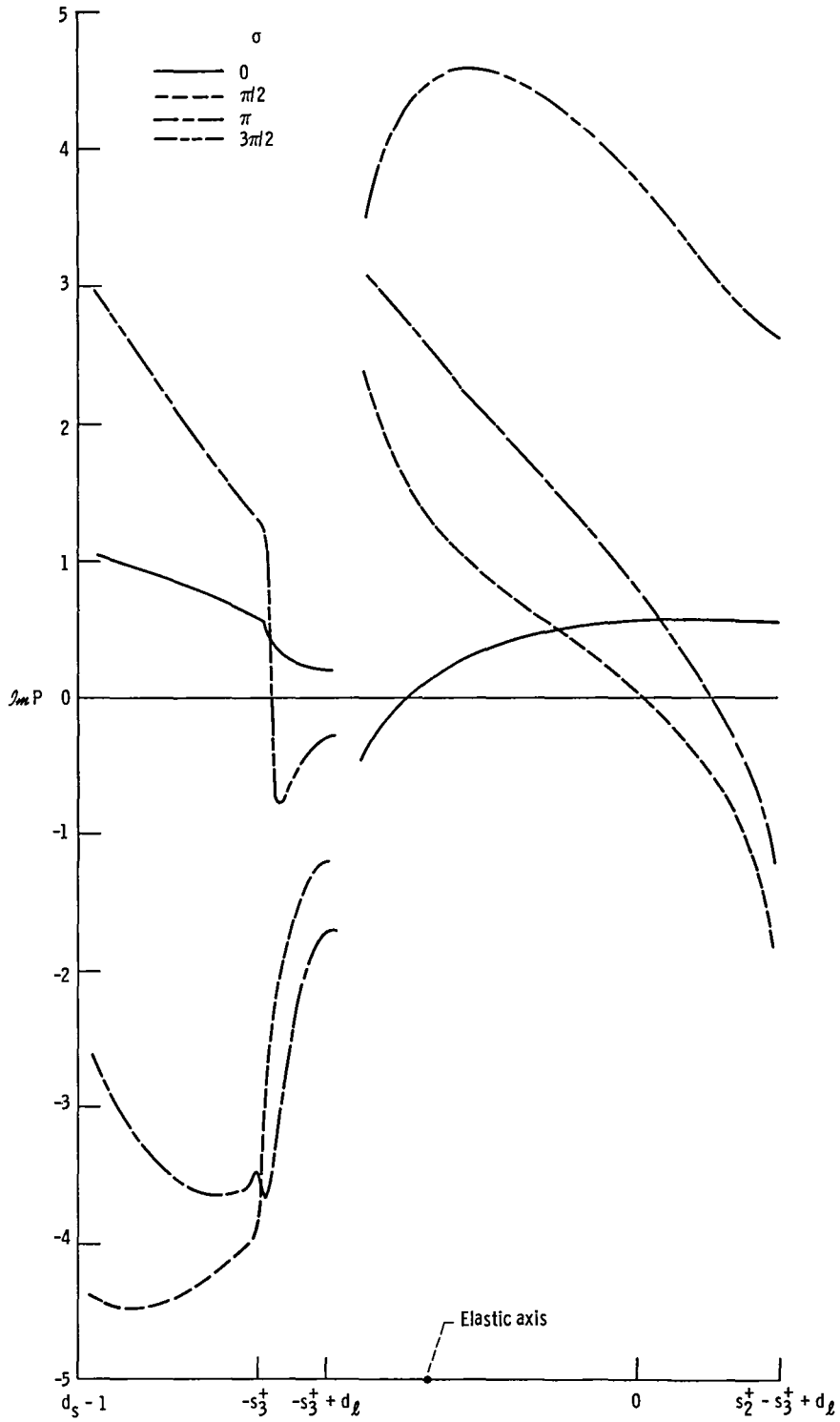

(d) Out-of-phase component (imaginary part) of pressure acting on upper surface.

Figure 11. - Concluded.

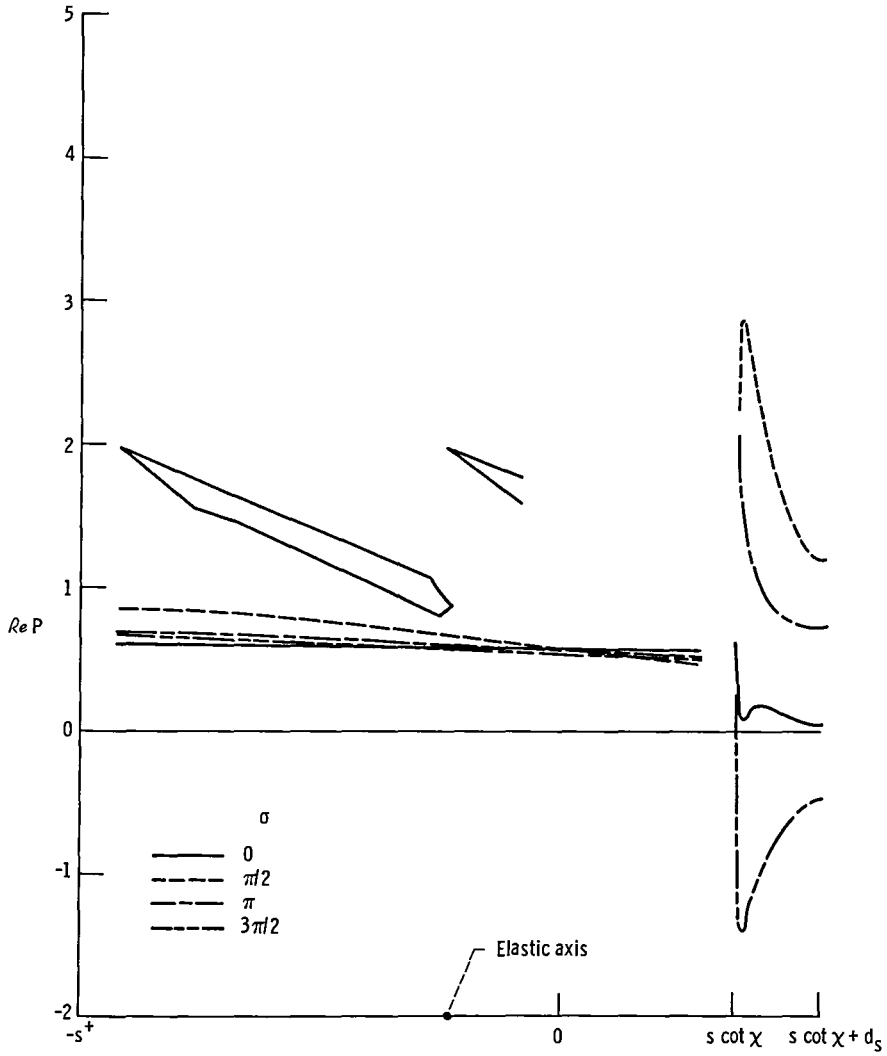

(a) In-phase components (real part) of pressure acting on upper surface.

Figure 12. - Nondimensional surface-pressure amplitudes on blade 5 undergoing pure pitching about its center; reduced frequency $(1/2)\,\omega_1 = 0.5$.

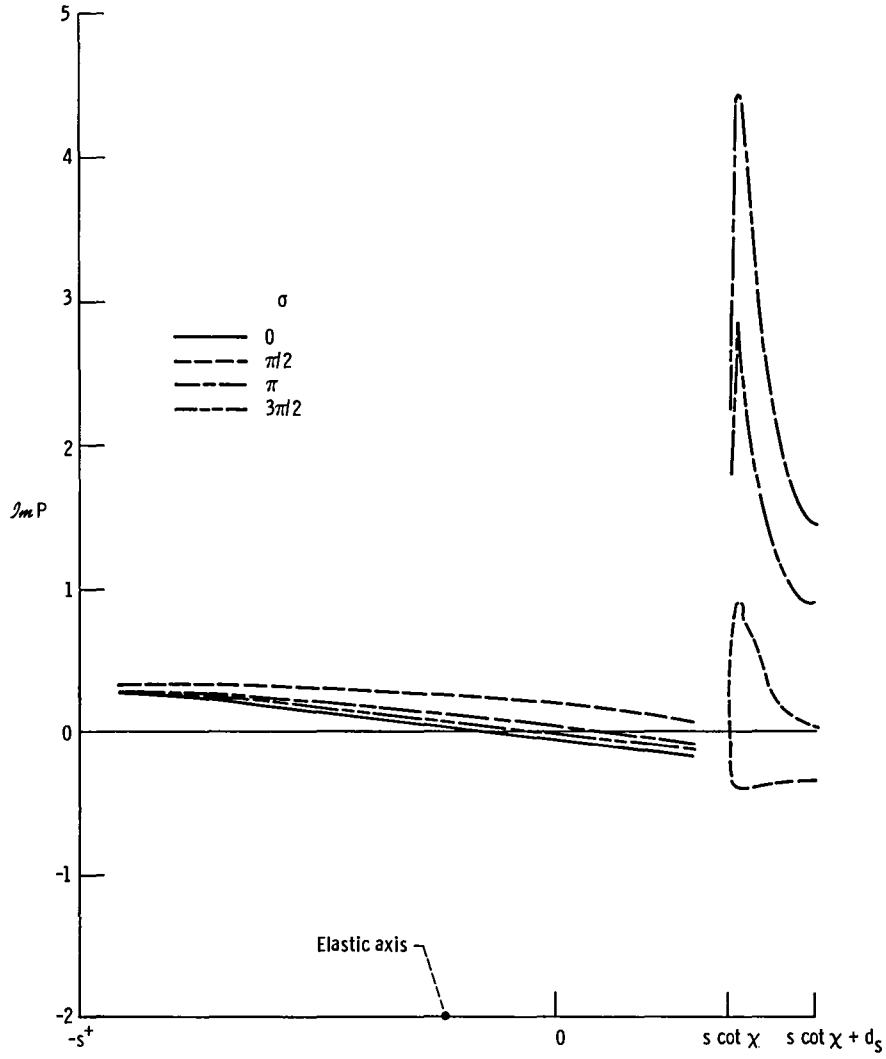

(b) Out-of-phase component (imaginary part) of pressure acting on upper surface.

Figure 12. - Continued.

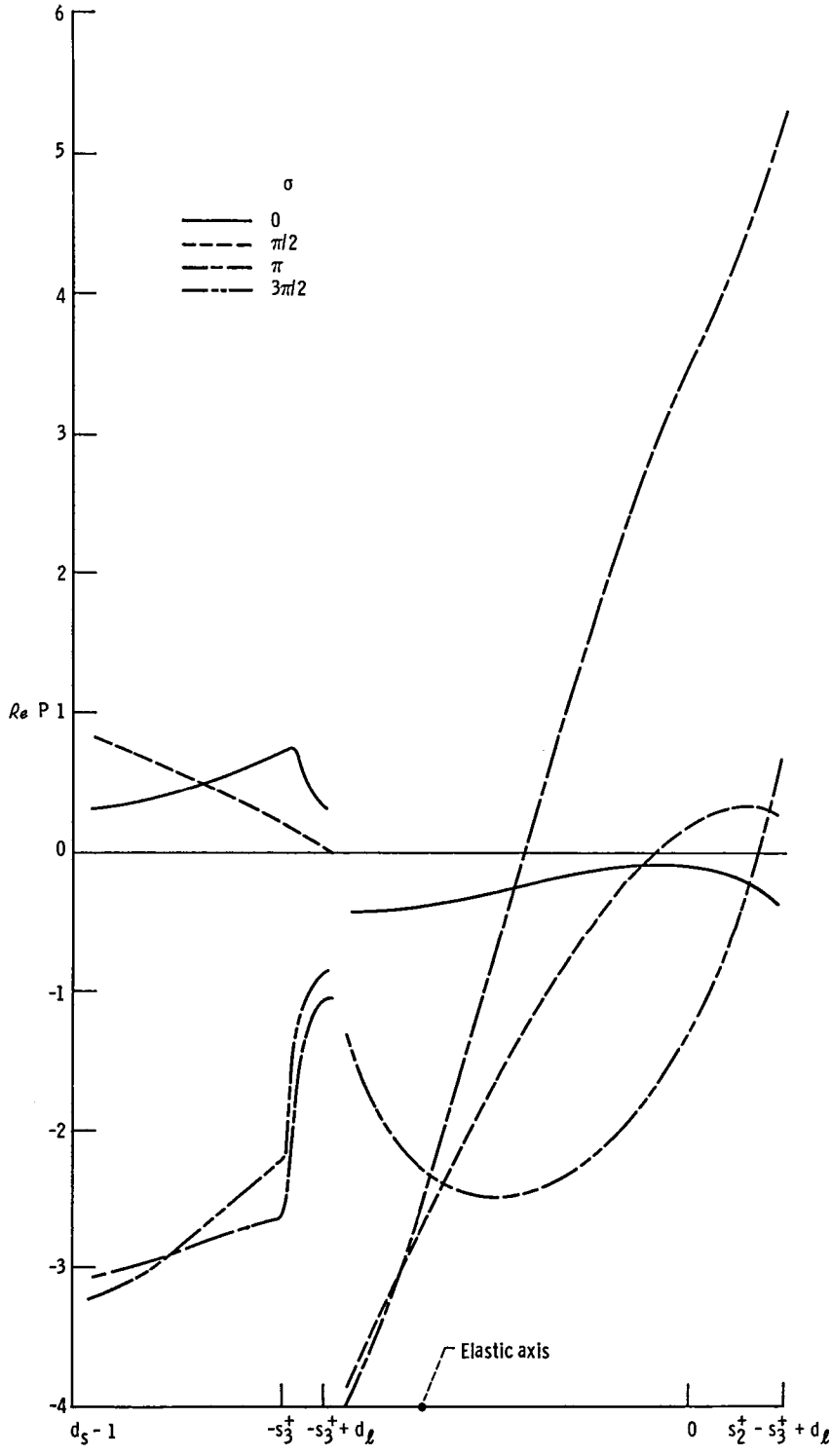

(c) In-phase component (real part) of pressure acting on lower surfaces.

Figure 12. - Continued.

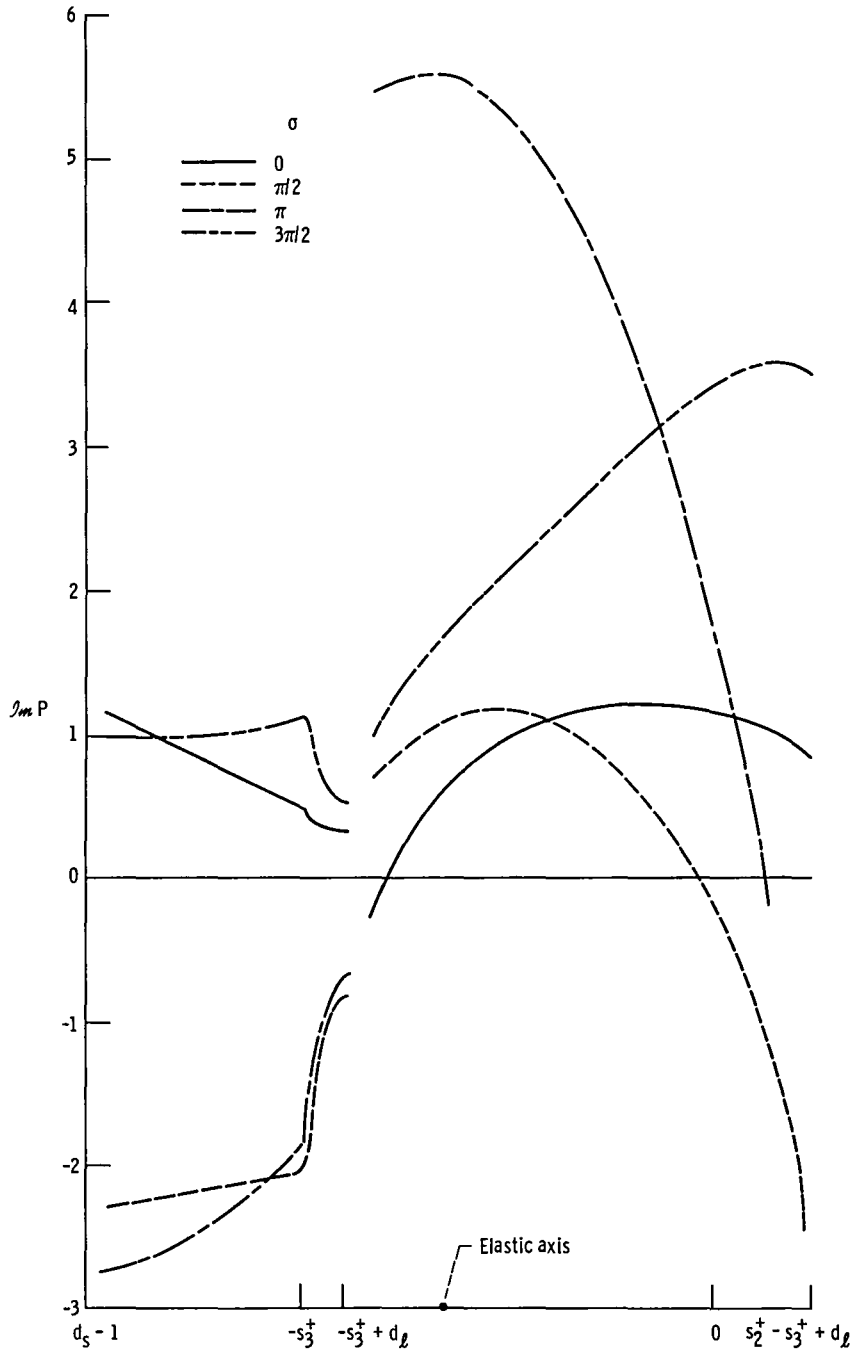

(d) Out-of-phase component (imaginary part) of pressure acting on lower surface.

Figure 12. - Concluded.

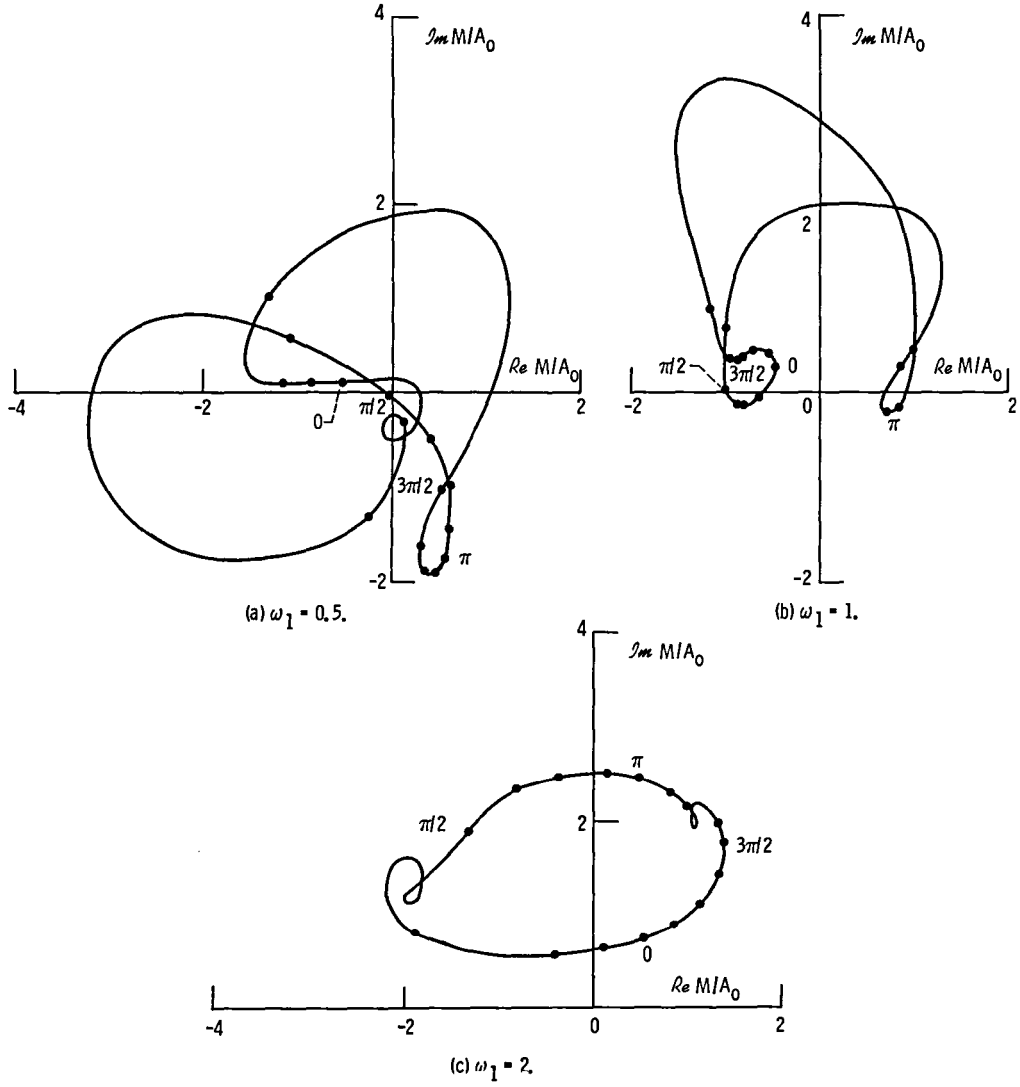

Figure 13. - Moment coefficient for pitching motion about center of blade 1. ($M_1 = 1.4$; $P_{21} = 2.11$.)

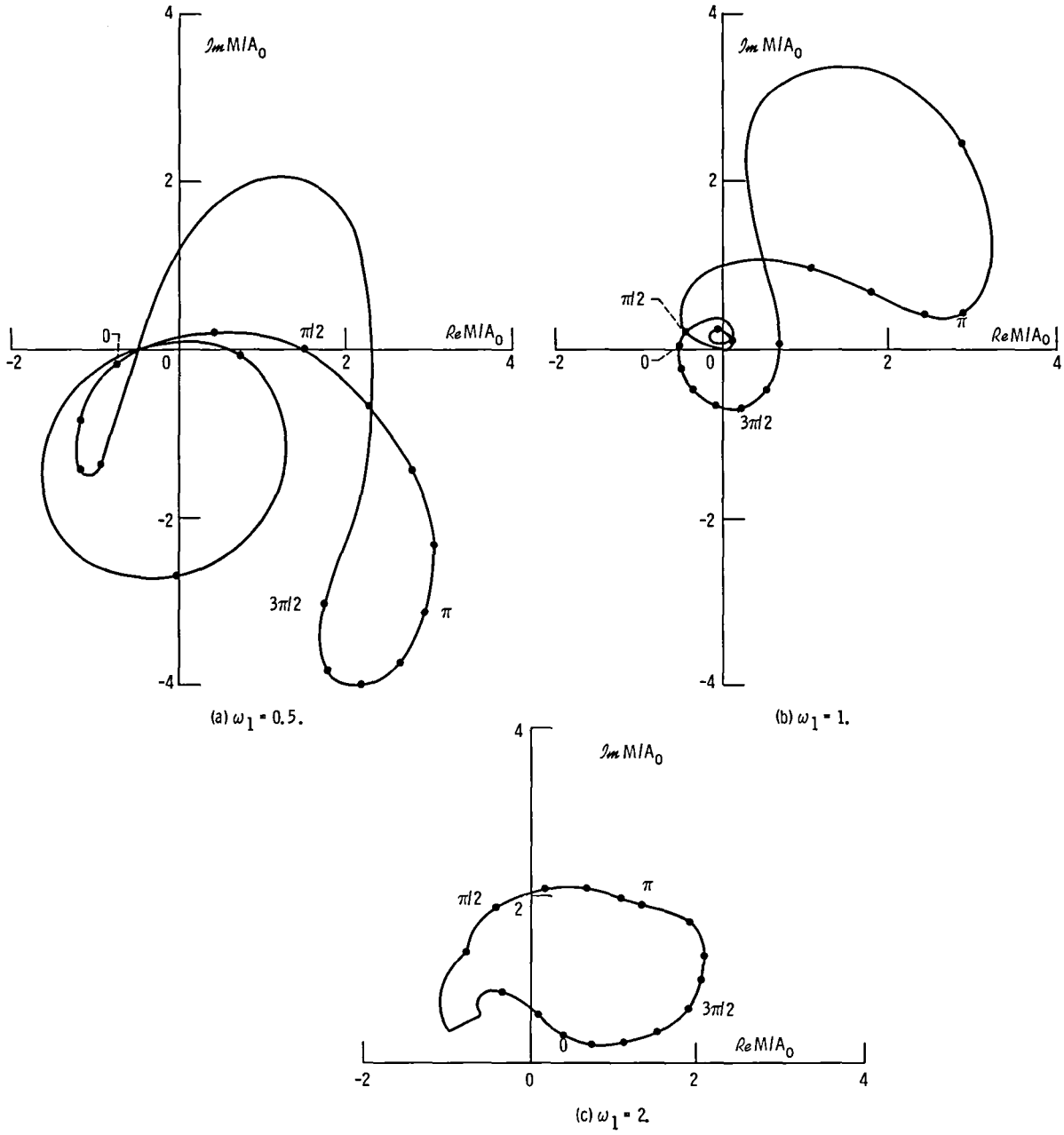

Figure 14. - Moment coefficient for pitching motion about center of blade 2. ($M_1 = 1.6$; $P_{21} = 2.76$.)

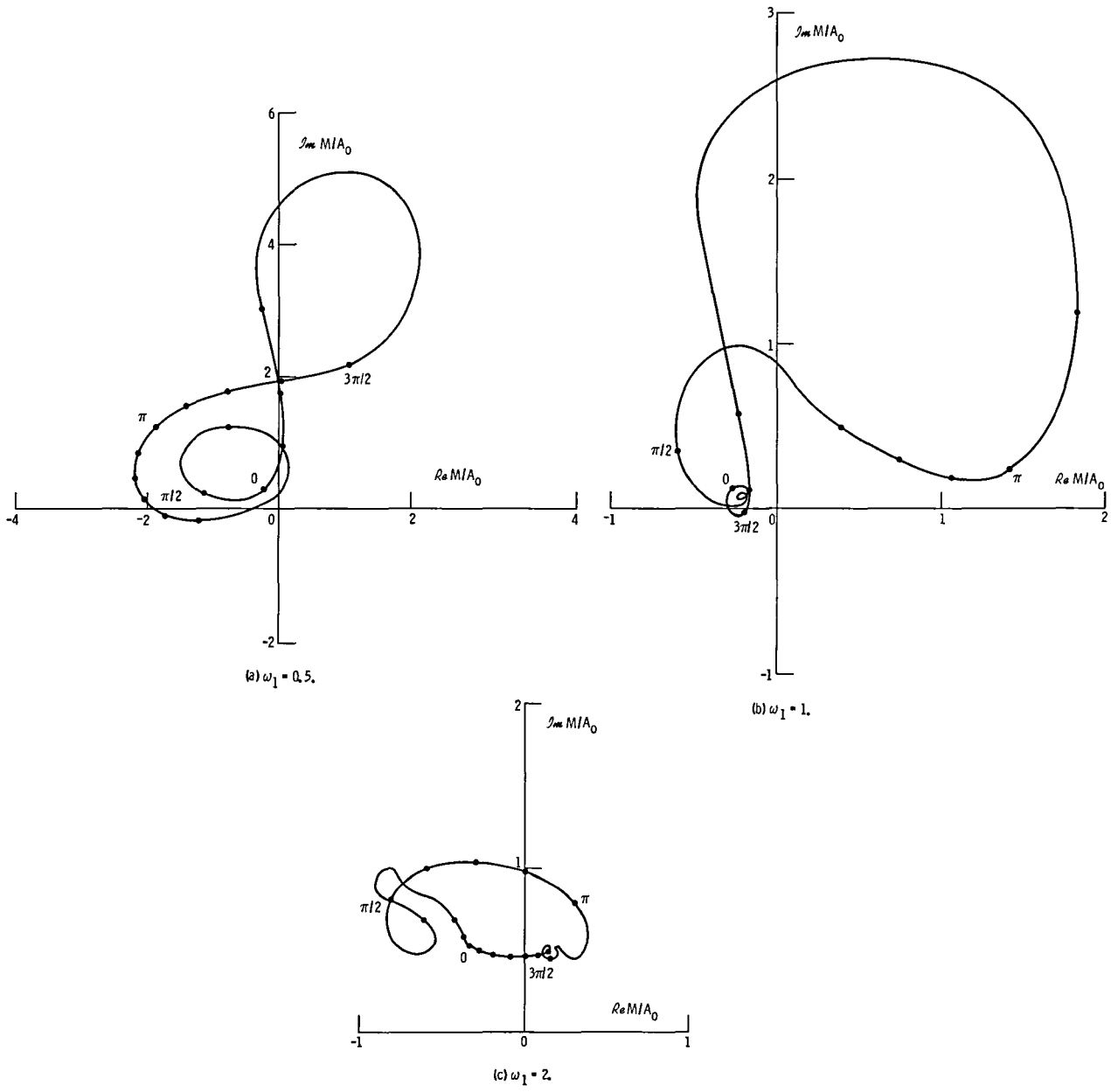

Figure 15. - Moment coefficient for pitching motion about center of blade 3. ($M_1 = 1.6$; $P_{21} = 2.81$.)

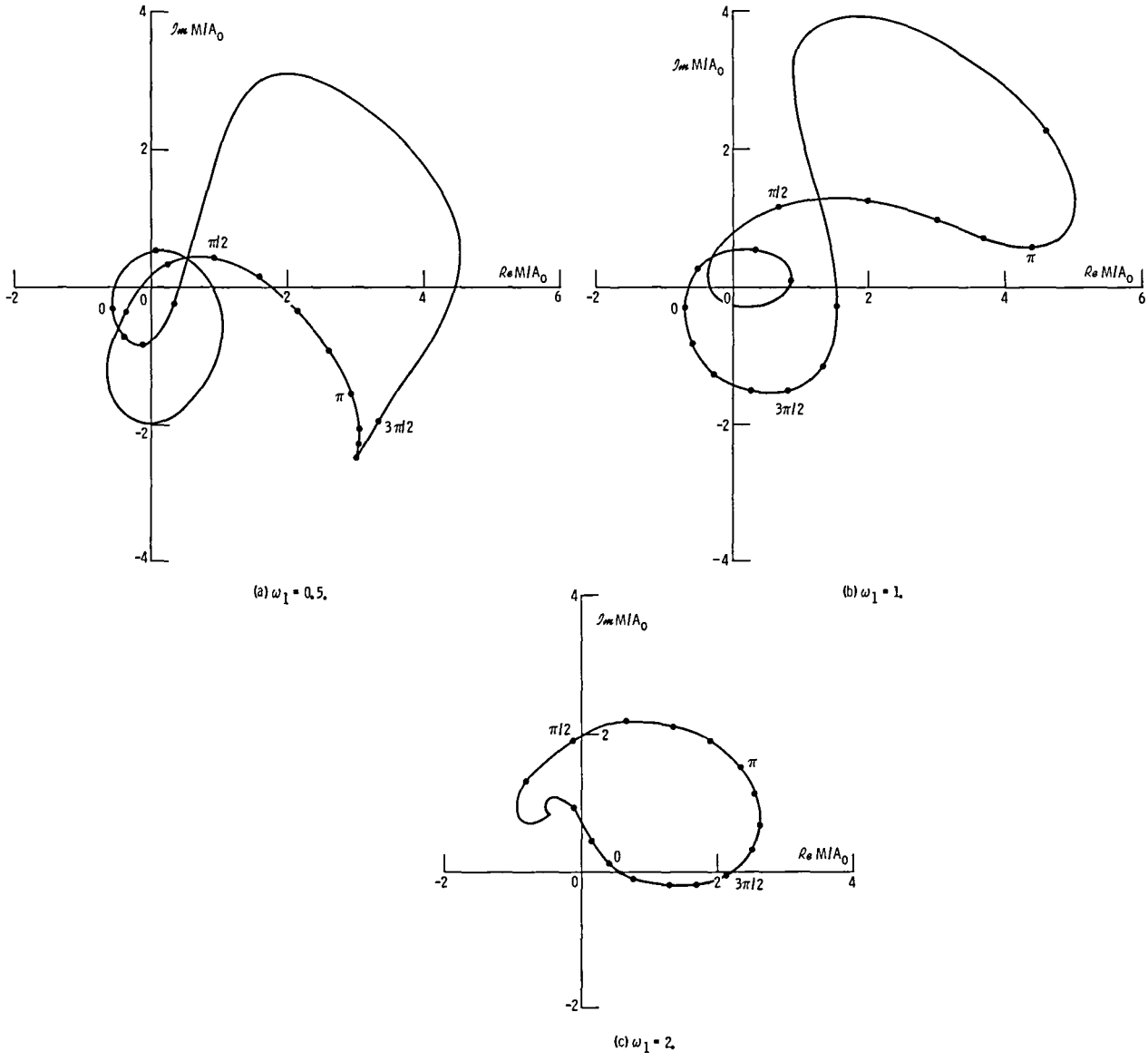

Figure 16. - Moment coefficient for pitching motion about center of blade 4. ($M_1 = 1.8$; $P_{21} = 3.49$.)

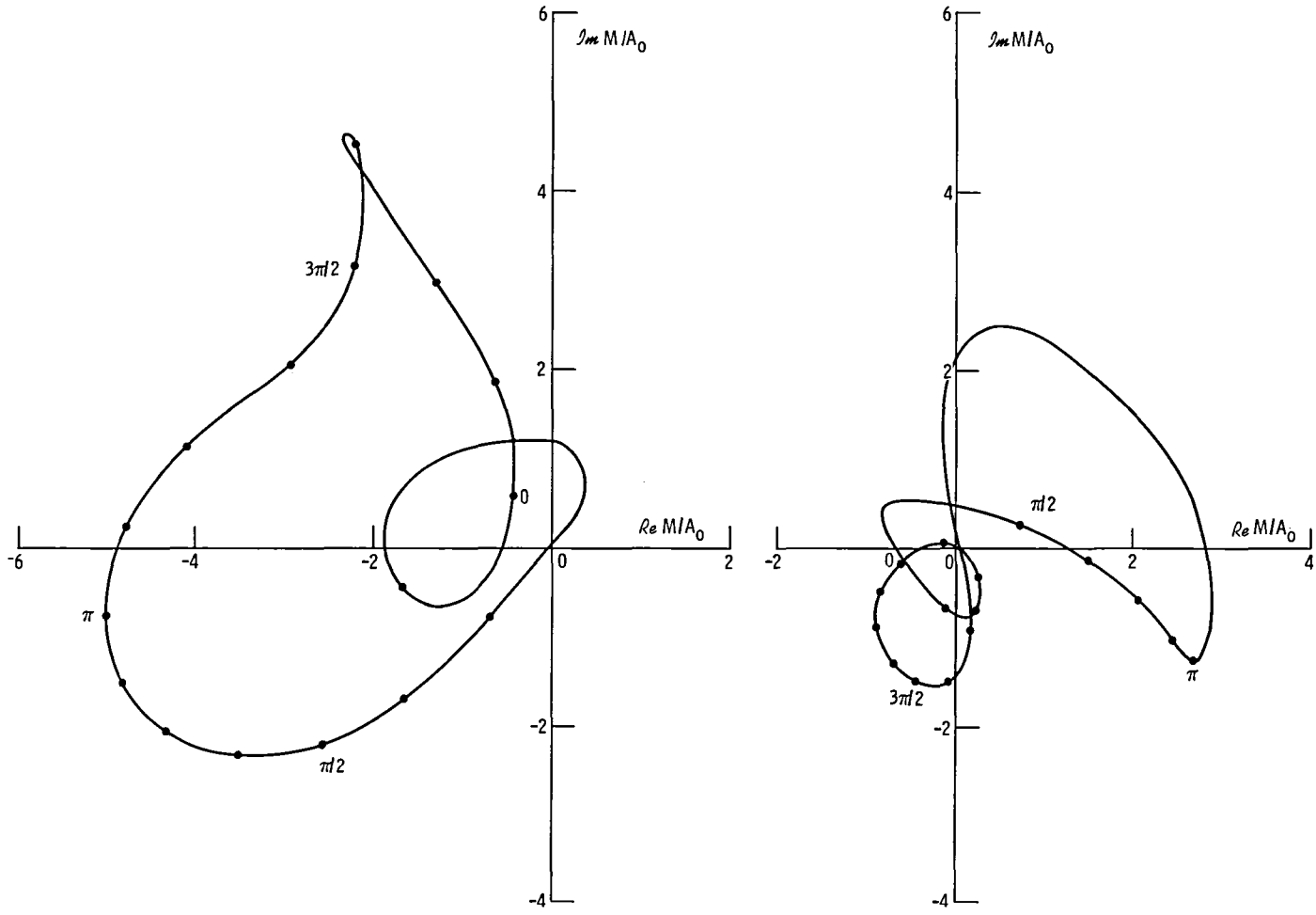

Figure 17. - Moment coefficient for pitching motion about center of blade 5. ($M_1 = 1.8$; $P_{21} = 3.61$.)

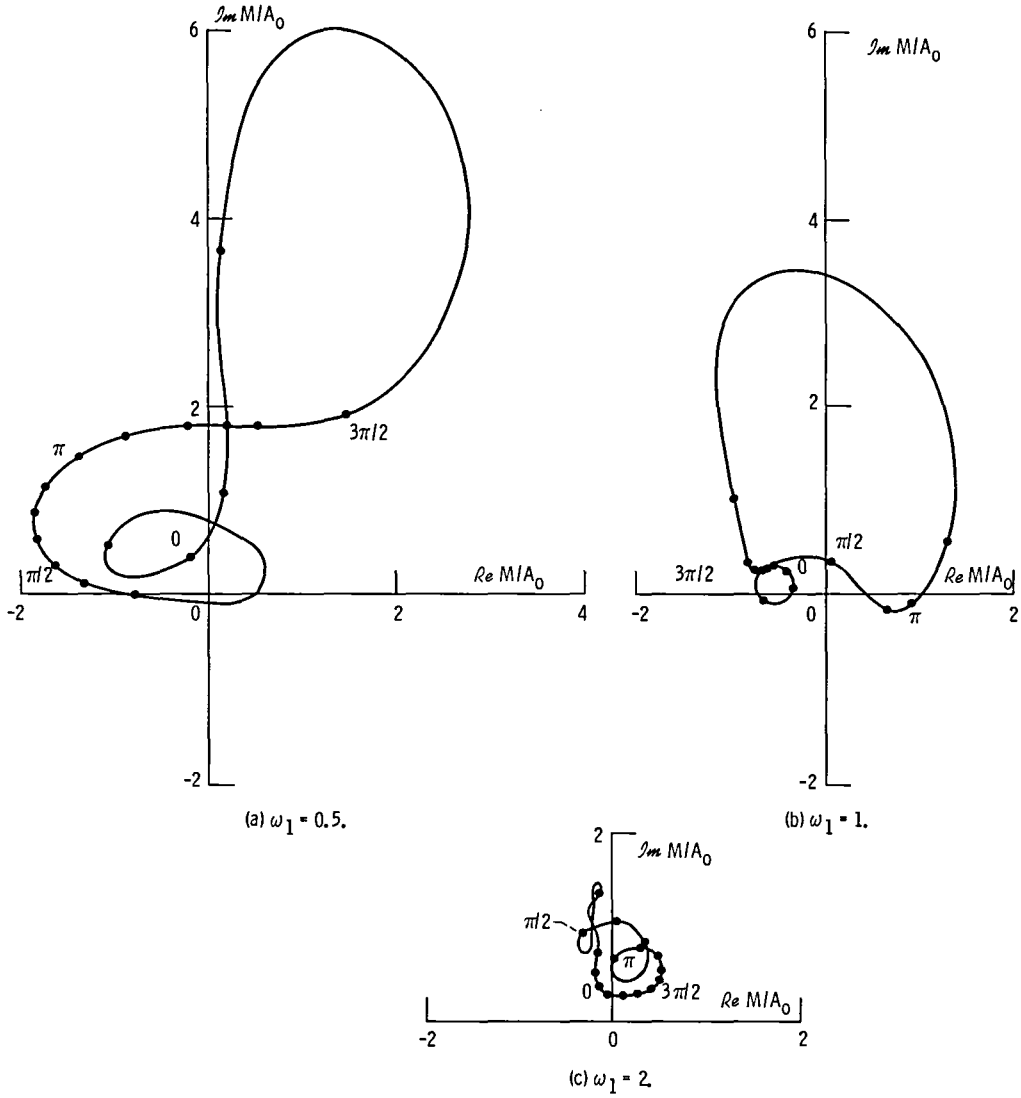

Figure 18. - Moment coefficient for pitching motion about center of blade 6. ($M_1 = 1.8$; $P_{21} = 3.68$.)

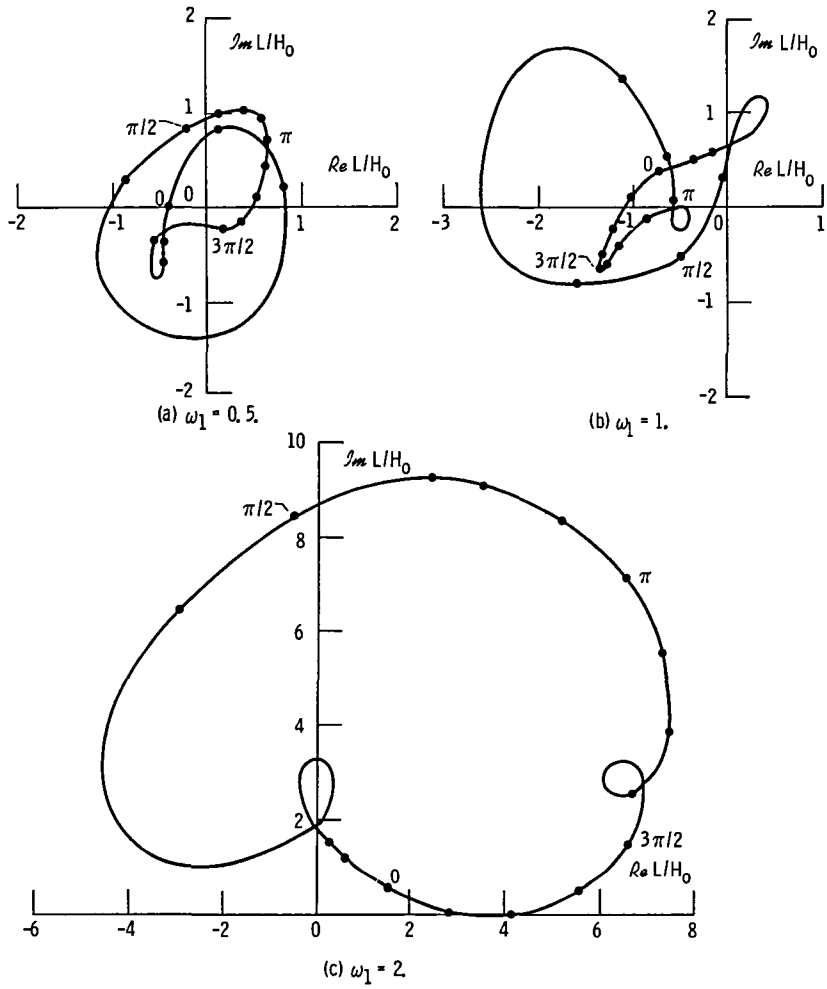

Figure 19. - Lift coefficient for plunging motion of blade 1. (M_1 = 1.4; P_{21} = 2.11.)

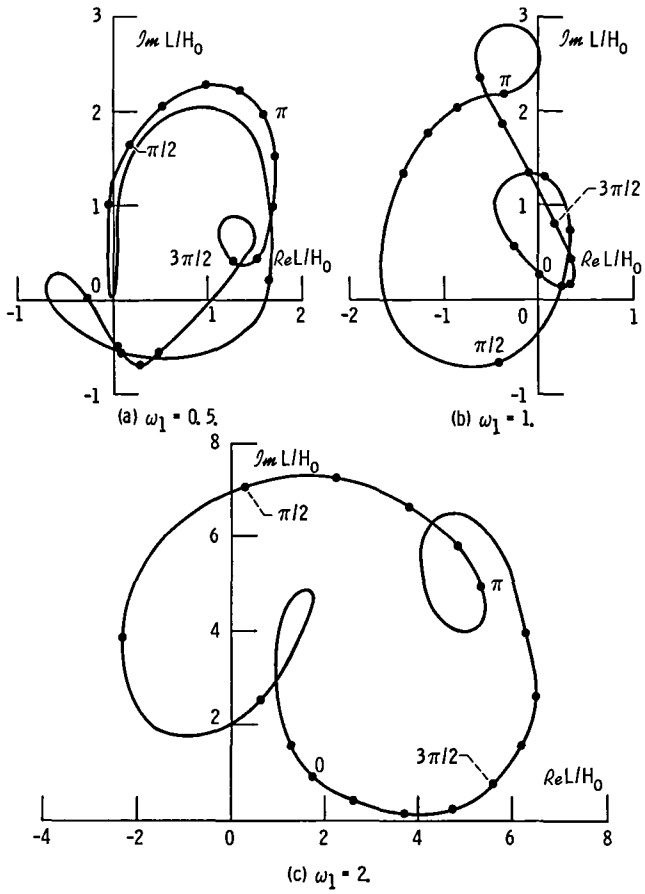

Figure 20. - Lift coefficient for plunging motion of blade 2. (M_1 = 1.6; P_{21} = 2.76.)

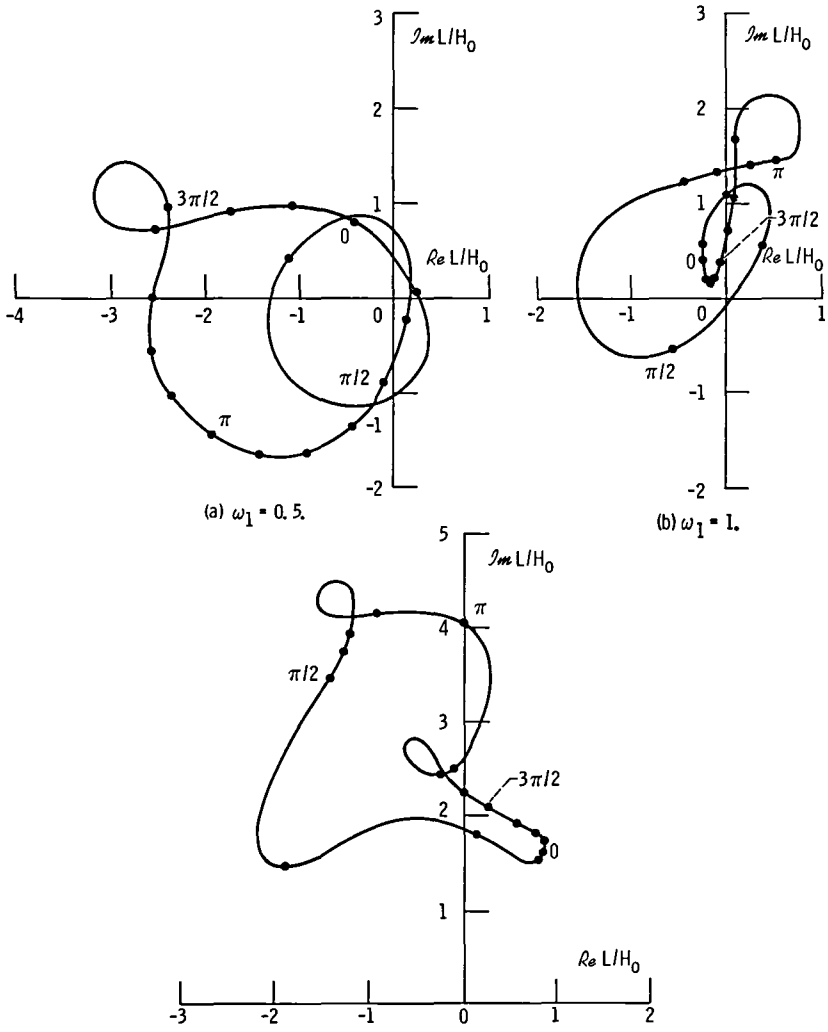

Figure 21. - Lift coefficient for plunging motion of blade 3. ($M_1 = 1.6$; $P_{21} = 2.81$.)

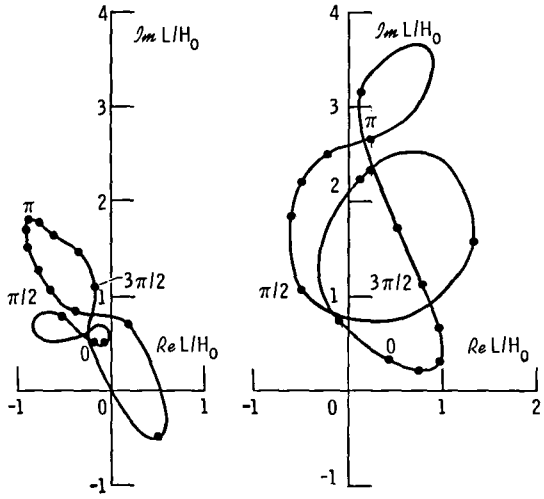

(a) $\omega_1 = 0.5$.

(b) $\omega_1 = 1$.

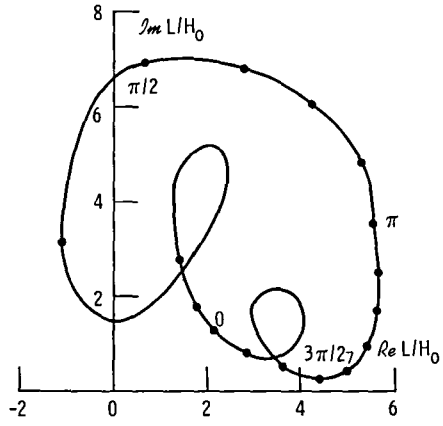

(c) $\omega_1 = 2$.

Figure 22. - Lift coefficient for plunging motion of blade 4. ($M_1 = 1.8$; $P_{21} = 3.49$.)

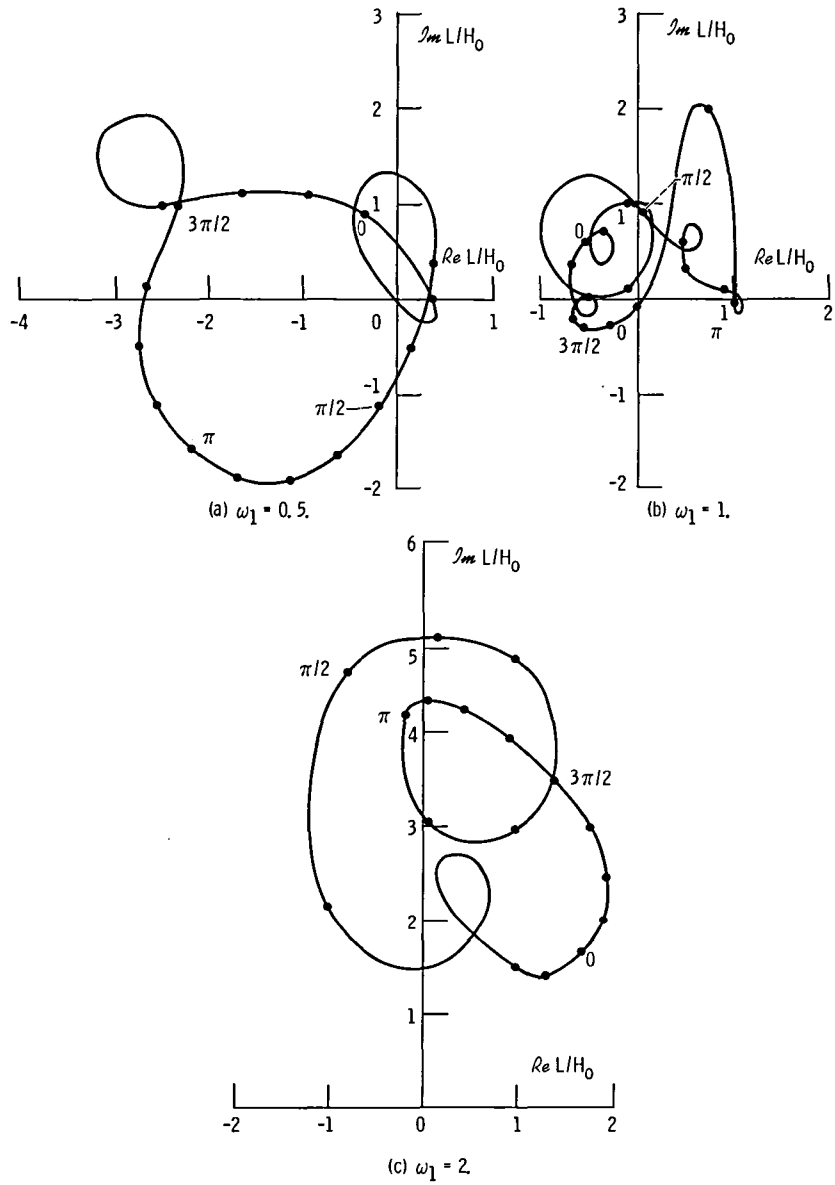

Figure 23. - Lift coefficient for plunging motion of blade 6. (M_1 = 1.8; P_{21} = 3.68.)

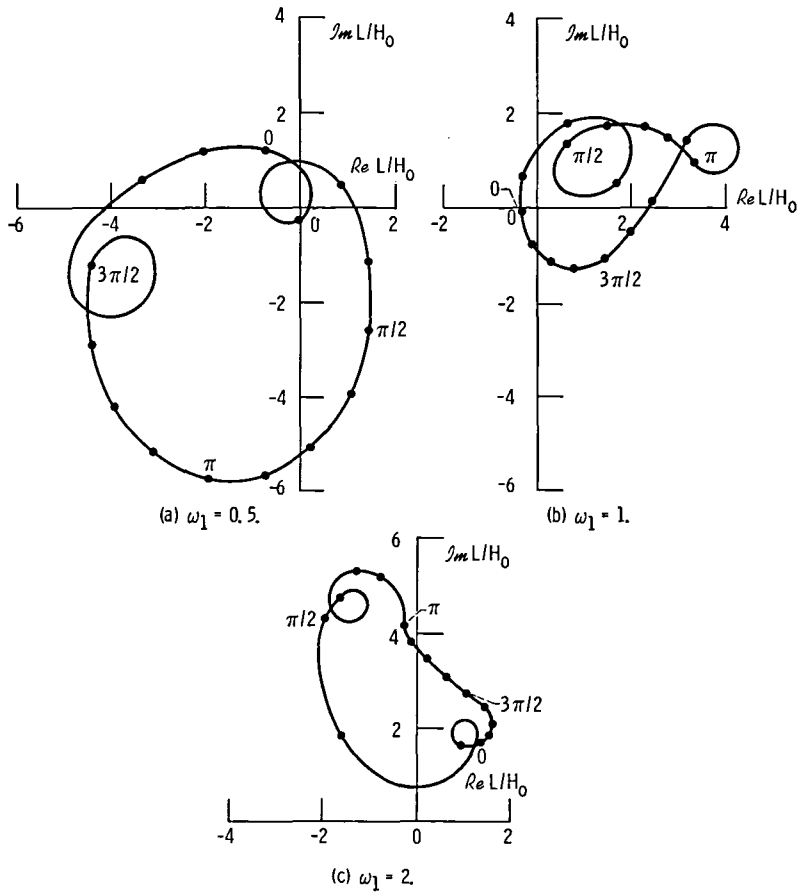

Figure 24. - Lift coefficient for plunging motion of blade 5. (M_1 = 1.8; P_{21} = 3.61.)

1. Report No.	2. Government Accession No.	3. Recipient's Catalog No.
NASA CR-3925		

4. Title and Subtitle	5. Report Date
Unsteady Flow in a Supersonic Cascade With Two In-Passage Shocks	September 1985
	6. Performing Organization Code

7. Author(s)	8. Performing Organization Report No.
Willis H. Braun	None
	10. Work Unit No.

9. Performing Organization Name and Address	11. Contract or Grant No.
Willis H. Braun 504 Lyme Circle Berea, Ohio 44017	NAS3-24100
	13. Type of Report and Period Covered
12. Sponsoring Agency Name and Address	Contractor Report
National Aeronautics and Space Administration Washington D.C. 20546	14. Sponsoring Agency Code
	505-90-22 (E-2129)

15. Supplementary Notes

Final report. Project Manager, Marvin E. Goldstein, Chief Scientist, NASA Lewis Research Center, Cleveland, Ohio 44135.

16. Abstract

A model for a supersonic blade row with two in-passage shock waves is developed. It accounts for three-dimensional effects in real flows by using an altered blade shape in a two-dimensional cascade. There is enough flexibility in the choice of blade shape to accommodate a desired entrance angle, exit angle, boundary-layer thickness and stage pressure ratio at a given entrance Mach number. The model divides the mean flow into regions of uniform or one-dimensional flow in which the solutions for the unsteady flow may be formed successively. The analysis makes use of previous solutions for unsteady flow in cascades and over an oscillating wedge. Six flow conditions are chosen in the range of parameters for which the two-shock model is valid for studies of flutter in torsion and bending. It is found, in keeping with previous results from a single-shock model, that in each case there is increasing instability with decreasing frequency.

17. Key Words (Suggested by Author(s))	18. Distribution Statement
Flutter; Compressor; Supersonic flow; Shock waves	Unclassified - unlimited STAR Category 02

19. Security Classif. (of this report)	20. Security Classif. (of this page)	21. No. of pages	22. Price*
Unclassified	Unclassified	89	A05

*For sale by the National Technical Information Service, Springfield, Virginia 22161

NASA-Langley, 1985

End of Document